AFRRI Reports

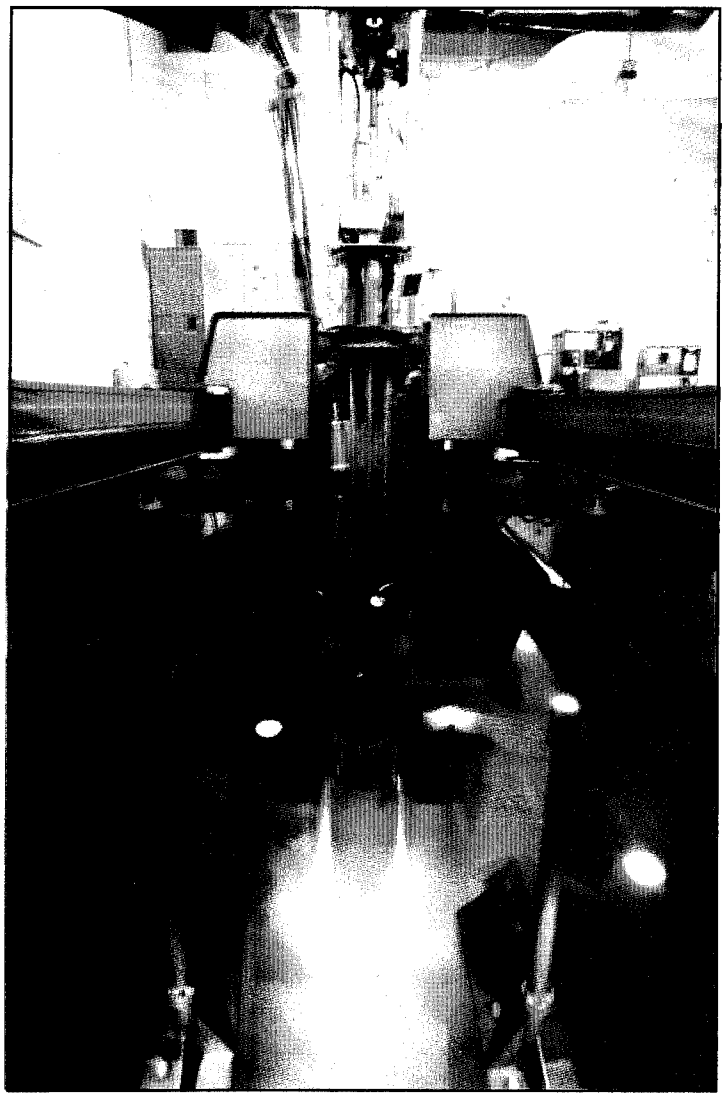

First Quarter
1995

Armed Forces Radiobiology Research Institute
8901 Wisconsin Avenue
Bethesda, Maryland 20889-5603

On the cover: The glow in the pool of water shielding the core of AFRRI's Mark-F TRIGA nuclear reactor is known as Cherenkov radiation and is caused by electrons from the reactor traveling at speeds greater than the speed of light in water. The effect is named for Pavel Alekseyevich Cherenkov, a Soviet scientist who, along with his co-investigators, won the 1958 Nobel Prize for Physics for their observations.
AFRRI photo by David H. Morse.

REPORT DOCUMENTATION PAGE

Form Approved
OMB No. 0704-0188

1. AGENCY USE ONLY *(Leave blank)*	2. REPORT DATE	3. REPORT TYPE AND DATES COVERED
	April 1995	Reprints

4. TITLE AND SUBTITLE

AFRRI Reports, First Quarter 1995

5. FUNDING NUMBERS

PE: NWED QAXM

6. AUTHOR(S)

7. PERFORMING ORGANIZATION NAME(S) AND ADDRESS(ES)

Armed Forces Radiobiology Research Institute
8901 Wisconsin Avenue
Bethesda, MD 20889-5603

8. PERFORMING ORGANIZATION REPORT NUMBER

SR95-1 - SR95-10

9. SPONSORING/MONITORING AGENCY NAME(S) AND ADDRESS(ES)

Uniformed Services University of the Health Sciences
4301 Jones Bridge Road
Bethesda, MD 20814-4799

10. SPONSORING/MONITORING AGENCY REPORT NUMBER

11. SUPPLEMENTARY NOTES

12a. DISTRIBUTION/AVAILABILITY STATEMENT

Approved for public release; distribution unlimited.

12b. DISTRIBUTION CODE

13. ABSTRACT *(Maximum 200 words)*

This volume contains AFRRI Scientific Reports SR95-1 through SR95-10 for January-March 1995.

14. SUBJECT TERMS

15. NUMBER OF PAGES
100

16. PRICE CODE

17. SECURITY CLASSIFICATION OF REPORT	18. SECURITY CLASSIFICATION OF THIS PAGE	19. SECURITY CLASSIFICATION OF ABSTRACT	20. LIMITATION OF ABSTRACT
UNCLASSIFIED	UNCLASSIFIED	UNCLASSIFIED	UL

CLASSIFIED BY:

DECLASSIFY ON:

CONTENTS

Scientific Reports

ELSEVIER

Mutation Research 334 (1995) 39–47

MR
Environmental Mutagenesis

Simplified and optimized kinetochore detection: cytogenetic marker for late-G_2 cells

M. Abend [a,*], W.F. Blakely [b], D. van Beuningen [a]

[a] *Ministry of Defense, Federal Armed Forces Medical Academy, Institute of Radiobiology, Neuherbergstr. 11, 80937 Munich, Germany*
[b] *Armed Forces Radiobiology Research Institute, Radiation Biophysics Department, Bethesda, MD 20889-5603, USA*

Received 23 December 1993; revision received 28 April 1994; accepted 3 May 1994

Abstract

Cytogenetic detection of kinetochore proteins using the CREST antibody coupled with secondary antibodies labeled with different fluorescent probes has been optimized for several in vitro mammalian cell lines. This study investigated selected parameters including the influence of common fixatives (methanol, ethanol, methanol : acetic acid (3 : 1)), detergents (Triton-X100, Tween), fluorescent probes (CY3, BODIPY, FITC), washing protocols, and an antifading agent (paraphenylenediamine) on the detection of kinetochore proteins in control and X-ray (240 kVp)-irradiated cells. Utilizing an optimized fixation and staining protocol, a brilliant visualization of kinetochores in interphase cells was obtained in control as well as X-ray-irradiated interhase cells. Application of this improved kinetochore staining methodology readily permits discriminating cells containing either single or paired kinetochores, the latter of which are characteristic of late-G_2 phase and prophase cells.

Keywords: Kinetochores; Late-G_2 phase; Fluorochrome conjugation; CY3; BODIPY; FITC

1. Introduction

Kinetochores are known as the area of attachment of the spindle apparatus for separation of chromatids during mitosis and meiosis (Earnshaw and Rattner, 1989). Brenner et al. (1981) and Bartholdi (1991) showed that cells express paired kinetochores (called prekinetochores) during the late-G_2 phase and prophase. The exact detection of late-G_2 phase cells can be of great interest in experiments evaluating the regulation of cells at the G_2/M transition after irradiation. Another example in which kinetochore staining procedures are used is to differentiate acentric from centric chromosome fragments in micronuclei. However, according to Eastmond and Tucker (1989) and Yager et al. (1990) the amount of unscorable micronuclei ranges from 15% to 30% due to an insufficient kinetochore stain. To overcome this problem, other authors either used a biotin-avidin antibody sandwich technique (Henning et al., 1988) or recommended in situ hybridization with centromeric probes to increase the signal (Heddle et al., 1991).

* Corresponding author. Tel. 049-89-3168-3203; Fax 049-89-3168-3395.

SSDI 0165-1161(94)00049-U

When counting cells with paired kinetochores, additional difficulties arise: labeling of kinetochores is reduced on X-irradiated cells at least 1 day after irradiation (own experience), and duplication of kinetochores does not occur simultaneously in the cell (Haaf and Schmid, 1989). Therefore, an excellent staining of the kinetochores is needed in order to differentiate between kinetochores lying close together and paired kinetochores. Furthermore, each of the 40–50 kinetochores of the utilized cells has to be examined individually in order to decide whether it is paired or not. Usually, kinetochores are in different focus levels in the cell. Focusing each cell at different levels is very time consuming and eye stressing. It would be a great advantage to have one focus level.

The aim of our study was to optimize the labeling of kinetochores by modifying the staining procedure and by comparing the use of different fluorochrome conjugates, such as FITC (fluorescein 5-isothiocyanate), BODIPY (trademark of Molecular Probes) and CY3 (cyanine fluorochrome no. 3, trademark of Dianova).

2. Materials and methods

Cells and cell cultures

Three mammalian cell lines were used. NCTC clone L929 (mouse fibroblasts) and Chang cells (human liver cells) were purchased from Flow Laboratories (Meckenheim, Germany). HL-60 (human leukemia) cells were a gift of Prof. Dr. Grosse-Wilde (Institut für Immungenetik, Universitätsklinikum Essen). L929 and Chang cells were grown in Earle's modification of Eagle's minimum essential medium (MEM) supplemented with 20% heat-inactivated fetal calf serum and subcultured twice per week. HL-60 cells were treated similarly, but were cultured in RPMI 1640 medium. Cultures were incubated at 37°C in a humidified atmosphere buffered by 5% CO_2 in air and hydrogen carbonate at pH 7.4. All chemicals for media were purchased from Boehringer, Mannheim, Germany.

L929 cells and Chang cells were harvested by trypsinization of the monolayer (0.05% trypsin containing 0.02% EDTA in calcium- and magnesium-free phosphate-buffered saline (PBS) (Boehringer)). HL-60 cells were grown in suspension.

Radiation conditions

L929 cells and Chang cells were plated at 0.1×10^6 cells/ml in 25-cm^2 culture flasks and HL-60 cells in 75-cm^2 flasks. After plating for 24 h, cells were irradiated at room temperature (RT) as exponentially growing cultures with single doses of 240 kV X-rays (Isovolt 320/10; Seifert, Ahrensburg, Germany), filtered with 3 mm Be. Absorbed dose was measured with a Duplex dosimeter (PTW, Freiburg, Germany). The absorbed dose rate was about 1 Gy/min at 13 mA. L929 cells and Chang cells were irradiated with 2–6 Gy; HL-60 cells were irradiated with 0.1–2.5 Gy.

Preparation of slides

After trypsinization where needed, cells were washed twice in PBS and were cytospun ($< 40 \times g$/min, 5 min) at several time points (0, 4, 7, 10, 13, 15, 17, 20, 24, 27, 30, 33, 36, 40, 45, 50 h) after irradiation. Slides were air dried for 10 min, fixed in either methanol (99%) at RT or −20°C, ethanol at RT or methanol and acetic acid for 10 min, air dried for 10 min again, and washed in PBS for 10 min prior to the incubation of antibodies. Doing a cytospin is an easy, comfortable and established way to produce scorable slides (Cherry et al., 1989; Eastmond and Tucker, 1989). Therefore, the growth of cells on a coverslip or slide, as described by several other authors (Bartholdi, 1991; Degrassi and Tanzarella, 1988; Fantes et al., 1989; Nüsse et al., 1989), can be avoided.

Immunofluorescence

Slides were incubated with 100 μl of polyclonal antikinetochore antibodies (pooled CREST-Serum, Sigma, Deisenhofen, Germany, diluted 1:5 to 1:100 in PBS or Triton X-100 or Tween) at RT in a humidified chamber for 1 h. Slides were carefully prerinsed with PBS or distilled water before the 10-min wash in a cuvette containing PBS or distilled water. The secondary

antibody (100 μl) was conjugated either to the fluorochrome CY3 (goat antihuman IgG (H + L) diluted 1:50 in PBS; Dianova, Hamburg, Germany), BODIPY (goat antihuman IgG (H + L) diluted 1:10 in Tween or PBS (1:50); Molecular Probes, Eugene, OR, USA), or FITC (rabbit antihuman IgG diluted 1:10 in Tween or PBS (1:50); Dako, Hamburg, Germany) and was applied to the slide for 30 min at RT in a humidified chamber. DNA was counterstained with 100 μl DAPI (4′,6-diamidino-2-phenylindol, 10 μg/100 ml distilled water; Serva, Heidelberg, Germany) during the last 5 min of incubation. The slides were prerinsed with PBS or distilled water and placed in a cuvette containing PBS or distilled water for 10 min, air dried for 15 min, and were either stored at 4°C in darkness for at least 6 weeks without significant changes in the staining intensity or mounted in glycerin with or without paraphenylenediamine (PPD, 1 mg/ml, according to Johnson and Araujo, 1981) and scored at least 1 h afterwards (reveals a clearer image due to reduced background stain, unpublished experience).

Microscopic observation, photometry, and photographs

The slides were examined (magnification 400–1000 ×) with an epifluorescence microscope (Diaplan 20, Leica, Wetzlar, Germany), equipped with an ultraviolet filter (excitation at 270–380 nm; emission at 410–580 nm) for the DAPI stain, a green filter (excitation at 530–560 nm; emission at > 580 nm) for the CY3 kinetochore stain and a blue filter (excitation at 450–490 nm; emission at > 515 nm) for the FITC or BODIPY kinetochore stain.

Fluorescence intensity of the kinetochores of cells was measured using a microscope photometrical detector (MPV2, Leica). Typically, one cell nucleus was placed in the detection field for these measurements.

Photographs were taken with this microscope in combination with the Orthoplan (Leica), using black and white film (Ilford, 400 ASA).

Analysis of the data

All tables and graphs were based on three separate experiments. Semiquantitative results (Tables 1, 3–5) were accomplished on the basis of at least 200 cells examined per parameter and experiment. Quantitative results (Figs. 1–3, Table 2) were based on at least 120 measurements per experiment and curve, which resulted in about 1000 measurements per figure. The double exponential curve fit and the SEM were calculated with the aid of statistical software (Sigma Plot, Version 5.0, Jandel, Erkrath, Germany).

Microscopic observation of fluorochrome-labeled kinetochores was evaluated based on several parameters. Staining intensity was qualitatively measured by eye or quantitatively scored by the use of the microscopic photometer as described above. Nonspecific or background staining by the fluorochrome probes was qualitatively evaluated by eye. An additional parameter, homogeneity, addressed the ability of the staining protocol to provide a uniform detection efficiency of kinetochores in various cells observed in a single microscopic field at 400–1000 × magnification.

3. Results and discussion

Fixation of cells

Several common fixatives were examined for their effect on the detection of kinetochores using three cell lines 0 and 50 h after irradiation. The kinetochore staining intensity of three cell lines using CY3, FITC, or BODIPY secondary antibodies revealed no significant differences when fixed with either prechilled methanol

Table 1
Influence of different fixatives on the staining intensity of fluorochrome labeled kinetochores determined 0 and 50 h after irradiation

Fixative	Cell line		
	L929	Chang	HL-60
Methanol (−20°C)	+++	+++	+++
Methanol (RT)	+++	+++	+++
Ethanol (RT)	+++	+++	+++
Methanol + acetic acid	(+)	(+)	(+)

+++, strong; (+), not detectable by eye. Pluses represent the semiquantitative results of at least 200 cells examined per fixative and experiment (two repeats were performed).

(−20°C), ethanol, or methanol at room temperature (Table 1). However, the use of methanol combined with acetic acid as a fixative agent resulted in a drastic reduction of the ability to detect kinetochore (Table 1). This apparent destruction of kinetochore antigen recognition sites by acetic acid has been previously described (Earnshaw et al., 1989; Henning et al., 1988). The results of these studies support the use of methanol or ethanol at RT or −20°C as a fixative, similar to the recommendations of others (Degrassi and Tanzarella, 1988; Henning et al., 1988, 1990; Nüsse et al., 1989).

Immunofluorescence

The immunofluorescence staining procedure was performed according to the following two equations:

Kinetochore (Kin) + 1st antikinetochore antibody (CREST-Ab) → Kin-CREST-Ab (1)

Kin-CREST-Ab + 2nd antiantibody-fluorochrome conjugate → labeled Kin (2)

First antibody. Pooled CREST-Serum has an advantage over the serum derived from an individual person: Muro et al. (1990) reported that not all patients (20%) who express the symptoms of the CREST syndrome (calcinosis, Raynaud's phenomenon, esophageal dysmotility, sclerodactyly, telangiectasia) exhibit the whole spectrum of antikinetochore antibodies. Additionally, the titer of the antibodies is reported to differ among patients (Verheijen et al., 1992). While others (see above) report inhomogeneous kinetochore staining when using antibodies derived from single individuals, our experience with different lots of the 'pooled' CREST-Serum consistently revealed the same staining quality regardless of the cell line examined and the time (when using a 1:10 dilution) after irradiation. Typically, CREST-Serum was diluted 1:5 to 1:100 in our studies. Concentrations between 1:10 and 1:100 revealed comparable results up to 20 h after irradiation (data not shown). However, even later (up to 50 h) after irradiation, the 1:10 dilution displayed a more homogeneous staining result, which occurred concomitantly with an increased number of micronuclei and apoptotic cells (data not shown), suggesting a connection between reduced kinetochore stain and appearance of damaged cells.

Secondary antibodies. Goat or rabbit antihuman IgGs conjugated with either FITC, BODIPY or CY3 were utilized as secondary antibodies for detection of kinetochores. CY3 is a recently developed fluorochrome (Ernst et al., 1989, Southwick et al., 1989). It reveals a stronger fading than FITC or BODIPY (Fig. 1). Fig. 1, representing L929 cells 0 h after irradiation, shows that BODIPY has a slightly better photostability than FITC, as described by the manufacturer (Bioprobes, 1989, 1990). When adding an antifading drug (PPD) to the mounting media of L929 cells 0 h after irradiation, the three fluorochromes show comparable fading characteristics (Fig. 2). However, when comparing the fluorescence *intensities* of the fluorochromes with each other (mounted only in glycerin), a twofold or threefold stronger

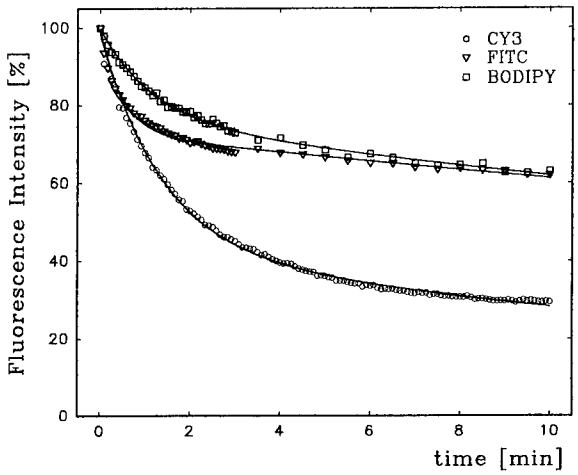

Fig. 1. Fading characteristics of three fluorochromes without an antifading drug determined on L929 cells 0 h after irradiation. Different fluorescence intensity values of the fluorochromes were normalized to 100 at the onset of measurements. Symbols represent the mean of at least three experiments with 120 measurements per experiment and curve. Typical SEM was < 3% of the mean.

signal for CY3 can be observed than for FITC or BODIPY. The results of one representative experiment (L929, 0 h after irradiation) are displayed in Fig. 3. The mean of three such experiments is shown in Table 2 (row 1). Table 2 also shows that BODIPY's fluorescence intensity is comparable to that of FITC. This differs from the manufacturer's reported characteristics of BODIPY (Bioprobes, 1989, 1990). Similar findings (see Table 2) were found with different lots of the BODIPY conjugate in repeated experiments. Possible delays in the overseas shipment of this reagent may account for these BODIPY results.

Due to the fluorescence intensity of CY3-labeled kinetochores (without antifading drugs), kinetochores are still detectable by eye until about 31% of their initial fluorescence intensity remains (Table 2). Alternatively, FITC- and BODIPY-labeled kinetochores are detectable until 82% and 75%, respectively, of their originally far lower signals remain. The detection level can be decreased to less than 70%, 60%, and 71% of CY3-, FITC- and BODIPY-labeled kinetochores respectively (Table 2) when PPD is added to the mounting media (lowest detection level for CY3 was not exactly quantified because the lowest remaining CY3 signal during the 10-min interval of measurements was 70%). In order to obtain this effect, the slides have to be mounted in glycerin containing PPD for at least 1 h, RT (but no longer than 48 h). The time window for kinetochore detection in cells correlates with the fading characteristic and the staining intensity of the fluorochromes utilized. Using CY3, kinetochores are detectable for 8 min (without PPD, Table 2). In contrast, FITC-labeled kinetochores have to be detected in 0.5 min. BODIPY-labeled kinetochores are detectable for 2.5 min due to their lower fading characteristic compared to FITC (Fig. 1, Table 2). After incubating the fluorochromes in mounting media containing PPD, the time window for detection of CY3- and FITC-labeled kinetochores rose to > 10 min and 9 min, respectively. In contrast, BODIPY is not greatly affected by PPD. For this fluorochrome, we found only a minor increase of detection time from 2.5 min to 3 min (Figs. 1–3).

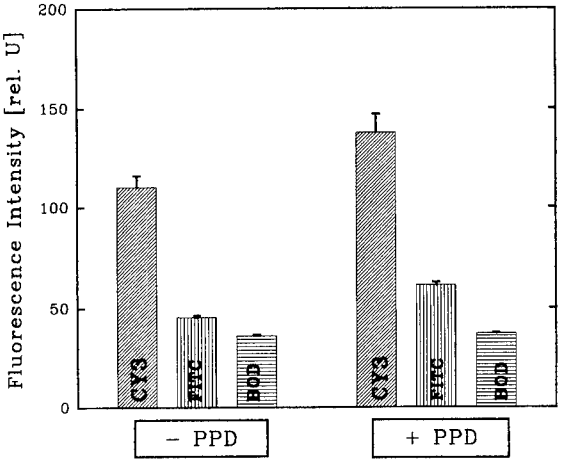

Fig. 3. Comparison of the fluorescence intensities of three fluorochromes with or without an antifading drug determined on L929 cells 0 h after irradiation. Data are from one representative experiment including 200 measurements altogether. – PPD, glycerin mounting media only; + PPD, glycerin mounting media with PPD.

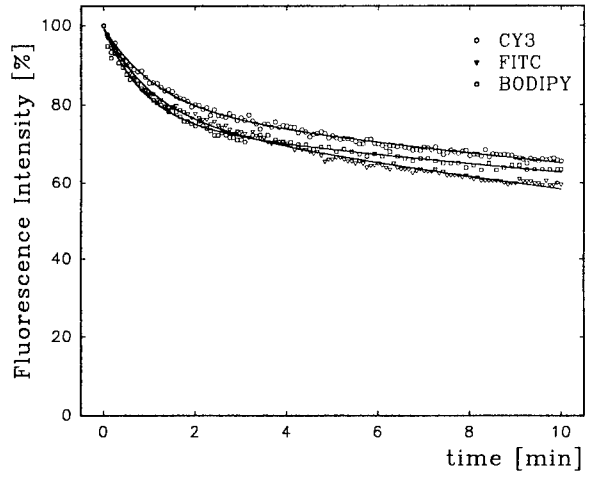

Fig. 2. Fading characteristics of three fluorochromes with an antifading drug determined on L929 cells 0 h after irradiation. Different fluorescence intensity values of the fluorochromes were normalized to 100 at the onset of measurements. Symbols represent the mean of at least three experiments with 120 measurements per experiment and curve. Typical SEM was < 3% of the mean.

Focus problem. Cells mounted in glycerin or PPD (which was stored at −20°C) reveal kinetochores located in various focus levels even when incu-

Table 2
Summary of the fluorescence characteristics of three fluorochromes without and with an antifading agent in the mounting medium determined on L929 cells 0 h after irradiation

	−PPD			+PPD		
	CY3	FITC	BODIPY	CY3	FITC	BODIPY
Relative fluorescence intensity [a]	2.4	1.1	1.1	2.7	1.5	1.0
Detection level (% of baseline)	31	82	75	< 70	60	71
Detection time (min)	8	0.5	2.5	> 10	9	3

−PPD, glycerin mounting media only; +PPD, glycerin mounting media with PPD.
[a] Data were normalized to BODIPY-labeled kinetochores mounted in glycerin or PPD. The mean of 120 measurements per experiment is given (two repeats were performed).

bated for 1–2 h at RT. To examine kinetochores of a cell at different focus levels is eye stressing and time consuming. This can be avoided when using glycerin at RT as shown in Table 3 for L929 cells 0 h after irradiation. The explanation for the temperature dependence of this observation is unknown. CY3-labeled kinetochores mounted in glycerin at RT provided the best results with regard to the staining intensity of the kinetochores and their location in nearly one focus level, in comparison to the other fluorochromes mounted in glycerin with or without PPD (Table 3). This could be also shown for CY3 conjugates up to 50 h after irradiation (data not shown). CY3, diluted 1:50, was appropriate. Concentrations of FITC and BODIPY were 5 times higher (at least 1:10).

Table 3
Influence of the mounting media on kinetochore detection in various focus levels, and the staining intensity of various fluorochrome-conjugated probes determined on L929 cells 0 h after irradiation

Fluorochrome	Mounting media	Focus	Staining intensity
CY3	Glycerin, RT	+ + +	+ + +
CY3	Glycerin + PPD	+ +	+ + +
FITC	Glycerin, RT	+ +	+
FITC	Glycerin + PPD	+ +	+ +
BODIPY	Glycerin, RT	+ +	+ +
BODIPY	Glycerin + PPD	+ +	+ +

Focus, + + +, nearly all kinetochores in one focus level; + +, most of the kinetochores are in different focus levels. Staining intensity, + + +, strong, + +, medium, +, weak. Pluses represent the semiquantitative results of at least 200 cells examined per fluorochrome and experiment (two repeats were performed).

Detergents

In this study FITC and BODIPY had to be diluted in Tween or PBS (1:50) to obtain a countable signal as shown by others (Holowacz and De Boni, 1991; Miller et al., 1991). Diluting the IgG CY3 conjugate in Tween (1:5–1:100) or Triton X-100 (1:5–1:100) increased both the signal on the kinetochore region and the unspecific labeling of the cytoplasm of L929 cells 0 h after irradiation (Table 4) but also at later time points

Table 4
Influence of detergents on kinetochore staining intensity, background (nonspecific) staining, and homogeneity of staining with CY3-conjugated probe determined on L929 cells 0 h after irradiation

Detergent	Staining intensity	Background	Homogeneity
None	+ +	+	+ + +
Tween			
1:5	+ + +	+ + +	+ +
1:10	+ + +	+ +	+ +
1:50	+ + +	+ +	+ + +
1:100	+ + +	+ +	+ + +
Triton X-100			
1:5	+ +	+ + +	+ +
1:10	+ +	+ + +	+ +
1:50	+ + +	+ +	+ + +
1:100	+ + +	+ +	+ + +

Staining intensity, + + +, strong, + +, medium. Background, + + +, high, + +, medium, +, low. Homogeneity, + + +, high, + +, medium. Pluses represent the semiquantitative results of at least 200 cells examined per detergent and experiment (two repeats were performed).

and in HL-60 cells (data not shown). Highly concentrated detergent solutions led to an inhomogeneity of stained cells; hence, the use of detergents did not improve the CY3 results.

Incubation of antibodies

Some authors recommend incubating the slides with the antibodies in a humidified chamber at 37°C (Henning et al., 1990; Miller et al., 1991; Nüsse et al., 1989). In our laboratory incubation at either 37°C or RT does not influence the fluorescence intensity. This is contrary to Henning's findings (1990) of an enhanced signal detection when the antibody is incubated at 37°C. He also used pooled CREST-Serum, but his staining protocol was different and that might explain the differences.

Washing procedure

Prerinsing and washing of CY3-stained kinetochore L929 cells (0–50 h after irradiation) only with PBS after each incubation with antibodies increased the background (nonspecific cytoplasmic staining of the cells and the slide itself, Table 5). This can be avoided efficiently when using only distilled water after each antibody incubation step. Use of this reagent resulted in negligible background staining of the cytoplasm or on the slides. That made it difficult to distinguish cells localized closely together. In order to recognize cells easily we therefore decided to prerinse and wash the cells with PBS after incubation with the first antibody and utilized distilled water after incubation with the second antibody.

Table 5
Influence of different washing procedures on kinetochore staining and background (nonspecific) staining with CY3-conjugated probe determined on L929 cells 0–50 h after irradiation

Washing procedure	Staining intensity	Background
PBS	+ + +	+ +
Distilled water	+ + +	(+)
PBS + distilled water	+ + +	+

Staining intensity, + + +, strong. Background, + +, medium, +, low, (+), not detectable by eye. Washing procedure, PBS, prerinse and washing of slides only in PBS after each antibody incubation; distilled water, prerinse and washing of slides only in distilled water after each antibody incubation; PBS + distilled water, prerinse and washing of slides in PBS after the first and in distilled water after the second antibody incubation. Pluses represent the semiquantitative results of at least 200 cells examined per washing procedure and experiment (at least two repeats were performed).

Comparable effects were found when using FITC and BODIPY conjugates. However, after washing only with distilled water not only the background but also the kinetochore staining intensity appeared to be reduced (data not shown).

Detection of late-G_2 cells

Paired kinetochores are reported to be observed during the late-G_2 phase and prophase (Brenner et al., 1981). In order to differentiate both phases, cellular DNA was stained with DAPI in the presented study. Late-G_2 phase cells were characterized by paired kinetochores and the absence of readily identified DAPI-stained chromosomes. Fig. 4 displays DAPI-stained DNA of two cells, and the CY3-labeled kinetochores of the same HL-60 interphase cells. The cell showing paired kinetochores and homogeneously distributed staining of cellular DNA is identified as being in late-G_2 phase. The labeling of CY3-stained kinetochores on the other cell lines (not shown) is comparable to the quality shown for HL-60 cells. In contrast, kinetochores are less clearly labeled when using FITC or BODIPY conjugates. Hence, a further discrimination of the G_2 phase in early- and late-G_2 phase or G_2pk (G_2 phase with *p*aired *k*inetochores) becomes apparent.

First measurements of G_2pk on unirradiated L929 and HL-60 cells reveal high differences of 3.8% ($\pm$0.3, SEM) and 7.5% ($\pm$0.2, SEM) respectively. However, changes in the G_2pk compartment become even more prominent after irradiation or can be comparable to the baseline, depending on the cell line observed (data submitted for publication). Therefore this optimized technique can be useful for a more precise detection of perturbations in the G_2 phase kinetics after irradiation, hyperthermia, or exposure to chemical agents.

In conclusion, a simplified and, for selected parameters, optimized kinetochore staining procedure is presented: cells were cytospun and fixed in methanol (RT); kinetochores were labeled with

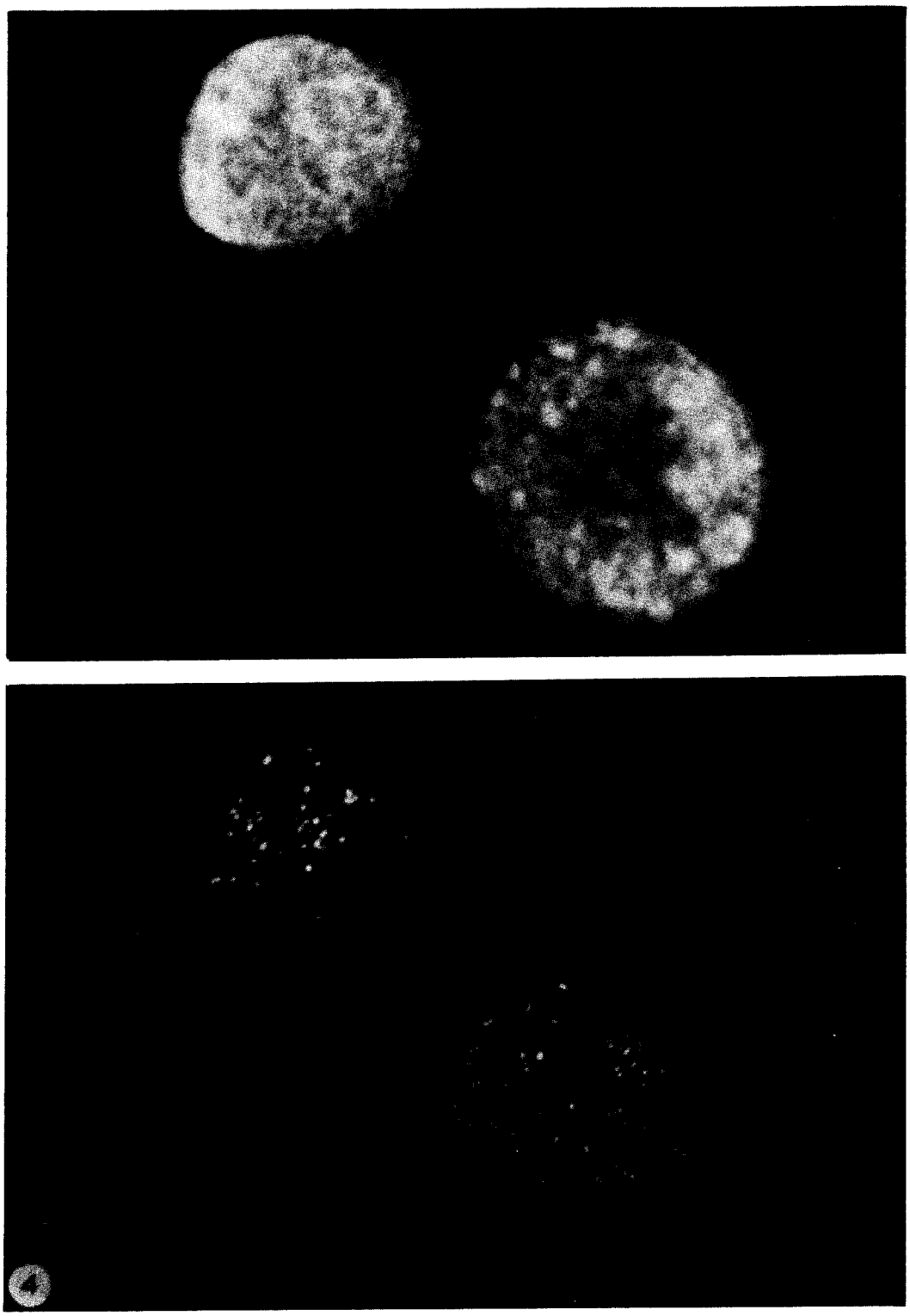

Fig. 4. Photograph illustrates stained DAPI DNA and CY3-stained kinetochores of HL-60 cells 20 h after irradiation. Magnification 1000 ×. (top) Interphase nuclei stained with DAPI. (bottom) Same cells stained for kinetochores, showing one cell with paired kinetochores.

CREST-Serum (1 : 10) and antihuman IgG CY3 conjugate (1 : 50) in a humidified chamber at RT, counterstained with DAPI, and mounted in glycerin (RT). Proliferation of cells on a slide or coverslip, use of prechilled fixatives, incubation of antibodies at 37°C, and use of detergents and antifading drugs as recommended by others was not necessary. Additionally, this simplified staining procedure leads to a constant staining result even up to 50 h after irradiation and can be measured comfortably for about 10 min with strongly labeled kinetochores that are almost all in one focus level. Furthermore, five times fewer CY3 antibodies are required in comparison to FITC or BODIPY conjugates.

Acknowledgements

We thank Mr. W. Hiersekorn for his expert technical assistance and Dr. W. Kaffenberger for helpful discussions. This work was supported by the German Ministry of Defense and the Armed Forces Radiobiology Research Institute under work unit 04640.

References

Bartholdi, M.F. (1991) Nuclear distribution of centromeres during the cell cycle of human diploid fibroblasts, J. Cell Sci., 99, 255–263.

Bioprobes (1989) BODIPY: The new fluorescein substitute, Bioprobes, 10, 3–4.

Bioprobes (1990) BODIPY: Fluorescent secondary antibodies and other proteins, Bioprobes, 11, 8–10.

Brenner, S., D. Pepper, M.W. Berns, E. Tan and B.R. Brinkley (1981) Kinetochore structure, duplication, and distribution in mammalian cells: analysis by human autoantibodies from scleroderma patients, J. Cell Biol., 91, 95–102.

Cherry, L.M., A.J. Faulkner, L.A. Grossberg and R. Balczon (1989) Kinetochore size variation in mammalian chromosomes: an image analysis study with evolutionary implications, J. Cell Sci., 92, 281–289.

Degrassi, F. and C. Tanzarella (1988) Immunofluorescent staining of kinetochores in micronuclei: a new assay for the detection of aneuploidy, Mutation Res., 203, 339–345.

Earnshaw, W.C. and J.B. Rattner (1989) A map of the centromere (primary constriction) in vertebrate chromosomes at metaphase, Prog. Clin. Biol. Res., 318, 33–42.

Earnshaw, W.C., H. Ratrie III and G. Stetten (1989) Visualization of centromere proteins CENP-B and CENP-C on a stable dicentric chromosome in cytological spreads, Chromosoma, 98, 1–12.

Eastmond, D.A. and J.D. Tucker (1989) Identification of aneuploidy-inducing agents using cytokinesis-blocked human lymphocytes and an antikinetochore antibody, Environ. Mol. Mutagen., 13, 34–43.

Ernst, L.A., R.K. Gupta, R.B. Mujumdar and A.S. Waggoner (1989) Cyanine dye labeling reagents for sulfhydryl groups, Cytometry, 10, 3–10.

Fantes, J.A., D.K. Green, P. Malloy and A.T. Summer (1989) Flow cytometry measurements of human chromosome kinetochore labeling, Cytometry, 10, 134–142.

Haaf, T. and M. Schmid (1989) Centromeric association and non-random distribution of centromeres in human tumour cells, Hum. Genet., 81, 137–143.

Heddle, J.A., M.C. Cimino, M. Hayashi, F. Romagna, M.D. Shelby, J.D. Tucker, P. Vanparys and J.T. MacGregor (1991) Micronuclei as an index of cytogenetic damage: past, present, and future, Environ. Mol. Mutagen., 18, 277–291.

Henning, U.G.G. (1990) Modification of the kinetochore immunofluorescence staining method for human fibroblasts for use with a commercially available anticentromere antibody, Mutation Res., 234, 251–252.

Henning, U.G.G., N.L. Rudd and D.I. Hoar (1988) Kinetochore immunofluorescence in micronuclei: a rapid method for the in situ detection of aneuploidy and chromosome breakage in human fibroblasts, Mutation Res., 203, 405–414.

Holowacz, T. and U. De Boni (1991) Arrangement of kinetochore proteins and satellite DNA in neuronal interphase nuclei: changes induced by gamma-aminobutyric acid (GABA), Exp. Cell Res., 197, 36–42.

Johnson, G.D. and G.M. de C. Araujo (1981) A simple method of reducing the fading of immunofluorescence during microscopy, J. Immunol. Methods, 43, 349–350.

Miller, B.M., H.F. Zitzelsberger, H.-U. Weier and I.-D. Adler (1991) Classification of micronuclei in murine erythrocytes: immunofluorescent staining using CREST antibodies compared to in situ hybridization with biotinylated gamma satellite DNA, Mutagenesis, 6, 297–302.

Muro, Y., K. Sugimoto, T. Okazaki and M. Ohashi (1990) The heterogeneity of anticentromere antibodies in immunoblotting analysis, J. Rheumatol., 17, 1042–1047.

Nüsse, M., S. Viaggi and S. Bonatti (1989) Induction of kinetochore positive and negative micronuclei in V79 cells by the alkylating agent diethylsulphate, Mutagenesis, 4, 174–178.

Southwick, P.L., L.A. Ernst, E.W. Tauriello, S.R. Parker, R.B. Mujumdar, S.R. Mujumdar, H.A. Clever and A.S. Waggoner (1990) Cyanine dye labeling reagents-carboxymethylindocyanine succinimidyl esters, Cytometry, 11, 418–430.

Verheijen, R., B.A.W. de Jong, E.H.H. Oberyé and W.J. van Venrooij (1992) Molecular cloning of a major CENP-B epitope and its use for the detection of anticentromere autoantibodies, Mol. Biol. Rep., 16, 49–59.

Yager, J.W., D.A. Eastmond, M.L. Robertson, W.M. Paradisin and M.T. Smith (1990) Characterization of micronuclei induced in human lymphocytes by benzene metabolites, Cancer Res., 50, 393–399.

Pergamon

Pharmacology Biochemistry and Behavior, Vol. 50, No. 4, pp. 521–526, 1995

0091-3057/95 $9.50 + .00

0091-3057(94)00331-9

Behavioral Effects of Vehicles: DMSO, Ethanol, Tween-20, Tween-80, and Emulphor-620

CARL ANDREW CASTRO, JOHN B. HOGAN, KIMBERLY A. BENSON, CHRISTINA W. SHEHATA AND MICHAEL R. LANDAUER[1]

Behavioral Sciences Department, Armed Forces Radiobiology Research Institute, 8901 Wisconsin Avenue, Bethesda, MD 20889-5603

Received 28 March 1994

CASTRO, C. A., J. B. HOGAN, K. A. BENSON, C. W. SHEHATA AND M. R. LANDAUER. *Behavioral effects of vehicles: DMSO, ethanol, Tween-20, Tween-80, and emulphor-620.* PHARMACOL BIOCHEM BEHAV **50**(4) 521–526, 1995.—Experimental drugs and compounds that do not easily dissolve in water or saline are frequently combined with vehicles like solvents, detergents, or vegetable oils. Yet very little has been reported on the behavioral effects of vehicles. In this study, we assessed the effects of a vegetable oil (emulphor-620), two detergents (Tween-20 and Tween-80), and two solvents [dimethyl sulphoxide (DMSO) and ethanol] on the locomotor activity in CD2F1 male mice. Locomotor activity was monitored for 12 h after vehicle administration (IP). The concentrations for each vehicle were expressed as percent of vehicle in saline (v/v). Emulphor-620 did not affect locomotor activity at any concentration tested (2%, 4%, 8%, 16%, and 32%). Tween-20 significantly decreased locomotor activity at a concentration of 16% and Tween-80 at 32%. DMSO significantly decreased locomotor activity at concentrations of 32% and 64%. In contrast, ethanol produced a biphasic behavioral response: increased activity at a concentration of 16% and decreased activity at a concentration of 32%. These results will facilitate the selection and concentration of vehicles to be used in combination with experimental drugs or test agents.

Locomotor activity Vehicles DMSO Tween-20 Tween-80 Ethanol Emulphor-620

MANY experimental drugs and compounds do not dissolve readily in water or saline and, thus, are difficult to administer. For example, radioprotective eicosanoids such as 16,16 prostaglandin E_2 and misoprostol (12,13,16,17), antitumor agents such as ellipiticine and acronycine (6,28), adenosine derivatives such as N^6-cyclohexyladenosine and 5′-N-ethylcarboxamidoadenosine (8,20), and anticonvulsant drugs such as primidone and carbamazepine (19) can each be administered only in combination with a vehicle. Compounds used most often as vehicles have been solvents, detergents, or vegetable oils (4,10,21). The most commonly used solvent vehicles in both in vivo and in vitro models include dimethyl sulphoxide (DMSO) and ethanol [e.g., (2,26)]. The polyoxyethylene sorbitan monolaurate detergents Tween-20 and Tween-80 are commonly used vehicles in pharmacological and physiological studies [e.g., (5,19,25,27)]. Of the vegetable oil vehicles, the polyethoxylated castor oil emulphor-620 is used most often probably because it is the preferred vehicle for the investigation of pharmacological effects of the much studied cannabinoid compounds [see (18)].

Surprisingly, very little has been reported on how these vehicles affect behavior. This study characterized the behavioral effects of DMSO, ethanol, Tween-20, Tween-80, and emulphor-620 by measuring their effects on the locomotor activity of mice.

METHOD

Subjects

Subjects were male outbred (BALB/c × DBA/2)F1 mice (Charles River Breeding Laboratory, Raleigh, NC), also known as CD2F1 mice, weighing 24–30 g. All mice were quar-

The opinions and assertions contained in this report are the views of the authors and do not necessarily reflect those of the Department of Defense. During the conduct of this study, the investigators adhered to the Animal Welfare Act and the Guide for the Care and Use of Laboratory Animals, National Institutes of Health Publication No. 86-23.

[1] To whom requests for reprints should be addressed.

antined on arrival and representative animals were screened for evidence of disease. Mice were housed in groups of 10 in Microisolator cages (Lab Products, Maywood, NJ) on hardwood chip contact bedding in a facility approved by the American Association for Accreditation of Laboratory Animal Care. Animal rooms were maintained at 21 ± 2°C with 50 ± 10% humidity on a 12 L : 12 D cycle. Commercial rodent chow and acidified water (pH 2.5) were freely available.

Apparatus and Procedure

Computerized Digiscan activity monitors (Omnitech Electronics, Columbus, OH) were used to quantify locomotor activity. Each monitor used an array of infrared photodetectors spaced 2.5 cm apart to determine horizontal locomotor activity, which was expressed as the total distance travelled. Immediately after all injections (IP), mice were placed into individual Plexiglas activity chambers (20 × 20 × 30 cm). Activity was continuously monitored every 5 min for the first 2 h to ascertain the onset of effects; thereafter, activity was continuously recorded at 1-h intervals for the next 10 h. All testing took place during the dark portion of the light : dark cycle. Each animal was tested only once. Food and water were available throughout the testing period.

Vehicle Compounds

Saline (0.9% sodium chloride) was obtained from Abbott Laboratories (North Chicago, IL); emulphor-620 (Alkamuls) from Rhone-Poulenc (West Point, GA); ethanol (100%) from Pharmco Products Inc. (Weston, NJ), DMSO; and Tween-20 and Tween-80 from Sigma Chemical Company (St. Louis, MO). Because vehicle concentrations are typically administered as a percent of the diluent, the vehicles used in this study are expressed as percent of vehicle in saline (v/v). We used a 25 gauge needle for each IP injection in a volume of 10 ml/kg.

Data Analysis

Locomotor activity was analyzed using a repeated measures analysis of variance (23). Vehicle compound was the between-subjects effect, and time was the within-subject effect. Separate analyses were made for the minute and hour data and all p-values used were Greenhouse-Geisser corrected (23). When a significant interaction of the main effect and time was present, a Student-Newman-Keuls test (23) was used to assess differences in treatments at each time point. A log transform was used in the analysis to help stabilize variances.

The behavioral median effective dose (ED_{50}) of each vehicle was estimated using weighted least square fits of functional forms of the locomotor activity vs. percent vehicle concentration. The standard error of each ED_{50} was estimated using error propagation, and these errors were then used to compute 95% confidence intervals. The ED_{50} was defined as the percent concentration of the vehicle in saline (v/v) that reduced locomotor activity to 50% of saline control value. ED_{50} values were calculated at 1 and 2 h after vehicle administration.

RESULTS

Behavioral ED_{50}s

The behavioral ED_{50}s, expressed as a percentage of vehicle in saline, and the confidence intervals of each vehicle at 1 and 2 h after injection are presented in Table 1. Precise ED_{50}s could not be determined for emulphor-620 at either 1 or 2 h after injection because at the highest concentration tested (32%) it did not reduce locomotor activity by at least 50%. For the same reason, an exact ED_{50} could not be determined for Tween-80 at 1 h after injection. Higher concentrations of these two vehicles were not evaluated because their viscous properties prevented IP administration with a 25 gauge needle.

Saline

The locomotor activity of mice administered saline is compared with that of noninjected mice in Figs. 1A and 2A. The total distance travelled by each of these groups of mice was not significantly different, (all p-values > 0.61), indicating that the injection procedures had no effect on locomotor activity. However, both the minute and hour data indicated that activity in both groups decreased over time, all F-values > 22.14, all p-values < 0.0001.

Vegetable Oil (Emulphor-620)

Emulphor-620 did not alter the distance travelled by the mice at any concentration tested. For both the minute and hour data (Figs. 1B and 2B), neither the main effect of emulphor-620 nor the emulphor-620 × time interactions were significant, all p-values > 0.18. The main effect of time, how-

TABLE 1

EFFECTIVE DOSES (ED_{50}) AND CONFIDENCE INTERVALS (CI) FOR LOCOMOTOR BEHAVIOR IN MICE EXPRESSED AS PERCENTAGE OF VEHICLE IN SALINE

		Behavioral ED_{50}s and CIs*	
Vehicle	Chemical Name	% at 1 h	% at 2 h
Emulphor	Polyethoxylated castor oil	> 32.0	> 32.0
Tween-20	Polyoxyethylene sorbitan monolaurate	9.6 (8.4–11.0)	14.4 (11.1–18.7)
Tween-80	Polyoxyethylene sorbitan monooleate	> 32.0	30.1 (28.9–31.3)
DMSO	Dimethyl sulfoxide or sulfinylbis [methane]	27.0 (24.4–29.9)	32.3 (30.3–34.4)
Ethanol	Ethyl alcohol	27.7 (26.6–28.3)	31.25 (30.2–32.3)

*ED_{50}s and CIs were calculated at 1 and 2 h after IP administration.

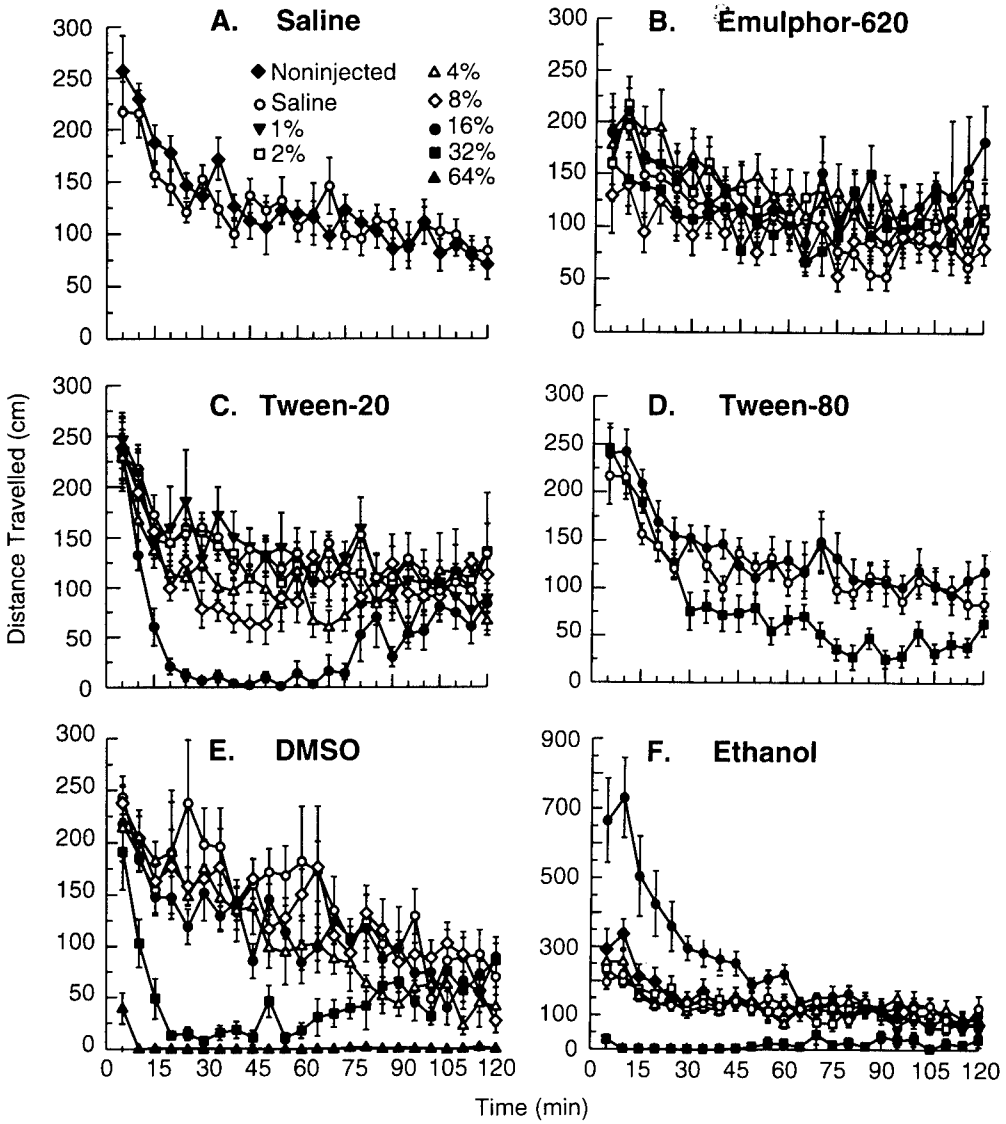

FIG. 1. Onset of locomotor behavior expressed as distance travelled (mean ± SEM) 5–120 min after administration (IP) of six commonly used drug vehicles. All vehicle compounds were administered as percent of vehicle in saline (v/v). n = 8–12 mice per group.

ever, was significant, all F- values > 26.24, all p-values < 0.0001, indicating again that the activity of the mice in both groups decreased during the testing period.

Detergents (Tween-20 and Tween-80)

Only the highest Tween-20 concentration tested (16%) significantly decreased the distance travelled by the mice. As illustrated in Figs. 1C and 2C the Tween-20 × time interactions were significant for both the minute and hour data, all F-values > 1.36, all p-values < 0.05. Post hoc analyses of these interactions indicated that, compared with all other groups tested, the 16% concentration of Tween-20 significantly decreased the distance travelled at 15 to 75 min after administration and, to a lesser extent, decreased the distance travelled for the first 2 h after administration (p-values < 0.05).

Only the 32% concentration of Tween-80 decreased the distance travelled by the mice. As shown in Figs. 1D and 2D, the Tween-80 × time interactions were significant for both the minute and hour data, all F-values > 1.81, all p-values < 0.005. Post hoc analyses revealed that the distance travelled by mice receiving a 32% concentration was significantly decreased at 30 min, 35 min, 50–115 min and 2 h following administration compared with that by mice receiving either a 16% concentration of Tween-80 or saline (p-values < 0.05).

Solvents (DMSO and Ethanol)

The 32% and 64% concentration of DMSO significantly decreased the distance travelled following administration (Figs. 1E and 2E). For both the minute and the hour data, the main of effects of DMSO and time and as well as the DMSO × time interactions were significant, all F-values > 3.27, all p-values < 0.0001. Analyses of the minute data revealed that the distance travelled by the mice receiving a 32% concentra-

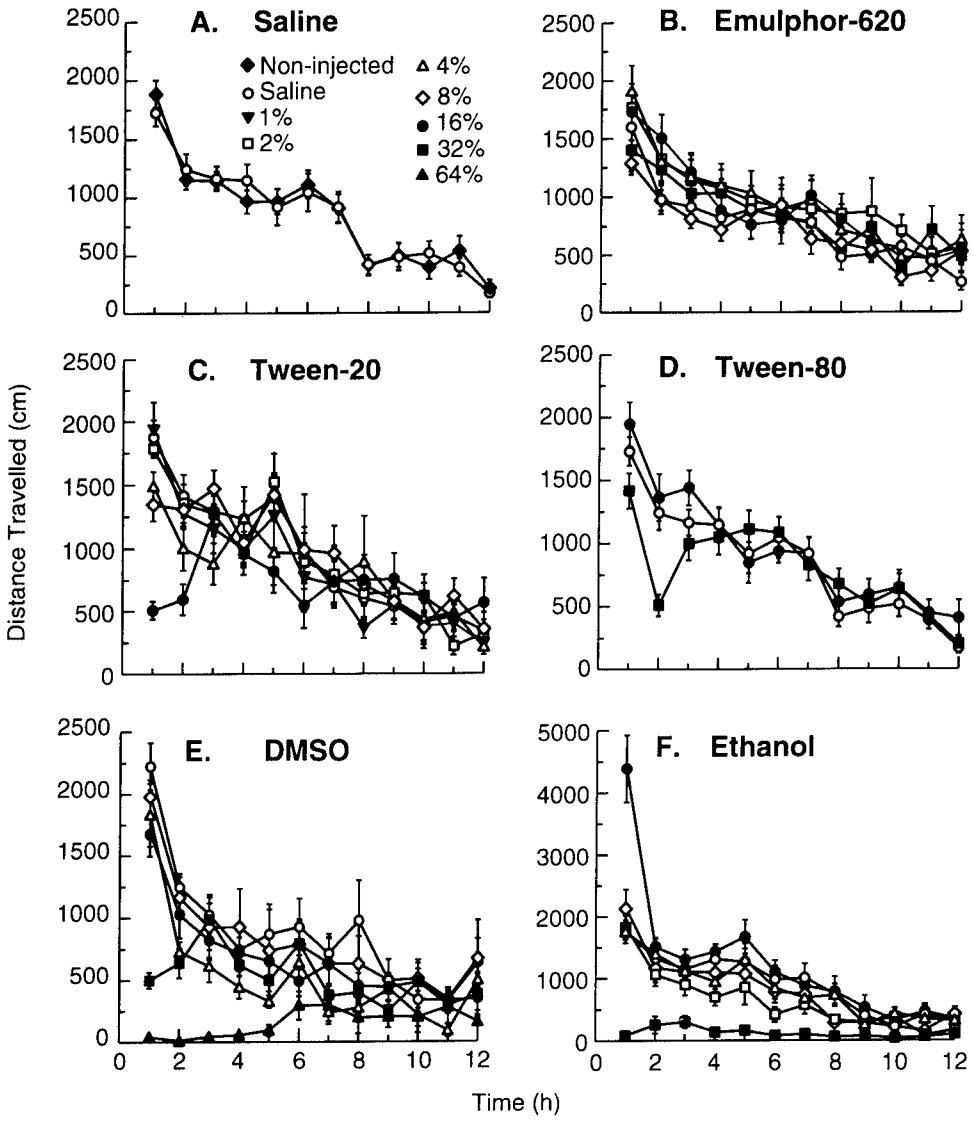

FIG. 2. Duration of locomotor behavior expressed as distance travelled (mean ± SEM) 1-12 h after administration (IP) of six commonly used drug vehicles. All vehicle compounds were administered as percent of vehicle in saline (v/v). n = 8-12 mice per group.

tion was significantly decreased at 10-75 min after administration (p-values < 0.05) and that the distance travelled by the mice receiving a 64% concentration significantly decreased at 5-120 min following administration (p-values < 0.05). Analyses of the hour data indicated that the distance travelled by the mice receiving a 32% concentration was decreased at 1 h and that the distance travelled by the mice receiving a 64% concentration was decreased at 1-6 h (p-values < 0.01).

The effects of ethanol on the distance travelled by the mice were biphasic (Figs. 1F and 2F). The activity increased after administration of a 16% concentration and decreased after administration of a 32% concentration. Consistent with this description of the data, the main effects of ethanol and time as well as the ethanol × time interactions were significant, all F-values > 1.70, all p-values < 0.002. Post hoc analyses of the ethanol × time interactions for the minute data revealed that the mice receiving a 16% concentration travelled a greater distance than all other groups at 5-45 min after administration (p-values < 0.05). Analyses also revealed that the mice receiving a 32% concentration travelled a lesser distance than all other groups at 5-120 min after administration (p-values < 0.05). Post hoc analyses of the ethanol × time interactions for the hour data indicated that the mice receiving a 16% concentration travelled a greater distance than all other groups only at 1 h after administration (p-values < 0.01) and that the mice receiving a 32% concentration travelled a lesser distance than all other groups at 1-8 h after administration (p-values < 0.01).

DISCUSSION

Three major classes of compounds used as vehicles for drugs are vegetable oils, detergents, and solvents. This study assessed the effects of representative compounds from each of these classes on the locomotor activity in mice. Our results demonstrate that the vegetable oil emulphor-620 did not affect

the locomotor activity at any concentration tested (2–32%), that the detergents Tween-20 and Tween-80 depressed locomotor activity at respective concentrations of 16% and 32%, that the solvent DMSO decreased locomotor activity at concentrations of 32% and 64%, and that the solvent ethanol had a biphasic effect, increasing locomotor activity at a concentration of 16% and decreasing it at a concentration of 32%. Because emulphor-620 did not affect locomotor activity in our study, it may be better than the solvents or detergents tested in this study when behavioral toxicity is considered as an end point. Ashby and Mirkora (2) have recommended that vegetable oils replace DMSO as a vehicle for insoluble compounds. Kocsis et al. (15) have shown that DMSO reduces locomotor activity, and Fossom et al. (9) demonstrated that it impairs operant performance in the rat.

Vegetable oils, however, may not always be the vehicles of choice. Emulphor-620 has been reported to alter serum lipid levels, lipoprotein patterns, and tissue lipid content in dogs (11). Indeed, in many instances a detergent or solvent vehicle is preferred. For example, Tween-80 was found to be the only adequate solubilizer for use in smooth muscle preparations when compared with ten other vehicles including DMSO and ethanol (4). Moreover, Tween-80 has been used as a vehicle to evaluate the behavioral effects of experimental drugs and toxicants without apparent adverse side effects (24). Similarly, O'Hara and colleagues (21) found DMSO to be a better vehicle than ethanol or emulphor-620 for evaluating the toxicity of chlorinated hydrocarbons in the isolated hepatocyte system. Therefore, depending on whether the experimental model is in vivo or in vitro and the end point selected, a vehicle compound from any one of the three classes may be appropriate.

Frequently, however, investigators use a combination of vehicles to administer an experimental drug or test agent. Emulphor-620 and ethanol are often used in combination to administer a variety of agents including delta-9-tetrahydrocannabinol (22), fungicides (1), insecticides (3) and antibiotics (28). When these vehicles are used in combination, relatively low concentrations are given, usually consisting of 5% emulphor and 5% ethanol in 90% saline (v/v) (1,3,22,28). Although our results indicated that lower concentrations of emulphor-620 and ethanol alone did not alter locomotor activity (see Figs. 1B, 1F, 2B, 2F), a combination of emulphor-620 and ethanol may. In fact, a vehicle solution consisting of emulphor (5%) and ethanol (5%) has been shown to lower the blood pressure and increase the heart rate of dogs (11). Thus, if more than one vehicle is used to administer an experimental drug or test agent, it is important to determine the effects not only of the individual vehicles but also of the combinations.

A vehicle solution having no apparent effect when administered alone may dramatically alter the response of the drug being investigated. For example, DMSO reportedly precipitates crystallization or deposition of experimental drugs and test agents upon contact with biological fluids, thus extending its time course (2). DMSO has also been shown to lower the sensitivity of rats to the rate-decreasing effects of *d*-amphetamine on an operant behavioral task (9) and to enhance the toxicity of the antineoplastic agent bleomycin (14). Similarly, Tween-80 has been shown to lower the anticonvulsant effects of primidone and carbamazepine because it reduces drug absorption (19), and Tween-20 has been shown to decrease the bioavailabilty of a benzodiazepine receptor ligand 20-fold compared with the vehicle polyethylene glycol (PEG-400) (18). Thus, because vehicle solutions can alter the bioavailability and increase or decrease the toxicity of experimental drugs and compounds, it has been recommended that potency estimations be based not only on the doses administered but also on the brain and plasma concentrations of the experimental drug or test agent (19).

In conclusion, to minimize toxicity, it is best to dissolve experimental drugs and compounds in either saline or water. When this is not possible, it is important to ensure that the vehicle does not affect the response under investigation. Often this will require that the selected vehicle be compared with other vehicle compounds, as demonstrated in this study.

ACKNOWLEDGEMENTS

We thank William E. Jackson, III, for statistical advice and Donna K. Solyan for editorial assistance. This research was supported in part by a grant administered through the Department of Defense/ Department of Veterans Affairs Cooperative Research Program.

REFERENCES

1. Allen, A. A.; MacPhail, R. C. Bitertanol, a triazole fungicide, increases operant responding but not motor activity. Neurotoxicol. Teratol. 15:237–242; 1993.
2. Ashby, J.; Mirkova, E. Reevaluation of the need for multiple sampling times in the mouse bone marrow micronucleus assay: Results for DMBA. Environ. Mol. Mutagen. 10:297–305; 1987.
3. Bloom, A. S.; Staatz, C.; Dieringer T. Pyrethroid effects on operant responding and feeding. Neurobehav. Toxicol. Teratol. 5: 321–324; 1983.
4. Braak, K.; Frey, H.-H. Effects of solvents and detergents on the contractions of isolated smooth muscle preparations. J. Pharm. Pharmacol. 42:837–841; 1990.
5. Castro, V. L.; Bernardi, M. M.; Palermo-Neto, J. Evaluation of prenatal aldrin intoxication in rats. Arch. Toxicol. 66:149–152; 1992.
6. Chien, M. M.; Rosazza, J. P. Microbial transformations of natural antitumor agents: Use of solubilizing agents to improve yields of hydroxylated ellipticines. Appl. Environ. Microbiol. 40:741–745; 1980.
7. Constantine, J. W.; Lebe, W. S. Histamine release in dogs by emulphor EL-620. Experientia 35:338–339; 1978.
8. Durcan, M. J.; Morgan, P. F. Evidence for adenosine A_2 receptor involvement in the hypomobility effects of adenosine analogues in mice. Eur. J. Pharmacol. 168:285–290; 1989.
9. Fossom, L. H.; Messing, R. B.; Sparber, S. B. Long lasting behavioral effects of dimethyl sulfoxide and the "peripheral" toxicant *p*-bromophenylacetylurea. Neurotoxicology 6:17–28; 1985.
10. Gad, S. C.; Chengelis, C. P. Acute toxicology testing perspectives and horizons. Caldwell, NJ: Telford Press; 1988.
11. Hacker, M.; Koeferl, M.; Hong, C. B.; Fagan, M. A. Cremohor and emulphor induced alterations of serum lipids and lipoprotein electrophoretic patterns of dogs. Res. Commun. Chem. Pathol. Pharmacol. 31:119–128; 1981.
12. Hanson, W. R.; Ainsworth, E. J. 16,16-Dimethyl prostaglandin E_2 induces radioprotection in murine intestinal and hematopoietic stem cells. Radiat. Res. 103:196–203; 1985.
13. Hanson, W. R.; Gardina, D. J. Misoprostol, a PGE_1 analog protects mice from fission-neutron injury. Radiat. Res. 128:S12–S17; 1991.
14. Hascher, W. M.; Baer, K. E.; Rutherford, J. E. Effects of dimethyl sulfoxide (DMSO) on pulmonary fibrosis in rats and mice. Toxicology 54:197–205; 1989.
15. Kocsis, J. J.; Harkaway, S.; Snyder, R. Biological effects of the metabolites of dimethylsulfoxide. Ann. NY Acad. Sci. 243:104–109; 1975.
16. Landauer, M. R.; Davis, H. D.; Kumar, K. S.; Weiss, J. F. Behavioral toxicity of selected radioprotectors. Adv. Space Res. 12(2):273–283; 1992.

17. Landauer, M. R.; Walden, T. L.; Davis, H. D. Behavioral effects of radioprotective agents in mice: Combination of WR-2721 and 16,16 dimethyl prostaglandin E_2. In: Riklis, E., ed. Frontiers in radiation biology. New York: VCH Publishers; 1990:199–207.
18. Lister, R. G.; LeDuc, B. W.; Greenblatt, D. J.; File, S. E. Poor bioavailability of CGS 8216 in a water/tween vehicle following intraperitoneal injection. Psychopharmacology (Berlin) 91:260–261; 1987.
19. Loscher, W.; Nolting, B.; Fassbender, C. P. The role of technical, biological and pharmacological factors in the laboratory evaluation of anticonvulsant drug. I. The influence of administration vehicles. Epilepsy Res. 7:173–181; 1990.
20. Nikodijevic, O.; Sarges, R.; Daly, J. W.; Jacobson, K. A. Behavioral effects of A_1- and A_2-selective adenosine agonists and antagonists: Evidence for synergism and antagonism. J. Pharmacol. Exp. Ther. 259:286–294; 1991.
21. O'Hara, T. M.; Borzelleca, J. F.; Clarke, E. C.; Sheppard, M. A.; Condie, L. W. A $CCl_4/CHCl_3$ interaction study in isolated hepatocytes: Selection of a vehicle. Fundam. Appl. Toxicol. 13: 605–615; 1989.
22. Perlin, E.; Smith, C. G.; Nichols, A. I.; Almirez, R.; Flora, K. P.; Cradock, J. C.; Peck, C. C. Disposition and bioavailability of various formulations of tetrahydrocannabinol in the Rhesus monkey. J. Pharm. Sci. 74:171–174; 1985.
23. SAS/STAT users guide, vol. 2, GLM. version 6.03. Cary, NC: SAS Institute; 1988.
24. Tilson, H. A.; Hong, J. S.; Sobotka, T. J. High doses of aspartame have no effects on sensorimotor function or learning and memory in rats. Neurotoxicol. Teratol. 13:27–35; 1991.
25. Venkatesh, K.; Levi, P. E.; Hodgson, E. The effect of detergents on the purified flavin-containing monooxygenase of mouse liver, kidney and lungs. Gen. Pharmacol. 22:549–552; 1991.
26. Waddell, W. J.; Marlowe, C.; Yamamoto, T.; Clark, M. J. Inhibition of the metabolism of urethane in the mouse by dimethyl sulfoxide (DMSO). Drug Metab. Dispos. 17:469–472; 1989.
27. Whalley, H. E.; Bootman, J.; Rees, R. 4CMB: Investigation of activity in a mouse micronucleus test. Mutat. Res. 100:361–364; 1982.
28. Zirvi, K. A.; Gilani, S. H.; Hill, G. J. Embryotoxic effects of doxorubicin and N-trifluoracetyladriamycin-14-valerate (AD-32). Teratology 31:247–252; 1985.

Digestive Diseases and Sciences, Vol. 40, No. 1 (January 1995), pp. 211–218

Effect of Radiation and Radioprotection on Small Intestinal Function in Canines

JORGE L. HERRERA, MD, ROY M. VIGNEULLE, PhD, THOMAS GAGE, MD, THOMAS J. MacVITTIE, PhD, JAMES B. NOLD, DVM, PhD, and ANDRE DUBOIS, MD, PhD

Radiation with doses >7.5 Gy damages the canine intestinal mucosa, and pretreatment with WR2721 reduces this damage. However, the effects of radiation and of WR2721 on *in vivo* intestinal transport are unclear. Therefore, we determined canine survival, intestinal transport, and mucosal histology following unilateral abdominal irradiation. Isoperistaltic ileostomies were prepared in 23 dogs under general anesthesia and aseptic conditions. After a three-week recovery period, animals were given either placebo or WR2721, 150 mg/kg intravenously, 30 min prior to 10 Gy cobalt-60 abdominal irradiation. Ileal transport and histology were determined in both groups before exposure and one, four, and seven days after irradiation. Seven-day survival was significantly improved by pretreatment with WR2721 (91% vs 33%, $P < 0.02$). On day 4, both mucosal integrity and net intestinal absorption were significantly better ($P < 0.05$) after WR2721 than after placebo. Thus, radiation-induced damage to the ileal mucosa is accompanied by a reduction in net ileal absorption of water and electrolytes *in vivo*. In addition, pretreatment with WR2721 improves animal survival while reducing ileal damage and improving intestinal absorption.

KEY WORDS: radiation; intestinal absorption; small intestine; radioprotection.

Therapeutic and accidental irradiation of the abdomen may profoundly alter both the structure and function of the small intestine, probably because the high rate of cell turnover makes this organ especially sensitive to the effects of ionizing radiation (1, 2). Manifestations of dose-dependent intestinal radiation injury may range from minimal histologic changes associated with few symptoms at lower doses to severe villous damage with associated intestinal fluid and electrolyte loss, leading to death at higher doses. This array of symptoms occurs three to seven days after exposure and has been named intestinal radiation syndrome (3–5).

While the effects of radiation on the morphology of the small intestine are well known (2, 4), the pathogenesis of the intestinal radiation syndrome remains controversial. The formation of free radicals during exposure to radiation is considered to be important in producing intestinal damage (6). Thus, attention has been focused on the use of endogenous and exogenous thiol compounds, which act as free-radical scavengers, in preventing radiation-

Manuscript received November 12, 1993; revised manuscript received April 29, 1994; accepted August 1, 1994.

From the Armed Forces Radiobiology Research Institute, Bethesda, Maryland 20889-5145; Walter Reed Army Institute of Research, Washington DC, 20307-5001; and the Uniformed Services University of the Health Sciences, Bethesda, Maryland, 20814-4799.

Dr. Herrera's present address: Division of Gastroenterology, University of South Alabama College of Medicine, Mastin Building Suite 4G, 2451 Fillingim Street, Mobile, Alabama 36617.

Dr. Nold's present address: Hazleton Wisconsin Inc., Pathology Department, 3301 Kinsman Boulevard, Madison, Wisconsin 53704.

Supported by the Armed Forces Radiobiology Research Institute, Defense Nuclear Agency, under work units B3161 and 00082. Views presented in this paper are those of the authors; no endorsement by the Defense Nuclear Agency or the Uniformed Services University of the Health Sciences has been given or should be inferred. Research was conducted according to the principles enunciated in the "Guide of the Care and Use of Laboratory Animals" prepared by the Institute of Laboratory Animal Resources, National Research Council.

Address for reprint requests: Dr. Andre Dubois, Department of Medicine, Uniformed Services University, 4301 Jones Bridge Road, Bethesda, Maryland 20814-4799.

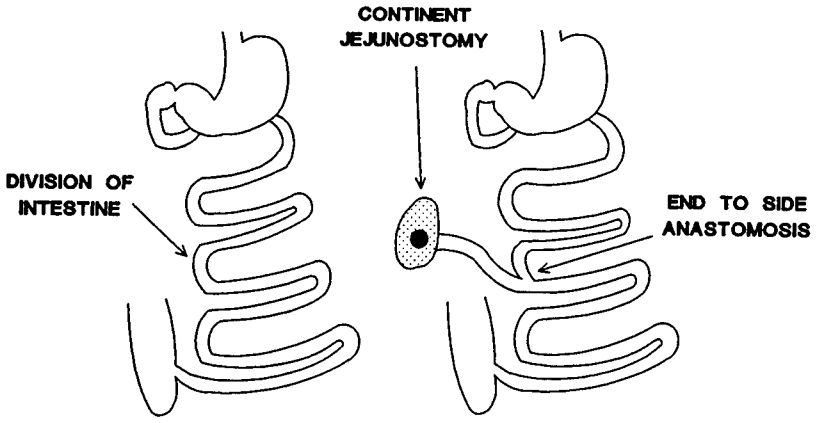

Fig 1. Schematic illustration of the surgical preparation. On the left, presurgery; on the right, postsurgical montage.

induced intestinal damage. *S*-2-(3-Aminopropylamino)ethylphosphorothioic acid (WR2721; Ethiofos, U.S. Biosciences, Blue Bell, Pennsylvania) (7, 8), is a thiol compound that has been shown to improve cell survival of normal tissues after irradiation (9–11).

Most studies of radiation injury and radioprotectants have either documented the histologic changes caused by acute radiation exposure (6, 12) or have assessed *in vitro* functional changes induced by radiation (13, 14). However, no data are available regarding the *in vivo* effects of radioprotectants in preventing or inhibiting the physiologic changes induced by radiation. Therefore, we used a previously developed large-animal model (15) to study the function and morphology of the small bowel during the acute period that follows irradiation and to assess the efficacy of WR2721 in preventing these changes.

MATERIALS AND METHODS

Animals. Twenty-three male purpose-bred beagles (age: 1–3 years, weight: 12–15 kg) were studied. Dogs were quarantined on arrival and screened for evidence of disease. They were maintained in an AAALAC-accredited facility in runs and were provided commercial dog chow and tap water *ad libitum*. Animal holding rooms were maintained at 21 ± 2° C with 50 ± 10% relative humidity using at least 10 changes per hour of 100% conditioned fresh air. They were on a 12 hr light–dark full spectrum lighting cycle with no twilight.

Animal Preparation. The surgical preparation used in the present study has been previously described (15), and it is illustrated in Figure 1. In brief, a midline laparotomy was performed under general anesthesia and aseptic conditions, and a loop of intestine was selected and transected at the midpoint between the duodenum and the cecum (transition jejunum–ileum). The distal end of the loop was brought out through the abdominal wall and sutured to the parietal peritoneum, muscles, and skin, creating a continent ileostomy. The proximal end of the loop was anastomosed end-to-side to the intestine 30 cm distal to the ileostomy, such that the afferent limb situated out of the nutrient stream was 30 cm. As described below, intestinal perfusion fluids were introduced into a segment situated 30 cm beyond the end-to-side anastomosis, ie, 60–80 cm from the ileostomy and in an area of intestine that was permanently maintained in the nutrient stream. Dogs were given 500 mg of ampicillin prophylaxis daily during two days prior to and for eight days after surgery.

Intestinal Transport Studies. After a three-week recovery period, the 14 unanesthetized dogs were habituated to stand quietly in a Pavlov stand composed of four poles and a sling with four holes for the legs of the animal. Intestinal transport was then measured using a triple-lumen intestinal perfusion tube as previously described (16, 17). In brief, the tube was composed of three perfusion lumens: one for infusion of the marker, and two for aspiration of the mixed intestinal contents. The proximal aspiration port was 10 cm distal to the infusion port, thus allowing a 10 cm mixing segment. The distal aspiration port was 20 cm distal to the proximal aspiration port, thus allowing a 20-cm test segment. A fourth lumen allowed the inflation and deflation of a balloon placed at the tip of the tube to facilitate tube placement (ie, 5 cm from the distal aspiration port). The perfusion tube was inserted into the ileostomy, the balloon was inflated with 3–5 ml of air, and the peristaltic activity of the intestine permitted gently advancing of the balloon to 85 cm from the skin. As a result, the intestinal study segment was in the distal ileum and 60–80 cm from the ileostomy. The intestine was perfused with a solution containing electrolytes (Na^+: 130 meq/liter, K^+: 5.0 meq/liter, Cl^-: 105 meq/liter, HCO_3^-: 30 meq/liter), xylose (3 g/liter), and polyethylene glycol (PEG-3700: 5 g/liter and [^{14}C]PEG-4000: 0.3 μCi/liter) as nonabsorbable markers.

After an equilibration period of 40 min, three 20-min collections were obtained. Collections were made by manual syringe aspiration at a rate of 1 ml/min from both proximal and distal aspiration ports. A 5-min stagger

period was allowed between proximal and distal aspiration ports, based on previously determined transit time measurements. Dogs were studied prior to irradiation (baseline) and at days 1, 4, and 7 after exposure. Net water, Na^+, K^+, and Cl^- fluxes were determined. Measurements of ^{14}C radioactivity corresponding to PEG concentrations were performed using liquid scintillation counting (Beckman Instruments, Boca, California). Na^+, K^+, and Cl^- concentrations were determined using a Beckman E4A Electrolyte Analyzer.

Endoscopic Studies. Immediately following intestinal transport studies, the animals were sedated with 2.2 mg Rompun intramuscularly (Mobay Corp., Shawnee, Kansas), and inhalation general anesthesia was administered by intubation using of 4% isoflurane in a 67% N_2O–33% O_2 gas mixture, followed by maintenance with 1% isoflurane in the same gas mixture. The animals were then endoscoped using an Olympus GIF-P3 fiberoptic endoscope (Olympus Corp, Lake Success, New York) introduced through the ileostomy. Mucosal biopsies were obtained with a fenestrated pinch biopsy forceps (FB-21 Olympus Corp) capable of obtaining a biopsy reaching into the muscularis mucosa. Biopsies were taken at levels corresponding to the sites of ileal dosimetry.

Histopathology of Mucosal Biopsies. Intestinal mucosal biopsies were oriented on filter paper and immersion-fixed in 10% neutral-buffered formalin. This method permitted the entire processing of the preparation, including sectioning, without removing the tissue from its support. Following routine embedding in paraffin, sectioning at 4 μm, and staining with hematoxylin and eosin (H&E), the biopsies were coded from a table of random numbers and examined by a pathologist unaware of the treatment groups from which biopsies originated. The biopsies were evaluated microscopically and graded according to the severity of the radiation damage using the following grading score: zero, no damage; 1, preservation of villus height but epithelial cell necrosis and minor or early degeneration of crypt epithelium, edema, and hemorrhage of some of the lamina propria; 2, blunting of a few villi with the presence of atypical epithelial cells and some collapsed crypts, increased necrosis, variable enterocyte loss, and crypt cell hyperplasia; 3, blunting and denudation of most villi, edema, and ulceration of most of the epithelial surface and many collapsed crypts (Figure 2).

Treatment, Irradiation, and Dosimetry. Thirty minutes before irradiation, WR2721 (150 mg/kg; 11 dogs) or placebo (12 dogs) was given in a blinded fashion as a slow 10-min intravenous infusion. The animals were exposed to a total dose of 10 Gy of cobalt-60 gamma rays delivered to the right lateral abdomen. The area of radiation was defined by a 24 × 40-cm opening in a 5-cm lead brick wall placed between the animal and the radiation source. The exposure rate was 3.7 Gy/min, and the ^{60}Co source-to-midline distance was 118 cm. The vertebral column, the chest, and the four limbs were shielded, and exposure of the bone marrow was reduced to less than 7% of the total dose. Intraileal dosimetry was performed as previously described (18) by catheterizing the ileostomy with a 100-cm plastic tube containing 40 groups of three lithium fluoride thermoluminescent dosimeters (TLDs) in gelatin capsules spaced at 2.5-cm intervals, and separated by nylon balls and lead beads. The TLDs were used to determine the radiation dose received by the ileal mucosa at sites located 2.5 cm, 5.0 cm, 7.5 cm, etc..., from the ileostomy. The lead beads and steel ball markers were included to determine the intraabdominal position of the intraileal tube on orthogonal x-rays taken immediately before irradiation (18). The dose received by the absorption study segment located 60–80 cm from the ileostomy was calculated as the mean value of the doses measured in this segment determined by a trapezoidal area-under-the curve technique.

Studies and Animal Care After Irradiation. After irradiation, the animals were housed in individual cages, and they were treated prophylactically with daily administration of 500 ml Ringer's lactate solution subcutaneously and 40 mg/kg gentamicin sulfate intramuscularly for 14 days. The animals were evaluated daily for appetite, hydration, health status, and diarrhea. Absorption studies and endoscopic biopsies were repeated after radiation exposure at days 1 (placebo: six dogs; WR2721: five dogs), 4 (placebo: six dogs; WR2721: eight dogs), and 7 (placebo: three dogs; WR2721: five dogs). However, biopsies could be processed in only one animal treated with WR2721 at day 7 because of technical reasons. If the animal's health deteriorated beyond a level which could be maintained using basic therapy, the animal was euthanized with T-61 Euthanasia Solution (Taylor Pharmacal Co., Decatur, Illinois; 60 mg/kg, intravenously).

Data Analysis. Survival in placebo and WR2721 groups at day 7 was compared using contingency table analysis. Changes in net intestinal water and electrolyte transport were compared using Kruskal-Wallis test (19). *Post hoc* tests of differences between placebo and WR2721 groups at days 1, 4, and 7 were made using the Mann-Whitney test (19).

RESULTS

After the ileal mucosa had been exposed to 8.0–9.5 Gy as determined by dosimetry, seven-day survival was 33% (4/12 animals) in placebo-treated animals, and 91% (10/11) in dogs receiving WR2721 prior to exposure ($P < 0.016$). For subsequent analysis, the animals in the placebo group were classified as nonsurvivors (ie, those euthanized before day 7) and survivors (ie, those living beyond day 8). The difference in survival rate was not related to differences in the radiation doses, since TLDs placed in the lumen of the distal ileum at the time of exposure recorded similar doses in the two groups (placebo: 9.25 ± 0.39 Gy; WR2721: 9.88 ± 0.42 Gy; NS). The mean dose received in the segment used for the measurement of absorption (60–80 cm from the ileostomy) was also similar in the two groups (placebo: 8.24 ± 0.38 Gy; WR2721: 8.67 ± 0.35 Gy; NS).

The extent of lesions observed in ileal biopsies varied according to treatment group, dose, and time

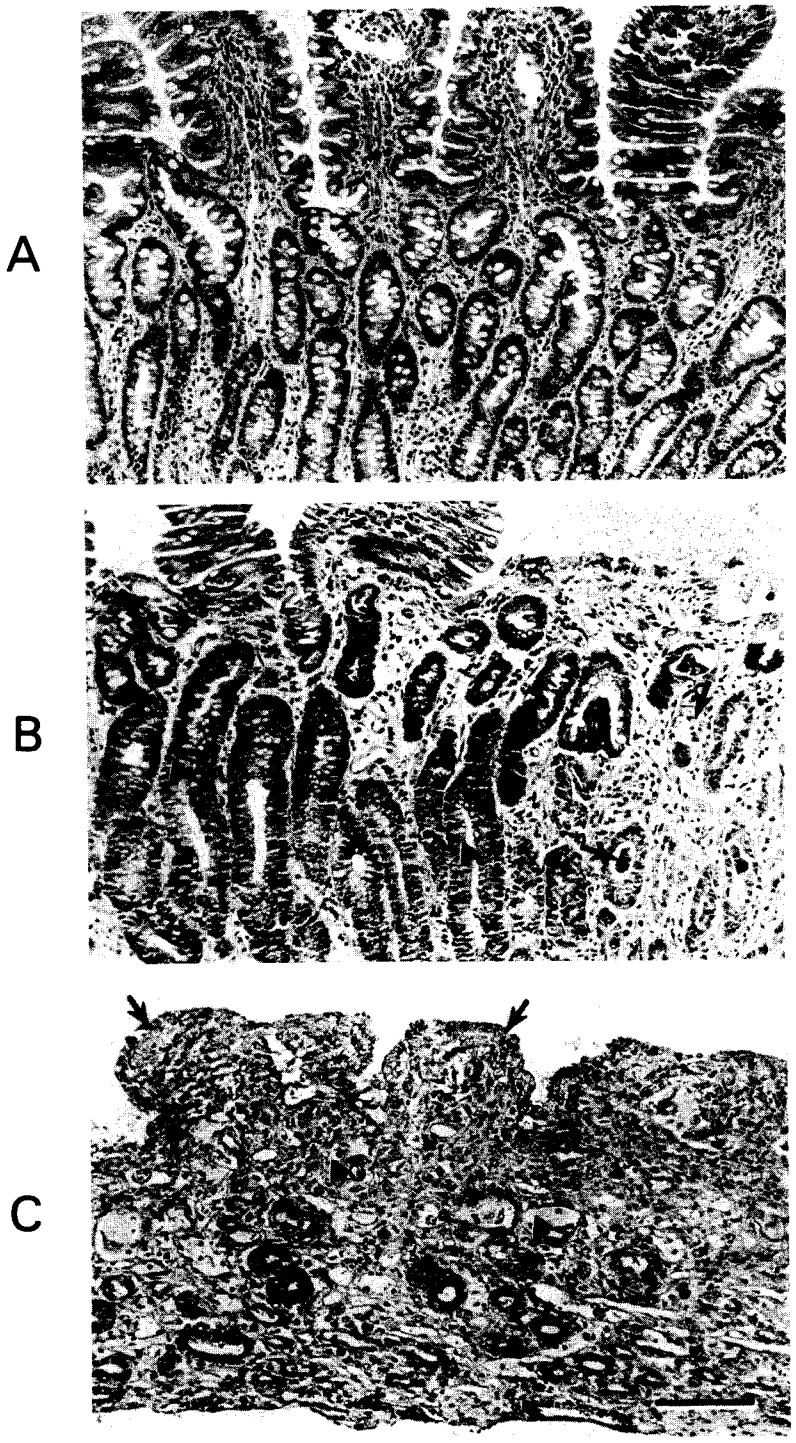

Fig 2. Intestinal biopsies (H&E, calibration bar is 50 μm). (A) Control normal mucosa (grade 0) with elongated villi and deep crypts lined by cuboidal to tall columnar epithelium; (B) biopsy obtained four days after 10 Gy irradiation plus WR2721 treatment showing moderate damage (grade 2) characterized by segmental crypt cell necrosis (arrows) and adjacent hyperplastic crypts (arrowheads); (C) specimen from four days after 9.4 Gy irradiation, no radioprotectant. Severe mucosal damage (grade 3) is present. The villi are severely blunted (arrows). Many crypts are collapsed while others are hypocellular and lined by hypertrophied epithelial cells (arrowheads).

TABLE 1. AVERAGE LOCAL DOSE AND HISTOPATHOLOGY GRADING SCORES* OF BIOPSIES FROM ILEUM OF IRRADIATED DOGS

	Day 1			Day 4		
Group	N	*Dose (Gy)*	*Score*	N	*Dose (Gy)*	*Score*
Placebo						
All	3	9.54 ± 0.83	1.0 ± 0.0	6	9.64 ± 0.24	2.5 ± 0.3†
Nonsurvivors	3	9.54 ± 0.83	1.0 ± 0.0	3	9.75 ± 0.41	3.0 ± 0.0†
Survivors	3	8.26 ± 1.53	1.0 ± 0.6	3	9.77 ± 0.48	2.0 ± 0.6
WR2721 survivors	5	8.22 ± 0.83	1.6 ± 0.5	8	9.31 ± 0.58	2.0 ± 0.4‡

*Score: 0 = normal, 1 = mild damage, 2 = moderate damage, 3 = severe damage. Values are mean ± SEM.
†$P < 0.05$ vs day 1 in corresponding treatment group.
‡$P < 0.05$ vs placebo nonsurvivors.

after irradiation (Figure 2). Histologic changes increased significantly at four days after irradiation compared to day 1 in the placebo group ($P < 0.05$), but not in the WR2721-treated group (Table 1). As a result, the score was significantly lower in the WR2721 group (in which 10/11 dogs survived) than in the placebo nonsurvivor group.

A trend towards a suppression of net water and ion transport occurred in the placebo group after irradiation (Figures 3–6), but the difference compared to baseline did not reach a level of statistical significance, probably due to the small number of animals in some of the groups. Nonetheless, the change in net intestinal transport of water on day 4 postirradiation was significantly less ($P < 0.05$) in the WR2721-treated group than in placebo-treated surviving and nonsurviving animals (Figure 3). At the same time, the change in Na^+ and Cl^- transport was significantly less ($P < 0.05$) in WR2721-treated animals than in nonsurviving placebo-treated animals, but the difference was not significant when compared to placebo-treated survivors (Figures 4 and 6). In contrast, the change in K^+ transport was significantly greater ($P < 0.05$) compared to placebo-treated survivors, but the difference compared to nonsurvivors did not reach statistical significance (Figure 5). These differences were transient, and intestinal transport of surviving animals in both treatment groups was not significantly different at day 7 (Figures 3–6).

DISCUSSION

In the present studies, we used a model previously developed to evaluate the time course of the effect of radiation on the small intestine in dogs while not modifying survival of the animals (15). In this model, sacrifice of the animals to obtain intestinal tissues is not required because surgical preparation of continent ileostomies allowed repeated ileoscopies and mucosal biopsies over time in the same dogs. The addition of a triple-lumen perfusion catheter technique to the model permitted measure-

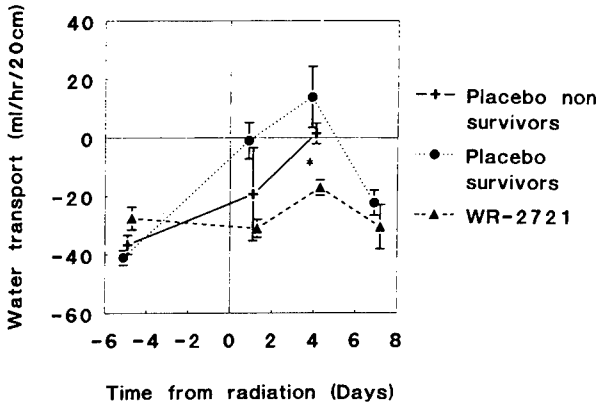

Fig 3. Time course of water transport in the canine ileum after unilateral abdominal exposure to 10 Gy cobalt-60. Negative values represent absorption, and positive values represent secretion. *$P < 0.05$ WR2721 versus placebo nonsurvivors and placebo survivors.

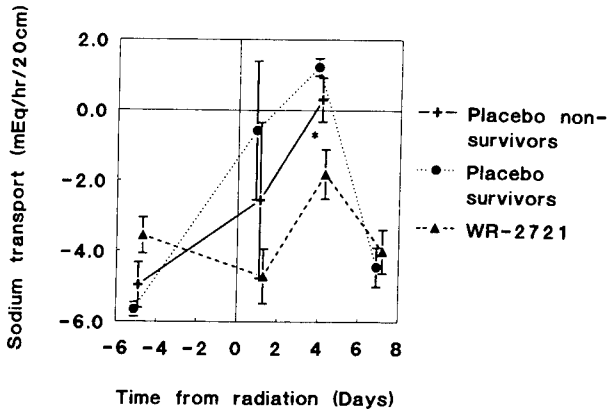

Fig 4. Time course of Na^+ transport in the canine ileum after unilateral abdominal exposure to 10 Gy cobalt-60. Negative values represent absorption, and positive values represent secretion. *$P < 0.05$ WR2721 versus placebo nonsurvivors.

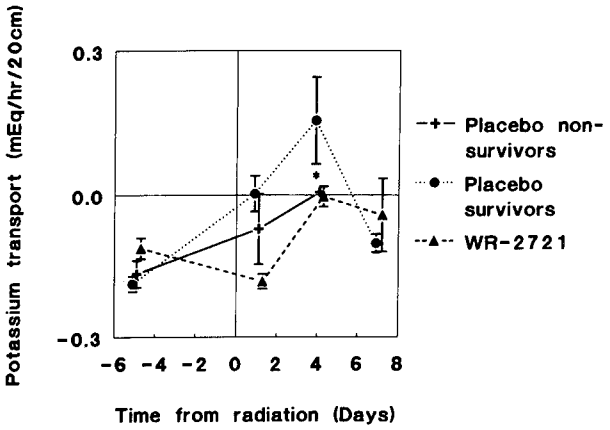

Fig 5. Time course of K^+ transport in the canine ileum after unilateral abdominal exposure to 10 Gy cobalt-60. Negative values represent absorption, and positive values represent secretion. *$P < 0.05$ WR2721 versus placebo survivors.

ment of intestinal transport, thus allowing repeated and concurrent determination of structural and functional changes of the canine ileum following irradiation.

After unilateral abdominal gamma irradiation with doses that resulted in ileal exposure to 8–9.5 Gy at 3.7 Gy/min, we observed that the seven-day survival rate was 33% in placebo-treated animals and that damage to the ileal mucosa and concurrent inhibition of net intestinal absorption was present within one to four days. We were unable to demonstrate a significant correlation between these alterations and survival in placebo-treated animals, although intestinal transport parameters returned to baseline by day 7 in surviving animals. Similar damage to the intestinal mucosa was observed four days

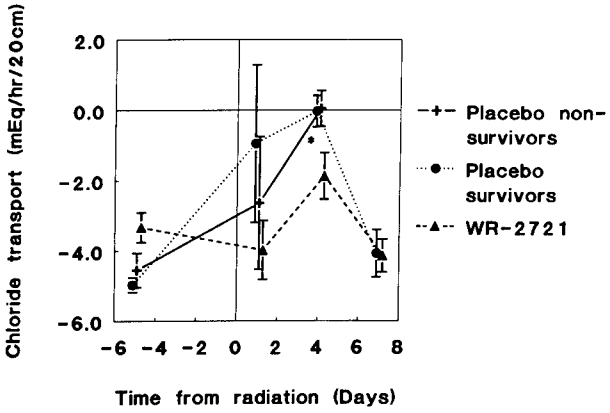

Fig 6. Time course of Cl^+ transport in the canine ileum after unilateral abdominal exposure to 10 Gy cobalt-60. Negative values represent absorption, and positive values represent secretion. *$P < 0.05$ WR2721 versus placebo nonsurvivors.

after 250 kVp x-irradiation of the abdomen with 9.38 Gy at 0.6 Gy/min, and these changes were accompanied by marked alterations of intestinal motility (20). Ten days after exposure, mucosal damage and abnormal motility had completely subsided, but a second exposure to the same dose of radiation caused chronic diarrhea, profound weight loss, and progressive changes in intestinal myoelectric activity (21). Similarly, symptoms of bloody diarrhea and changes in motility were observed after fractionated doses of 2.5 Gy of 250 kVp x-irradiation at 0.87 Gy/min given three times a week for three weeks (total dose 22.5 Gy) (22, 23). In these four studies, intestinal absorption was not measured, and no death occurred, which may have resulted from differences in dose rate and/or use of lower energy radiation. Thus, radiation-induced diarrhea appears to result from a combination of the alterations of intestinal transport of water and electrolytes, as demonstrated in the present studies, and of increased motility, as shown previously (20–23).

Radiation-induced functional changes observed *in vivo* in the canine small bowel occurred concurrently with histological alterations of the intestinal mucosa and followed a time course that was similar to that seen previously in isolated rat enterocytes exposed to 6Gy (13). In this *in vitro* model, intestinal transport was maximally altered three days after radiation, returning to baseline by day 7. This time course is consistent with suppression of intestinal transport enzymes caused by DNA damage, which would be prevented by WR2721. Recovery of intestinal transport would occur in placebo-treated survivors after the number of mucosal cells with intact DNA becomes sufficient to ensure absorption. Based on observations in rabbit ileum following whole-body exposure to gamma radiation (14), the functional alterations observed in the present studies could be due to changes in active basal electrolyte transport. Alternatively, the damage observed by histology on day 4 indicates that leakage of water and electrolyte across a more permeable intestinal mucosa may have occurred. In addition, functional recovery of the intestinal epithelium seven days after irradiation probably results from a combination of cellular regeneration and adaptation (2).

Treatment with WR2721 prevented or significantly reduced both mucosal damage and changes of intestinal transport from preirradiated values, while dramatically improving survival (90% vs 33%). It is interesting to note that changes in trans-

port of Na^+ and Cl^- were significantly less in WR2721-treated animals compared to placebo nonsurvivors, but not to placebo survivors, whereas the opposite was observed for K^+. Although no final conclusion can be drawn due to the small number of animals in each group, this observation suggests that improved survival after WR2721 pretreatment may be related to a reduction of radiation-induced alterations of Na^+ and Cl^- intestinal transport. Our findings also suggest that WR2721 improves survival at least in part by inhibiting the functional and morphological damage to the intestinal mucosa in large animals, similar to the observations in rodents (24). Yuhas and Storer (24) first reported that WR2721 was able to protect mice against whole-body irradiation. Subsequent studies demonstrated that this agent provided bone marrow protection in guinea pigs, monkeys, dogs, and humans, although the effect on the intestine was not examined (25). In the intestinal epithelium, intraperitoneal administration of WR2721 reduced initial damage to stem cells in the crypts and thereby decreased the damaging effect of a given dose of radiation, the dose reduction factor being 1.25 to 1.6 (6). However, WR2721 had to be injected parenterally because its oral bioavailability and efficacy is low, possibly because it suppressed gastric emptying (26). This problem may be obviated in the case of protection of colonic mucosa by administering 50 mg WR2721 by enema, which was shown to prevent radiation injury to the rat colon while not being systemically absorbed (11). In a clinical study, however, lower doses of WR2721 (100–450 mg/enema) could be administered safely but did not protect the rectosigmoid mucosa from damage (27). Therefore, additional studies with higher dosages will be required to further evaluate this promising approach.

In the present study, we delivered the total radiation in a single dose rather than fractionating it over several days, as is done during most types of radiation therapy. However, the results of the present study are clinically relevant because mucosal abnormalities are observed following radiotherapy in 90% of patients receiving 30 Gy total dose, 40% of those receiving 10–30 Gy and 20% of those receiving less than 10 Gy (28), and these effects are also present when doses are fractionated. Hence, our data demonstrate that WR2721 could be potentially beneficial by diminishing radiation enteritis, decreasing clinical toxicity, and allowing the use of higher radiation dosages when needed. In addition, exposure to a dose as small as 0.25 Gy suppresses mitosis in the small intestine of humans (29), and this effect could be reduced by WR2721.

Several important conclusions may be drawn from the present experiments. First, parenteral administration of WR2721 is able to protect the ileal mucosa in a large animal model, to enhance its absorptive function, and to improve survival of the animals after exposure to radiation. Second, experiments performed using the present model may be used to further assess the effects of radiation on the small bowel and to determine the potential of other radioprotectants. Third, the present data provide clinically important information on the natural history of the alterations of intestinal histology and function following exposure to gamma radiation.

ACKNOWLEDGMENTS

We thank William E. Jackson for expert advice on statistical analysis of the data.

REFERENCES

1. Quastler H: The nature of intestinal radiation death. Radiat Res 4:303–320, 1956
2. Baer AR, Cheeseman CI, Thomson BR: The assessment of recovery of the intestine after acute radiation injury. Radiat Res 109:319–329, 1987
3. Geraci JP, Jackson KL, Mariano MS: The intestinal radiation syndrome: Sepsis and endotoxin. Radiat Res 101:442–450, 1985
4. Kinsella TJ, Bloomer WD: Tolerance of the intestine to radiation therapy. Surg Gynecol Obstet 151:273–284, 1980
5. Dubois A, Walker RJ: Prospects for management of gastrointestinal injury associated with the acute radiation syndrome. Gastroenterology 95:500–507, 1988
6. Hanson WR: Radiation protection of murine intestine by WR-2721, 16,16-dimethyl prostaglandin E_2, and the combination of both agents. Radiat Res 111:361–373, 1987
7. Sweeney TR: A survey of compounds from the antiradiation drug development program of the US Army Medical Research and Development command. Walter Reed Army Institute of Research, Washington, DC, 1979
8. Schein PS: WR-2721: A chemotherapy and radiation-protective agent. Cancer Invest 8:265–266, 1990
9. Milas L, Hunter N, Reid B, Thames H: Protective effects of *S*-2-(3-Aminopropylamino)ethylphosphorothioic acid against radiation damage of normal tissues and fibrosarcoma in mice. Cancer Res 42:1888–1897, 1982
10. Rasey JS, Nelson NJ, Mahler P, Anderson K, Krohn KA, Menard T: Radioprotection of normal tissue against gamma rays and cyclotron neutrons with WR-2721: LD_{50} studies and ^{35}S-WR-2721 biodistribution. Radiat Res 97:598–607, 1984
11. France HG Jr, Jirtle RL, Mansbach CM: Intracolonic WR 2721 protection of the rat colon from acute radiation injury. Gastroenterology 91:644–650, 1986
12. Sigdestad CR, Grdina DJ, Connor AM, Hanson WR: A comparison of radioprotection from three neutron sources

and ^{60}Co by WR-2721 and WR-151327. Radiat Res 106:224–233, 1986
13. Cheeseman CI, Thomson AB, Walker K: The effects of abdominal irradiation on intestinal transport in the rat as assessed with isolated epithelial cells. Radiat Res 101:131–143, 1985
14. Gunter-Smith PJ: Gamma radiation affects active electrolyte transport by rabbit ileum: Basal Na and Cl transport. Am J Physiol 250(Gastrointest Liver Physiol 13):G540–G545, 1986
15. Vigneulle RM, Herrera J, Gage T, McVittie T, Taylor P, Zeman G, Nold JB, Dubois A: Nonuniform irradiation of the canine small intestine: I. Effects. Radiat Res 121:46–53, 1990
16. Modigliani R, Rambaud JC, Bernier JJ: The method of intraluminal perfusion of the human small intestine. Digestion 9:176–192, 1973
17. Barbezat GO: Triple-lumen perfusion of the canine jejunum. Gastroenterology 79:1243–1245, 1980
18. Zeman G, Mohaupt TH, McVittie T, Dubois A, Vigneulle RM: Nonuniform irradiation of the canine small intestine: II. Dosimetry. Radiat Res 121:54–62, 1990
19. Siegel S: Nonparametric Statistics for the Behavioral Sciences. New York, McGraw-Hill, 1956
20. Summers RW, Flatt AJ, Prihoda M, Mitros FA: Effect of irradiation on morphology and motility of canine small intestine. Dig Dis Sci 32:1402–1409, 1987
21. Summers RW, Glenn CE, Flatt AJ, Elahmady A: Does irradiation produce irreversible changes in canine small jejunal myoelectric activity? Dig Dis Sci 37:716–722, 1992
22. Otterson MF, Sarna SK, Moulder JE: Effects of fractionated doses of ionizing radiation on small intestinal motor activity. Gastroenterology 95:1249–1257, 1988
23. Otterson MF, Sarna SK, Lee MB: Fractionated doses of ionizing radiation alter postprandial small intestinal motor activity. Dig Dis Sci 37:709–715, 1992
24. Yuhas JM, Storer JB: Chemoprotection against three modes of radiation death in the mouse. Int J Radiat Biol 15:233–237, 1969
25. Yuhas JM, Spellman JM, Culo F: The role of WR-2721 in radiotherapy and or chemotherapy. Cancer Clin Trials 3:211–216, 1986
26. Dubois A, Jones M, Bailey H, Flynn NM, Warrenfeltz J, Fiala N: Suppression of gastric emptying after WR-2721: A possible cause for its poor bioavailability. Gastroenterology 95:862, 1989 (abstract)
27. Montana GS, Anscher MS, Mansbach CM, Daly N, Delannes M, Clark-Pearson D: Topical application of WR-2721 to prevent radiation-induced proctosigmoiditis. Cancer 69:2826–2830, 1992
28. Tarpila S: Morphological and functional response of human small intestine to ionizing radiation. Scand J Gastroenterol 6(suppl 12):1–52, 1971
29. Trier JS, Browning TH: Morphologic response of the mucosa of human small intestine to x-ray exposure. J Clin Invest 45:194–205, 1966

EXPERIMENTAL CELL RESEARCH 216, 411–421 (1995)

Differences in Dispersion of Influenza Virus Lipids and Proteins during Fusion

R. JOEL LOWY,*,[1] DEBI P. SARKAR,†‡ MARK H. WHITNALL,* AND ROBERT BLUMENTHAL†

*Physiology Department, Armed Forces Radiobiology Research Institute, Bethesda, Maryland 20889-5603; †Department of Biochemistry, University of Delhi South Campus, New Delhi, India; and ‡Section of Membrane Structure and Function, LMMB, NCI, NIH, Bethesda, Maryland

Digitally enhanced low-light-level fluorescence video microscopy and immunochemical staining were used to examine influenza virus envelope lipid and protein redistribution during pH-induced fusion. Video microscopy was performed using viruses labeled with either the lipid analogue octadecylrhodamine B (R18) or fluorescein isothiocyanate (FITC) covalently linked to envelope proteins. Viruses were bound to human red blood cells, and the pattern and intensity of fluorescence were monitored for 30 min while cell–virus complexes were perfused with pH 7.4 or 4.8 media at temperatures either above or below 20°C. R18 showed complete redistribution and dequenching by 30 min at all incubation temperatures, confirming reports that viral fusion occurs at subphysiological temperatures. FITC-labeled protein showed spatial redistribution at 28°C but no change at low temperature. Electron microscopy observations of immunochemical staining of viral proteins confirmed both that protein redistribution at 37°C was slower than R18 and the failure of movement within 30 min at 16°C. Video microscopy monitoring of RNA staining by acridine orange of virus–cell complexes showed redistribution to the RBCs at all temperatures but only after low pH-induced fusion. The results are consistent with differential dispersion of viral components into the RBC and the existence of relatively long-lived barriers to diffusion subsequent to fusion pore formation.

INTRODUCTION

There is considerable interest in understanding the molecular and biophysical processes which result in the fusion of envelope viral membranes with the host target cell [30]. Recently, there has been increasing appreciation that there are likely to be molecular rearrangements of the fusion proteins resulting in oligomeric structures, which are thought to be the biologically active molecular entities catalyzing membrane fusion [6, 8]. Evidence for such associations has been obtained from kinetic studies of fusion using macroscopic fluorometry [7, 8], microscopic fluorometry [25], and stopped-flow techniques [11, 12], as well as FRAP [4, 5, 17, 20], translational and rotational mobility measurements [5, 22], patch clamp capacitance [40, 43], and cell biological approaches [16]. The study of viral fusion events has primarily focused on lipid mixing monitored by octadecylrhodamine dequenching, which has provided a convenient and extremely valuable method for monitoring membrane fusion [1, 21, 29]. Although it has been shown that viral envelope protein motion changes after activation of fusion [5, 22], little is known about the kinetics of redistribution of viral protein during the actual fusion process.

Reported here are our results from examining the redistribution of influenza proteins relative to lipid movements during fusion to human red blood cells. Experiments were conducted at both 37°C and reduced temperatures to slow the overall fusion kinetics and more clearly observe the temporal patterns of lipid and protein movements. Low-light-level video microscopy was used to observe the redistribution of the lipid marker R18 and viral proteins by using FITC-labeled viral particles. Electron microscopy immunochemical techniques were used to provide a second set of experimentally independent observations of viral protein movement. Video methods were also used to examine the effects of temperature and pH on the redistribution of viral RNA. Portions of these finding have been previously reported in abstract form [26–28].

METHODS

Materials. Octadecylrhodamine B chloride (R18), thiazole orange and acridine orange were obtained from Molecular Probes (Eugene, OR). FITC-insulin and 1-ethyl-3-(dimethylaminopropyl)-carbodiimide (EDC) were from Sigma Chemical Co. (St. Louis, MO). The antibody was a goat polyclonal prepared against influenza A-USSR (H1N1) and Victoria (H3N3) conjugated to FITC (ViroStat, Portland, ME).

[1] To whom correspondence and reprint requests should be addressed at Physiology Department, Armed Forces Radiobiology Research Institute, Bethesda, MD 20889-5603.

0014-4827/95 $6.00

Fluorescent virus preparation and spectrofluorometry. Influenza strains A/Japan/H2N2 and X31/H3N2 were grown in eggs and isolated according to Puri *et al.* [35] and showed similar results to one another. R18 labeling was performed as previously described [25]. The coupling of FITC–insulin to the viruses was done using a modification of the method described by Lonngren and Goldstein [24]. Briefly, 2 ml of virus in PBS containing 2 mg/ml protein was mixed with 1 ml of PBS containing 1 mg of insulin–FITC. A 0.1-ml aliquot of PBS containing 5 mg/ml of EDC was added and the mixture incubated at approximately 25°C for 4 h with gentle shaking. The total volume was brought to 6 ml with PBS and was centrifuged at 50,000 rpm (100,000*g*) for 1 h. The virus pellet was resuspended in 6 ml PBS and washed three additional times under the same centrifugation conditions. After the final wash the volume was brought to 2 ml and the viruses were used for experimentation. Preliminary results showed directly linking FITC to the virus resulted in labeled material but with unacceptably low fluorescent levels and high backgrounds, possibly due to leaching of incompletely bound FITC (data not shown); therefore, only the insulin conjugates were used in the present study. Fluorometric assays were done [35] to determine whether viruses labeled with FITC were still fusion competent. As FITC was not self-quenching at the labeling concentrations monitoring required viruses to be labeled with R18 as well and compared to viruses from the same preparative group labeled with R18 alone. Fluorescence dequenching was monitored at 37, 30, and 10°C. Decreasing temperature increased the lag times and decreased the rate of dequenching, as had been previously reported [33, 41]. As R18 dequenching by FITC-labeled viruses occurred at all temperatures and without a consistent pattern of change in kinetic parameters, it was concluded they could be used for protein redistribution in the microscopic imaging experiments.

Virus–red blood cell prebound conjugates. Human red blood cells were obtained from the NIH Blood Bank and used within 3 days. Cells were washed three times in cold PBS and stored at approximately 10% v/v. For the experiments with R18 and FITC–virus, RBCs were first attached to polylysine-coated glass coverslips (5 μg/ml) by flooding them with 1% (v/v) RBCs. After 15–30 min, coverslips were washed to remove unattached cells and chilled to ice temperature. Viruses were added at a concentration of about 20 μg/ml for a total of 4 μg/coverslip and allowed to bind at pH 7.4 for 30 min, washed once to remove unattached viruses, and held on ice until use. For the experiments with immunostaining or acridine orange, viruses were bound to the RBC first and then to coverslips, which considerably reduced the fluorescence background due to viruses on the coverslip surface. In these experiments viruses at approximately 40 μg/ml were mixed with a 0.3% (v/v) solution of RBCs on ice for 30 min, centrifuged 30 s in a microfuge, and then resuspended in PBS at the same concentration. The virus–cell complexes were allowed to attach to coverslips for 30 min on ice, washed once, and then used for experimentation.

Fluorescence microscopy and image processing. Coverslips with bound viruses (A/Japan) were mounted in a Divorak chamber and perfused with pH 7.4 PBS at either 28°C (room temperature) or 13 ± 2°C until the start of the experiment. After an initial observation period the perfusate was switched to either pH 7.4 or pH 4.8 PBS. Images were acquired every 5–10 min using a low-light-level fluorescence microscope and digital image processing system, built around a Zeiss IM 35 microscope. The objective lens was a Zeiss 100X 1.3 N.A. Neofluar. The light source was a 100 W Hg lamp, with appropriate levels of heat and neutral density filters. The fluorescein filters were a standard Zeiss set, consisting of a 490-nm short-pass excitation filter, a 500-nm dichroic mirror, and a 520-nm long-pass emission filter. The rhodamine filter set consisted of a 540-nm wide-band excitation and a 620-nm emission filter from Omega Optics (Brattleboro, VT) and a Zeiss 540 (Zeiss, Thornberg, NJ) dichroic mirror. The camera system was a KS 1380 image intensifier (Videoscope Int., Dulles, VA) coupled to a Newvicon video camera (Model 65, Dage-MTI, Michigan City, IN). Images were acquired under manual control with 256 frames of integration using Imaging Technology boards (Bedford, MA) controlled by a Heurikon M68 host computer (Madison, WI) and were transferred directly from the image processor to the hard disk for storage and later analysis. Images within an experiment were enhanced by using the same algorithm for all time points. Generally a local area contrast scheme [10] and appropriate look up tables were applied before photographic recording using a Polaroid video freeze frame unit (Cambridge, MA) and Panatonic X (ASA 100) black and white film. Initial experiments with singly and doubly labeled viruses demonstrated that there was no leakage of the fluorescein signal with the rhodamine filters but there was leakage of the R18 signal with the fluorescein filters. This was presumably due to the activation of the low absorption tail below 500 nm of R18 by the broad-band excitation filter. Therefore, to ensure unequivocal interpretation of the dye redistribution results, even at the limits of detection for each dye, viruses with only one fluorescent label were used for microscopy for the R18/FITC comparisons of dye conjugated live virus or antibody-stained fixed viruses. Background levels of fluorescence for both dyes were fairly high in these experiments, with the primary interference being from out-of-focus viruses and aggregates.

Virus immunochemical staining. Virus (X31)–cell conjugates were prepared using either R18 or unlabeled viruses as for the microscope perfusion experiments. Coverslips were rapidly covered with PBS, pH 4.8 or 7.4, at 16 or 37°C and incubated for the indicated times, 1 to 30 min. RBCs with R18-labeled viruses were examined unfixed with no subsequent processing at 22°C to confirm that complete R18 dequenching had occurred in all experiments by 5 and 30 min at the high and low temperatures, respectively (data not shown). Postincubation, unlabeled virus–RBCs were washed once with room temperature PBS, pH 7.4, and fixed for 20 min in 2% glutaraldehyde, 0.2% picric acid, and 0.1 *M* sodium cacodylate, pH 7.2. After six 5-min PBS washes, the cells were processed for electron microscopic immunocytochemistry as follows: 10 min in 10% normal goat serum/PBS, 30 min in biotin-linked goat antiserum directed against influenza A viral strains A-USSR (H1N1) and Victoria (H3N2) (Viro-Stat cat. no. 1301), final dilution 1:200 in 10% normal goat serum, two washes in PBS, one wash in Tris-buffered saline at pH 9.6 (TBS), 30 min in avidin-biotinylated peroxidase complex (Vector) at 1:100 in TBS, one wash in TBS, two washes in PBS, 9 min in a glucose oxidase/diaminobenzidine reaction solution (0.4 units/ml glucose oxidase, 0.4% glucose, 0.136% imidazole, 0.04% ammonium chloride, 0.05% diaminobenzidine in PBS), six rinses in PBS and 30 min in 2% osmium tetroxide/PBS. The cells were then embedded in either LR White or Epon. Embedment in LR White was as follows: six 5-min washes in PBS, two 30-min incubations in 70% ethanol, one 1-h incubation in pure LR White at room temperature, one overnight incubation in LR White at room temperature, and polymerization at 50°C for 2 days. For embedment in Epon, the cells were given three 5-min washes in PBS, two 5-min washes in water, and dehydrated in ethanols. The cells were then incubated in acetone (two 15-min steps), 1:1 acetone/Epon overnight at 4°C, and spun down the next day. The acetone/Epon over the pellet was replaced, the capsules were placed under vacuum for several hours, and then the capsules were polymerized at 60°C. Ultrathin sections were stained with lead citrate to improve contrast. Micrographs were taken in a Hitachi H-7000 electron microscope at magnifications of 20–60,000.

RNA localization. Virus (X31)–cell complexes using R18-labeled influenza viruses were prepared and observed as described above. Dually labeled virus particles could be used, as the fluorescence from RNA staining was approximately 20-fold brighter than R18 and there was no crossover with appropriate image intensifier settings. Experiments were performed by constantly perfusing coverslips first with pH 7.4 at the desired experimental temperature, 37 or 16°C, and then switching to pH 4.8 or by retaining them at pH 7.4 for controls. The R18 signal was monitored until R18 redistribution appeared complete at 20–30 min. Monitoring was then switched to the fluorescein optics,

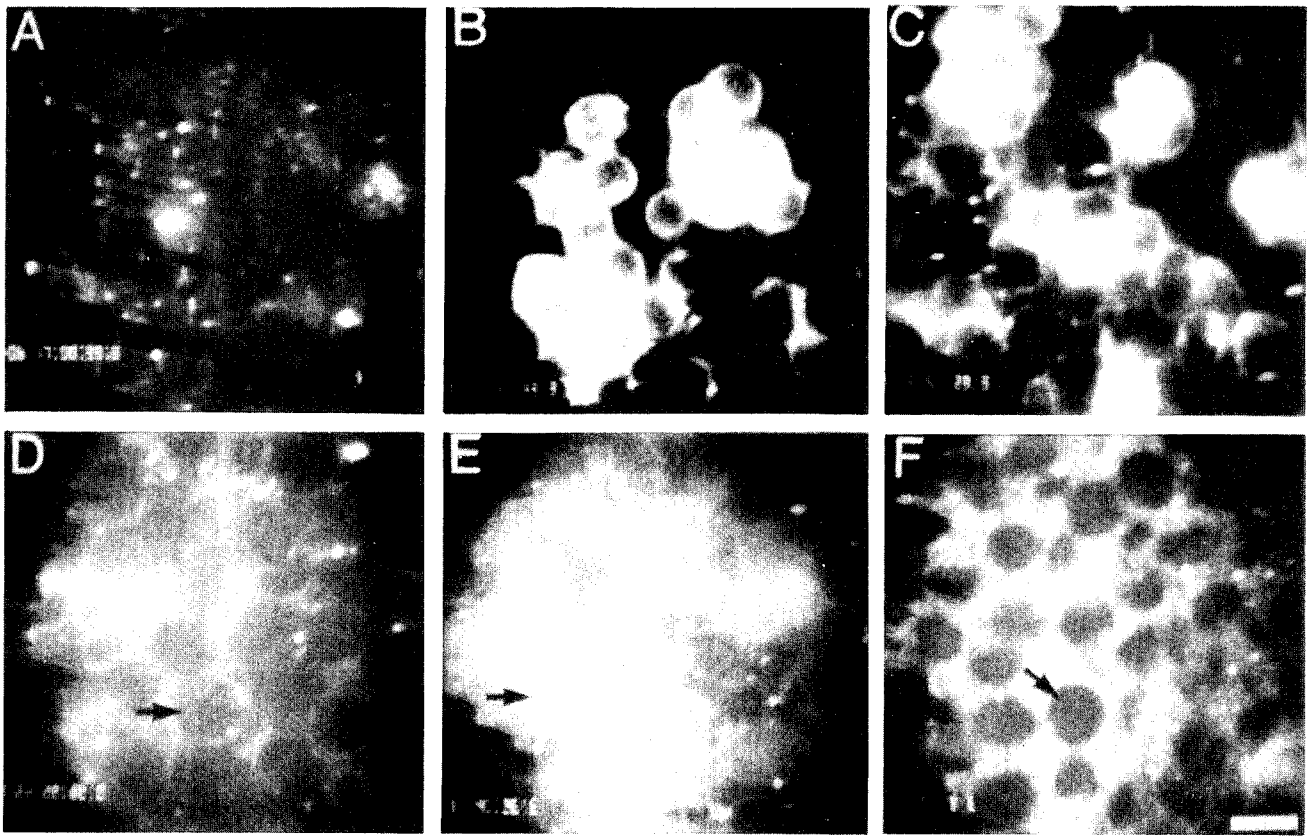

FIG. 1. Video fluorescence micrographs of R18 (A–C) and FITC–protein (D–F) distribution after perfusion for 30 min. PBS pH was 7.4 for A and D and pH 4.8 for B, C, E, and F. Incubation temperatures were 28°C for A, B, D, and E and 13 ± 2°C for C and F. During pH activation R18 at both 28 (B) and 13°C (C) loses the punctate pattern seen at neutral pH (A) and spreads across the cells accompanied by an increase in intensity due to dye dequenching. The FITC controls (D) show each cell (dark circles, arrow) being outlined by a bright mesh-like and punctate pattern due to viral particles on the coverslip between the cells. An increase in intensity in these semicircular regions was observed at 28°C (arrow) indicating redistribution of the FITC-labeled proteins onto the RBC surface. No change was seen for RBCs at 16°C (arrow). Bar, 10 μm.

and the chamber was perfused with pH 7.4 PBS containing 10 μg/ml acridine orange for 60–90 s at the experimental temperature, followed by pH 7.4 PBS at the experimental temperature. As soon as the chamber background decreased, images were acquired as rapidly as possible, as both punctate staining and volume staining were seen to decrease after 5–10 min. This decrease could be attributed to continued fusion and hemolysis, which result in loss of RNA and dye from the red blood cells.

RESULTS

Lipid and Protein Redistribution Observed during Fusion by Fluorescence Microscopy

Figure 1 shows video microscopy images of the distribution of R18 (A–C) and FITC-labeled viral protein (D–F) after a 30-min incubation at high temperature (28°C) and pH 7.4 (A and D) or pH 4.8 (B and E) or low temperature (13°C) and pH 4.8 (C and F). Images for perfusions at low temperature and neutral pH were nearly identical to those at the higher temperature (data not shown). Perfusion at pH 4.8 and 28°C (Fig 1B) demonstrates that R18, as expected, redistributes from the pH 7.4 punctate pattern (Fig. 1A) to a nearly uniform pattern of very bright fluorescence on very rounded cells, indicating high levels of dequenching and viral fusion [25]. Essentially identical results were obtained for low pH perfusion at low temperature (Fig. 1C). Due to limitations of the video camera and the film intrascene dynamic range, only the brightest cells can be displayed in Figs. 1B and 1C; the image regions containing rounded cells with "ring" fluorescence that appear dark were also uniformly stained but at a lower intensity. The observations at both perfusion temperatures were consistent with previous microscopic observations of R18 redistribution [25] and confirm the previous fluorometric results for fusion with both liposomes [41] and RBCs [34, 39], showing that influenza viral fusion occurs at subphysiological temperatures well below those previously thought to be the threshold for fusion activity.

The FITC experiments were considerably more diffi-

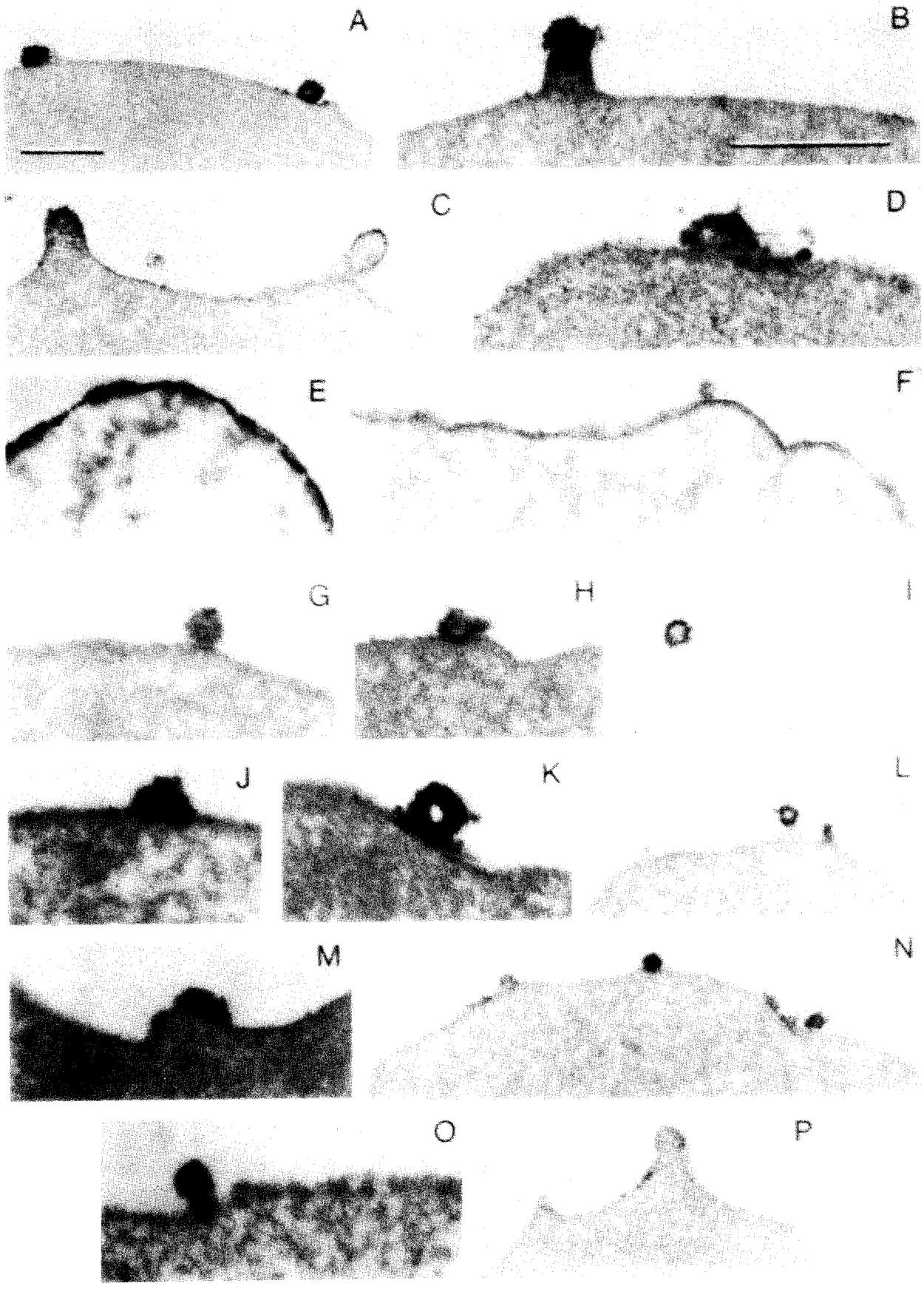
A
B
C
D
E
F
G
H
I
J
K
L
M
N
O
P

cult to perform than the R18 experiments, as the FITC signal was lower and the background fluorescence was higher. FITC was not self-quenched, so there was no intensity change during fusion but only a change in staining pattern to indicate dye–protein redistribution. The background was higher because the best focal plane for visualizing changes in staining also included viruses and aggregates attached to the glass coverslip surrounding the RBCs. These nonfusing particles appear as the bright net-like fluorescence while the surface of the individual RBCs are the semicircular regions. In the pH 7.4 controls, these regions are darker than the surrounding concentration of virus particles (Fig. 1D). Thirty minutes after induction of fusion by pH 4.8 perfusion at 28°C, the cell surfaces became overlayed with fluorescence of nearly the same intensity as the background, forming semicircular bright fluorescent regions corresponding to individual cells (Fig. 1E), which indicates the movement of FITC across the RBC membrane surface. The results at 13°C were strikingly different (Fig. 1F), as despite low pH perfusion the surface of the RBCs remained dark relative to the background fluorescence and nearly identical in appearance to the pH 7.4 controls. This lack of FITC staining suggests that viral proteins either are not moving into the target membrane or are doing so a very reduced rate compared to either protein at 28°C or R18 at high or low temperature.

Electron Microscopy Immunochemical Localization of Viral Protein

The localization of viral envelope proteins was also examined using EM level immunocytochemistry to provide a second independent approach that (1) has greater spatial resolution than light level video microscopy, (2) has a better signal-to-noise ratio for protein localization, and (3) uses unmodified viruses during fusion, eliminating the possibility of protein–dye conjugation artifacts.

Figure 2 shows distributions of viral protein on the surface of RBCs subsequent to incubation at pH 4.8 for 1, 5, and 30 min at 37°C (A–F) or 5, 10, 15, and 30 min at 16°C (G–P). The RBC electron density varies with loss of hemoglobin due to virally induced hemolysis, which is particularly pronounced at 30 min at 37°C. Loss of electron density was also observed at 16°C but was generally not as extensive (cf. Figs. 2F and 2O). At 37°C some (Fig. 2B) but not all viruses (Fig. 2A) showed clear fusion junctions at 1 min, but wide connections were prevalent by 5 min (Figs. 2C and 2D), at which time protein remained on the viral envelopes. By 30 min protein dispersion, however, was extensive (Figs. 2E and 2F), with staining in some cells nearly as intense as on the envelopes (cf. Figs. 2D and 2E). Occasionally a few remaining envelopes were seen, which were likely due to fusion-incompetent particles (Fig. 2F). However, it is important to note that influenza viral proteins were able to disperse completely and that the final equilibrium state at 30 min at 37°C was not small localized patches of proteins but appeared to be a relatively even distribution of proteins, indicating considerable free mobility within the membrane.

At 16°C at all times protein was restricted to viral envelopes or to regions of evagination approximately the same diameter as a viral particle. At 5 and 10 min clear junctions were not generally seen (Figs. 2G and 2K), but many particles had a flattened versus a more spherical appearance (Figs. 2H and 2J), which might reflect envelope structural changes associated with fusion. At 15 and 30 min, omega-shaped structures with varying degrees of neck-like or broad-based connections were visible, clearly showing aqueous continuity between the virus and RBC. All these structures showed viral proteins on their outer hemispherical surface and occasionally even along the length of the neck-like structures (Fig. 2O). The immediately adjacent membranes in most cases did not have apparent protein staining, although near a few structures there was a low level of staining. This may indicate some small amount of protein movement or could be nonspecific diffusion and readherence of the DAB reaction product. Even over extended regions, the RBC membrane was free of immunostaining at 30 min.

RNA Staining during Video Microscopy Observation of Virus–Cell Complexes

The feasibility of using video methods and the membrane-permeant dye acridine orange to localize RNA in unfixed virus–cell complexes pre- and postfusion was examined. Monitoring RNA movement was of interest as a means to correlate RNA redistribution with the movements of the protein and lipid. Also, RNA redistribution is an important additional indicator that a true fusion pore has formed during virus-cell fusion at reduced temperatures, as RNA is the contents marker for the virus and could not be transferred without an

FIG. 2. Electron microscopy immunochemical localization of influenza viral proteins. RBCs were incubated at pH 4.9 at 37°C for 1 (A, B), 5 (C, D), and 30 min (E, F) and at 16°C for 5 (G, H, I), 10 (J, K, L), 15 (M, N), and 30 (O, P) min prior to fixation. Immunostaining was as described under Methods. Virus–cell junctions are heterogeneous, varying from broad and extensive to narrow elongated necks. At all times for 16°C or at 1 and 5 min for 37°C, proteins remain on viral envelopes or on evaginated structures formed by extensively fused envelopes. Only at 30 min at 37°C is there dispersion of viral proteins into the plane of the RBC membrane. At all other times and temperatures and for all junction types little or no protein is seen on the adjacent RBC membrane. Bars, 0.5 μm. Magnifications are equivalent for A, C, F, I, L, N, and P and for B, D, E, G, H, J, K, M, and O.

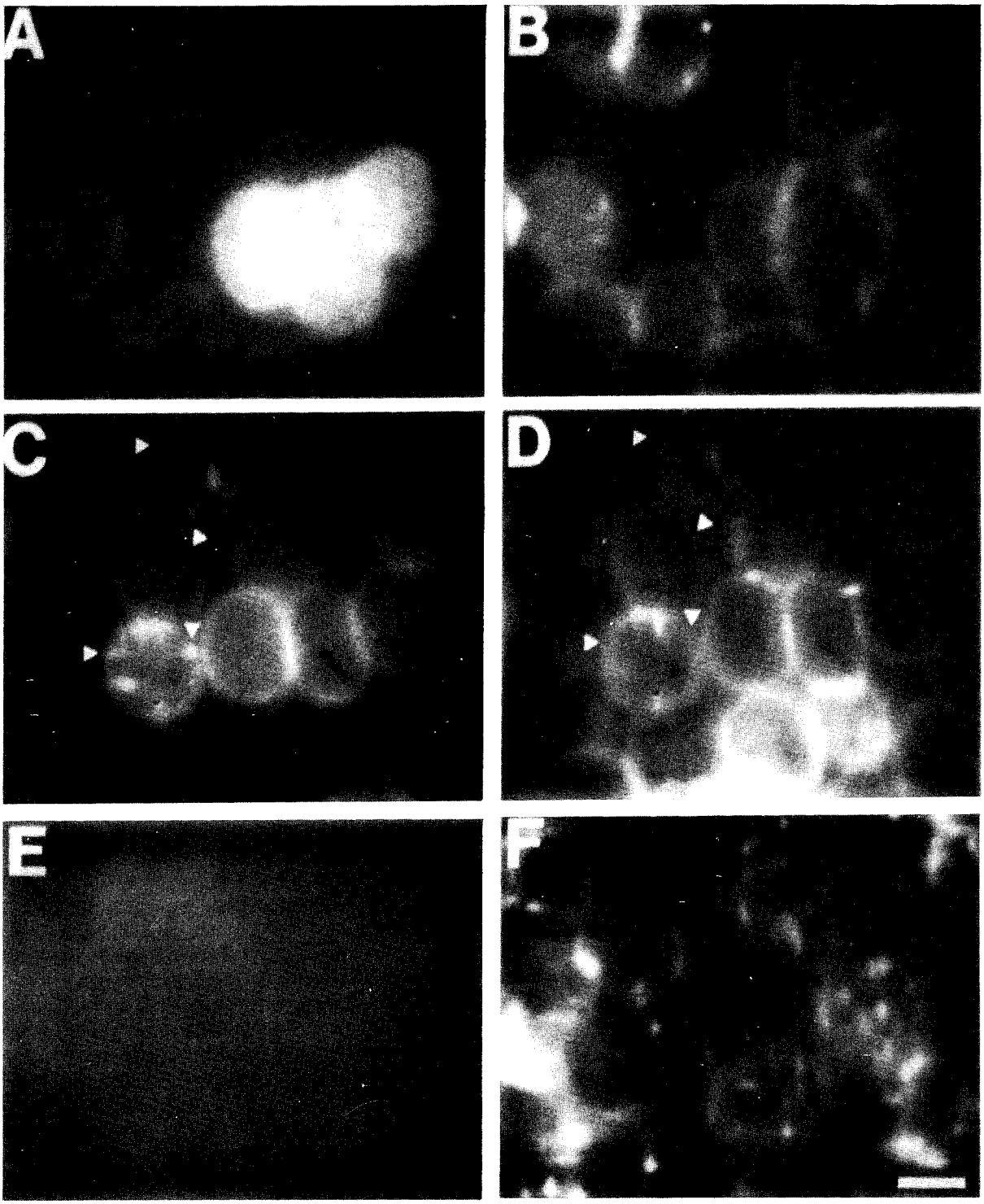

FIG. 3. Comparison of RNA and lipid distribution in virus–RBC complexes after perfusion for 30 min. Video images show patterns for acridine orange (AO) staining of RNA with fluorescein optics (A, C, and E) or R18 lipid (B, D, and F) with rhodamine optics. Virus–cell complexes were perfused at pH 4.8 at 37°C (A and B), pH 4.8 at 16°C (C and D), or pH 7.4 at 37°C (E and F) for 30 min and then rapidly stained with AO and observed (see Methods). R18 redistribution and dequenching occurs at low pH at both high and low temperatures (B and D), but not at neutral pH (F). AO staining for most cells shows a volume-filling pattern (A and C) which was 10- to 20-fold brighter than the R18 fluorescence. Punctate staining of AO occurred only at 16°C (C, arrowheads) but frequently the R18 has dispersed at this same location (D, arrowheads). No R18 redistribution occurs at pH 7.4 (F) and the faint background staining with AO (E) was only seen by increasing camera gain 10-fold. Bar, 5 μm.

aqueous junction formation between the virus and the cells.

Figure 3 shows both the R18 and the acridine orange staining pattern after 30 min for virus–cell complexes incubated at low pH (4.8) and 37°C (A and B), at low pH (4.8) and 16°C (C and D), and at neutral pH and 37°C (E and F). As expected, no redistribution of R18 occurred at neutral pH, and the typical punctate staining due to viral particles was readily observed (Fig. 3F). Nor was RNA staining observed at neutral pH (Fig. 3E). The low level of fluorescence outlining the RBCs in the neutral pH acridine orange (Fig. 3E) image was only visible at a 10-fold higher camera gain setting relative to Figs. 3A and 3C. Controls for nonspecific acridine orange staining of RBCs after pH 4.8 exposure without bound viruses showed a nearly identical pattern and level of background fluorescence (data not shown). These results demonstrated that residual association of acridine orange with the RBCs was very low in the absence of virus or viral fusion conditions to provide exogenous RNA. The acridine orange result was also consistent with the inability to stain intact influenza virus unless they had been previously treated with Triton X (data not shown). Presumably the tight association of the matrix proteins prevents RNA staining despite the lipid permeability of Acridine orange.

After pH 4.8 37°C incubation of virus–cell complexes, the R18 (Fig. 3B) images showed that all the cells had become rounded with R18 "ring" fluorescence, indicating viral fusion had occurred. The intensifier gain was purposely adjusted so that the brightest punctate objects could be observed; therefore, the cell surfaces do not appear as bright as in the Fig. 1 R18 images. The acridine orange staining was much brighter than the R18 staining, so differences in intensifier gain settings of approximately 20- to 30-fold resulted in good spectral separation of the images. The two predominant acridine orange staining patterns were (1) cells with very intense volume staining interspersed with (2) a large number of relatively weakly stained cells that also showed a circular membrane-associated fluorescence (Fig. 3A). No well-defined punctate acridine orange staining occurred, with or without spatial correlation to the few large objects remaining in the R18 images. These volume-filling patterns were consistent with RNA being dispersed after fusion into the RBC interior. Differences in staining intensity were likely due to varying levels of hemolysis, with intact cells having the brightest acridine orange fluorescence from higher amounts of retained intracellular RNA. The circular fluorescence pattern in the dimmer cells, which was still well above background, suggests that much of the RNA remaining after hemolysis was adhering to the plasma membranes of the inner RBCs. A higher diffuse background between the cells was noted in many of these samples and is consistent with RNA being released during hemolysis and then readhering to cell and coverslip surfaces. The presence of a few remaining punctate R18-staining objects (Fig. 3B) was consistently observed even under optimal fusion conditions and is attributable to inactive viruses [25].

The 16°C incubation samples also showed complete R18 redistribution (Fig. 3D), indicating lipid mixing subsequent to viral fusion, as illustrated in Fig. 1C. The acridine orange images (Fig. 3C) likewise showed volume staining in most cells but with more variation in intensity and lower general background, results that are consistent with a lower but more heterogeneous degree of RBC permeabilization, as would be expected at a lower temperature. Therefore, it appeared that, despite these reduced temperature conditions, fusion for most particles had occurred, with redistribution of membrane lipid and intracellular dispersal of the RNA to the target RBCs. In approximately 10–20% of the cells, a punctate acridine orange staining pattern was also observed (Fig. 3C, arrowheads), which in many instances did not correspond to punctate R18 staining. This suggests that some viruses may have been fortuitously observed after redistribution of envelope lipids while RNA remained in a compacted state.

DISCUSSION

Electron and Light Microscopy Observation of Protein and Lipid Movements

Previous video microscopy observations of single influenza virus particle fusion [25] combined with diffusion calculations suggested that lipid movement is restricted from the viral envelope to the target membrane surface. Subsequent to these reports there has been increasing experimental evidence that the influenza fusion process occurs through a series of steps, each involving molecular rearrangements which contribute to the overall macroscopic kinetics observed for viral fusion (see Introduction). There is relatively little information on viral envelope protein movements (see below), and none for influenza, to our knowledge, which attempts to describe these movements relative to other fusion processes, i.e., the more extensively described lipid movements. Knowledge of RNA entry is primarily from biochemical approaches with the kinetics related to endocytic entry and not the envelope fusion event itself [30]. The experiments reported here were designed to extend video microscopy methods to protein and RNA observation, determine whether protein movements appeared to be diffusionally restricted, and obtain evidence for RNA movements relative to lipid and protein. The expectations were that protein, like lipid would move more slowly than predicted by diffusional calculations and there would be kinetic differences between lipid and protein, but these would be similar to

their differences in free molecular in membrane diffusion rates.

The most surprising finding in these studies was the disassociation between viral envelope lipid and protein mixing into the RBC membrane, as protein appeared to move from the virions at a very much lower rate than lipid. A large difference in diffusional movements of viral molecular components during membrane fusion has not, to our knowledge, been reported previously. In these studies this difference was first detected during the live video observations of fusion at low temperature due to the lack of detectable protein movement to the target cells, even at times when the R18 had apparently redistributed to equilibrium. Conducting these experiments with unfixed material and continuous solution perfusion at low temperature makes it unlikely that the lipid redistribution was artifactual due to transient warming of the sample or nonfusion-mediated movement of virus envelope components to the RBC. However, there was concern that protein dispersal time was being overestimated in the video microscopy experiments. FITC-labeled protein redistribution kinetics could be artificially reduced due to changes in envelope protein functions or mobility, e.g., reduction in HA fusion competence, protein cross-linking or steric hindrance by insulin–FITC dye substituent groups. Threshold sensitivity of the video imaging system is greater for R18 than for FITC, both because of the intensity increase from the relief of R18 self-quenching and the lower signal-to-noise ratio with FITC due to the higher background of non-cellular bound virus. Systematic errors, if present, would again be toward overestimating the time for protein redistribution.

Standard EM immunochemical methods were used as a second independent method to examine distributions of unmodified viral proteins post-RBC fusion. These immunochemical results completely confirmed the live video microscopy observations, showing that at 30 min an even redistribution of envelope protein across the RBC surface had occurred at 37°C but little or no movement was seen at reduced temperature. The EM results were particularly informative about the kinetics of protein movement relative to lipid movement. At 5 and 30 min at 37 and 16°C, respectively, most of the envelope proteins were clearly restricted to small intensely staining virus-sized regions of the RBC surface, times at which this and previous studies have shown R18 to be well redistributed in the target RBC membrane. Five minutes is particularly long compared to R18/lipid mixing measurements of viral-cell fusion at 37°C, as spectrofluorometic dequenching measurements on a population of cells reached equilibrium within 60 s at 37°C [11], whereas single-particle measurements yielded a $t\frac{1}{2}$ of 41 s at pH 5.0 [25]. The structures the EM micrographs showed can be considered fusion intermediates as they existed subsequent to formation of fusion junctions that allowed lipid dispersal. Interestingly the nondispersed protein often appeared in small evaginations and/or envelope-like structures rather than completely planar structures or patches within the RBC plasma membrane. The types of unfused and partially fused viruses observed at both incubation temperatures were very similar to those previously reported [9, 13, 32], and the same progression of structures has been seen in other time course studies of envelope virus fusion. In these reports envelope structures and protein appear to be associated with virions throughout the process and even during late stages of fusion and penetration of endosomes. Recent micrographs of influenza fusing to HL-60 and CEM cell surfaces [14] show viruses joined to cells by fusion junctions that are either narrow necks, as in Figs. 2C and 2O, or expanded broad-based structures up to 100 nm wide as in Figs. 2D and 2M. Spike proteins were clearly discernible on the envelopes in their micrographs and were less distinct postfusion. Immunochemical localization of fowl plague virus showed protein localized on envelopes with a similar variation of structural forms from broad-based omega shapes to almost planar structures [31]. Therefore, it seems likely that the immunochemical localization of viral protein observed in restricted viral-sized regions accurately reflects its distribution during the fusion process and that a large temporal difference exists between the time of lipid and protein redistribution from the viral envelope into the target RBC membrane.

Video Microscopy Observation of Lipid and RNA Movements

The results with acridine orange staining support the idea that RNA can be localized in unfixed virus–cell fusion complexes during the fusion process. Very low levels of nonspecific staining were associated with the RBCs in the absence of virus or in pH conditions nonpermissive for fusion. Furthermore, it appears that until fusion is initiated the RNA in intact viruses is not accessible to staining despite acridine orange being membrane permeant and capable of penetrating the outer membrane envelope. At present it is not known whether staining is dependent on fusion pore formation or on the initial stages of capsid uncoating which remove the tightly associated matrix proteins. The presence of positive RNA staining in the RBC targets subsequent to low pH treatment at both 37 and 16°C is evidence that viral fusion at reduced temperature does not prevent the release of RNA into the target cell. Particularly noteworthy is that RNA staining was observed under the same time, temperature, and pH conditions in which lipid dispersion had taken place (Fig. 3D) but envelope proteins remained clustered (Figs. 2O and 2P). This result suggests that entry of the ribonuclear protein particles precedes complete dispersion of the viral

envelope structure and associated proteins. The identification of regions with punctate acridine orange staining but lacking R18 was suggestive that lipid mixing preceded RNA release. Definite conclusions on the exact timing of RNA entry will require additional kinetic studies, but these now appear feasible by using a combination of video and EM methods.

Simple Diffusional Considerations Do Not Explain Lipid and Protein Kinetics

An important question is whether the protein dispersion kinetics observed in this study can be readily explained by established diffusional mechanisms. One well-known potential barrier to virus protein movement in the RBC membrane is the spectrin meshwork. While lipids are generally unrestricted, RBC proteins are found to have approximately 100-fold smaller diffusion coefficients (D). D values for the most extensively studied protein, band 3, are generally 10^{-11} cm^2/s, which increases 40- to 50-fold when spectrin is not present or is disrupted [15, 38]. However, spectrin networks are unlikely to have a role in influenza virus molecular dispersion postfusion. Fusion of influenza at low pH has been shown to structurally disrupt the spectrin network of target RBCs and increase the mobility of both band 3 and HA to levels identical to spectrin-free conditions, e.g., $D = 4 - 5 \times 10^{-10}$ cm^2/s [44]. This D value for HA also corresponds well to that measured postfusion for Sendai virus proteins [3, 5]. Recent measurements of D for HA on CV-1 cells constitutively expressing HA were of similar magnitude (11.7×10^{-10} cm^2/s; [17]), which, like other nonerythroid cells should also be largely free of cytoskeletal restrictions [15].

Calculated rates of free protein diffusion also suggest that it is unlikely that the kinetics of protein dispersal observed in this study can be explained by this mechanism. First, a 100-nm-diameter influenza virus could be considered to appear fully dispersed when proteins had moved 1–5 μm from the site of envelope binding and fusion, which is a 30- to 150-fold dilution of the surface area. Simple diffusion predicts dispersion times of 5–50 s using values typical for viral protein $D = 10^{-10}$ to 10^{-9} cm^2/s [3, 17, 44]. Temperature effects for the present study can be estimated assuming an approximate doubling of D for each 10°C is applicable [3, 17]. This would increase these dispersion times to a maximum of 3 min at 16°C. A second calculation can be performed starting with the lipid transfer rate measured for single particles during virus-cell fusion. At pH 5 the $t_{\frac{1}{2}}$ was about 41 s [25]. D for the lipid analogue N-NBD-PE was 5-fold higher compared to D for HA in HA-expressing CV-1 cells at 22°C [17]. A similar difference in R18 and protein D values can be estimated from measurements with Sendai virus [3, 4]. Combining these experimental measurements we calculated a $t_{\frac{1}{2}}$ for protein movement of about 5 min at 37°C. Adjusting for temperature results in upper limits for the $t_{\frac{1}{2}}$ of protein dispersion of approximately 10 and 20 min at 28 and 16°C, respectively. The video microscopy observations of protein dispersal by 30 min at 28°C were consistent with the upper estimate of a $t_{\frac{1}{2}}$ of 10 min. Likewise, the even staining seen by EM at 30 min would also be expected from the 5 s to 5 min times calculated for diffusion at 37°C. However, the video and EM images obtained for other time and temperature combinations were not consistent with the diffusion predictions. The 20 minute maximum $t_{\frac{1}{2}}$ for 16°C implies that approximately 66% of the protein would move within 30 min, but experimentally little or no dispersion was detectable by either video or EM microscopy. Similarly, the same well-dispersed pattern on RBC plasma membrane observed at 30 min at 37°C would be expected at 5 min, but instead staining remained in small localized regions. Therefore simple diffusional considerations fail to adequately explain the protein movements seen during the viral fusion process either at early time points at physiological temperatures or for extended periods at temperatures below 20°C.

Previously reported results are also consistent with viral envelope lipids and proteins dispersing more slowly than predicted by simple diffusion. Lipids show reduced movements during HA-catalyzed fusion both for virus–cell [25] and for cell–cell fusion events [43]. Sophisticated analysis of R18 movement using realistic fusion junctional geometries predicts time constants in the millisecond time domain [36], whereas the $t_{\frac{1}{2}}$ of 41 s for lipid redistribution [25] is the minimum observed for single particles [18]. Detailed kinetic analysis of viral proteins undergoing fusion at reduced temperature has not been extensively studied for any virus-fusion target to date. However, the decreased protein mobility in this study is consistent with previous mobility fraction (Rf values) measurements of Sendai virus F proteins on RBCs. Unlike many reported results, the temperatures during fusion and for the mobility measurements of F proteins were the same [3]. The means of the Rf values were 0.61 to 0.32, respectively, at incubation temperatures of 37 and 25°C. Interestingly, distributions of Rf values were actually skewed; a large percentage of F proteins had essentially no detectable mobility at 25°C.

Further Identification of Barriers to Influenza Macromolecular Dispersion during Fusion Is Needed

As free diffusion values for proteins and lipids failed to predict the observed redistribution kinetics of virus envelope components, it seems possible that additional barriers to diffusion exist in the fusion state. A possible site and mechanism for a quantitatively large diffusion barrier would be the occurrence of a macromolecular

complex of HA molecules in association with the fusion junction forming the "fusion complex." Such an association of fusion proteins once assembled could have very slow dissolution rates due to protein–protein interactions. Closely associated proteins could cause steric hindrance and intramolecular interactions that would slow entry into the target membrane of both proteins and lipids. Formation of oligomeric associations has been proposed as being necessary for viral fusion and formation of stable fusion pores, and supportive experimental and theoretical evidence for such complexes is increasing [7, 8, 16, 19, 33, 37]. Although cell–cell fusion as catalyzed by HA may be different than viral fusion, studies using volume markers are consistent with initial formation of small fusion pores or a "sieve plate"-like structure of multiple small pores [37]. Capacitance measurements of HA-catalyzed cell–cell fusion indicated that the pore forms a narrow junction which continued to expand over 2 min [40]. Recently, based on simultaneous patch clamp and fluorescent imaging data, it has been further suggested that such a HA complex must begin to expand to a threshold size and incorporate lipid subsequent to aqueous junction formation in order for lipid transfer to occur [43]. During Sendai virus-mediated RBC–RBC fusion, F protein and HN concentrations are elevated in cell contact regions during fusion but disperse with time [2].

Regardless of the specific morphology, formation mechanism or lifetime of postfusion pore structures, the data support the notion that discrete fusion structural states exist subsequent to fusion pore formation. This study has shown that the collapse and relatively simultaneous dissolution of all molecular components into the target cell is unlikely to be the mechanism of influenza viral fusion. Importantly, the rates of viral molecular component entry are truly differential under physiological conditions, and the likely order of entry into the target cell is lipid mixing, followed by RNA entry, and finally a slow dispersion of envelope proteins.

We thank Drs. Anu Puri and Charles Pak for useful discussions and Karen Anderson for technical assistance with the electron microscopy immunostaining experiments. Dr. Lowy's work was supported by the Armed Forces Radiobiology Research Institute, Defense Nuclear Agency, under Work Units 00020 and 00105. Views presented in this paper are those of the authors; no endorsement by the Defense Nuclear Agency has been given or should be inferred. Research was conducted according to the principles enunciated in the Guide for the Care and Use of Laboratory Animals prepared by the Institute of Laboratory Animal Resources, National Research Council.

REFERENCES

1. Arbuzova, A., Korte, T., Muller, P., Herrmann, A. (1994) *Biochim. Biophys. Acta* **1190,** 360–366.
2. Aroeti, B., and Henis, Y. I. (1991) *J. Biol. Chem.* **266,** 15845–15849.
3. Aroeti, B., and Henis, Y. I. (1988) *Biochemistry* **27,** 5654–5661.
4. Aroeti, B., and Henis, Y. I. (1987) *Exp. Cell Res.* **170,** 322–337.
5. Aroeti, B., Jovin, T. M., and Henis, Y. I. (1990) *Biochemistry* **29,** 9919–9125.
6. Bentz, J., Ellens, H., and Alford, D. (1990) *FEBS Lett.* **276,** 1–5.
7. Blumenthal, R., Puri, A., Sarkar, D. P., Chem, Y., Eidelman, O., and Morris, S. J. (1988a) *in* Cell Biology of Virus Entry, Replication and Pathogenesis, UCLA Symposium on Molecular and Cellular Biology (Compans, R., Helenius A., and M. Oldstone, M., Eds.), Vol. 90, pp. 1–22, Alan R. Liss, New York.
8. Blumenthal, R., Puri, A., Walter, A., and Eidelman, O. (1988b) *in* Molecular Mechanisms of Membrane Fusion (Ohki, S., Doyle, D., Flanagan, T. D., Hui, S. W., and Mayhew, E., Eds.), pp. 367–383, Plenum, New York.
9. Braunwald, J., Nonnenmacher, H., and Tripier-Darcy, F. (1985) *J. Gen. Virol.* **66,** 283–293.
10. Chen, H., Sedat, J. W., and Agard, D. A. (1990) *in* Handbook of Biological Confocal Microscopy (Pawley, J. B., Ed.), pp. 141–150, Plenum, New York.
11. Clague, M. J., Schoch, C., and Blumenthal, R. (1991) *J. Virol.* **65,** 2402–2407.
12. Clague, M. J., Schoch, C., Zech, L., and Blumenthal, R. (1990) *Biochemistry* **29,** 1303–1308.
13. Dourmashkin, R. R., and Tyrrell, D. A. J. (1974) *J. Gen. Virol.* **24,** 129–141.
14. Duzgunes, N., Pedroso de Lima, M. C., Stamatatos, L., Flasher, D., Alford, D., Friend, D. S., and Nir, S. (1992) *J. Gen. Virol.* **73,** 27–37.
15. Edidin, M. (1990) *in* Current Topics in Membranes and Transport, Vol. 36, pp. 81–97, Academic Press, San Diego.
16. Ellens, H., Bentz, J., Mason, D., Zhang, F., and White, J. M. (1990) *Biochemistry* **29,** 9697–9707.
17. Fire, E. D., Zwart, E., Roth, M. G., and Henis, Y. I. (1991) *J. Cell Biol.* **115,** 1585–1594.
18. Georgiou, G. N., Morrison, I. E. G., and Cherry, R. J. (1989) *FEBS Lett.* **250,** 487–492.
19. Guy, H. R., Durell, S. R., Schoch, C., and Blumenthal, R. (1992) *Biophys. J.* **62,** 95–97.
20. Henis, Y. I., Herman-Barhom, Y., Aroeti, B., and Gutman, O. (1989) *J. Biol. Chem.* **264,** 17119–17125.
21. Hoekstra, D., De Boer, T., Klappe, K., and Wilschut, J. (1984) *Biochemistry* **23,** 5675–5681.
22. Junankar, P. R., and Cherry, R. J. (1986) *Biochim. Biophys. Acta* **854,** 198–206.
23. Kaplan, D., Zimmerberg, J., Puri, A., Sarkar, D. P., and Blumenthal, R. (1991) *Exp. Cell Res.* **195,** 137–144.
24. Lonngren, J., and Goldstein, I. J. (1978) *in* Methods in Enzymology, Vol. 50, Complex Carbohydrates, Part C, Victor (Ginsberg, Victor Ed.), pp. 160–162, Academic Press, New York.
25. Lowy, R. J., Sarkar, D. P., Chen, Y., and Blumenthal, R. (1990) *Proc. Natl. Acad. Sci. USA* **87,** 1850–1854.
26. Lowy, R. J., Sarkar, D. P., and Blumenthal, R. (1991) *J. Cell Biol.* **115,** 253a.
27. Lowy, R. J., Sarkar, D. P., and Blumenthal, R. (1992) *J. Cell. Biochem. Suppl.* **16C,** 131.
28. Lowy, R. J., Whitnall, M. H., and Blumenthal, R. (1993) *Biophys. J.* **64,** A188.
29. Loyter, A., Citovsky, V., and Blumenthal, R. (1988) *Methods Biochem. Anal.* **33,** 129–164.

30. Marsh, M., and Helenius, A. (1989) *Adv. Virus Res.* **36,** 107–151.
31. Matlin, K. S., Reggio, H., Helenius, A., and Simons, K. (1981) *J. Cell Biol.* **91,** 601–613.
32. Morgan, C., and Rose, H. M. (1968) *J. Virol.* **2,** 925–936.
33. Morris, S. J., Sarkar, D. P., White, J. M., and Blumenthal, R. (1989) *J. Biol. Chem.* **264,** 3972–3978.
34. Pak, C. C., Krumbiegel, M., and Blumenthal, R. (1994) *J. Gen. Virol.* **75,** 395–399.
35. Puri, A., Booy, F. P., Doms, R. W., White, J. M., and Blumenthal, R. (1990) *J. Virol.* **64,** 3824–3832.
36. Rubin, R. J., and Chen, Y. (1990) *Biophys. J.* **58,** 1157–1167.
37. Sarkar, D. P., Morris, S. J., Eidelman, O., Zimmerberg, J., and Blumenthal, R. (1989) *J. Cell Biol.* **109,** 113–122.
38. Saxton, M. J. (1990) *Biophys. J.* **57,** 1167–1177.
39. Schoch, C., Blumenthal, R., and Clague, M. J. (1992) *FEBS Lett.* **331,** 221–225.
40. Spruce, A. E., Iwata, A., White, J. M., and Almers, W. (1989) *Nature* **342,** 555–556.
41. Stegmann, T., White, J. M., and Helenius, A. (1990) *EMBO J.* **9,** 4231–4241.
42. Sugrue, R. J., and Hay, A. J. (1991) *Virology* **180,** 617–624.
43. Tse, F. W., Iwata, A., and Almers, W. (1993) *J. Cell Biol.* **121,** 543–552.
44. Yoshimura, A., Yamashina, S., and Ohnishi, S-I. (1985) *Exp. Cell Res.* **160,** 126–137.
45. Zhirnov, O. P. (1990) *Virology* **176,** 274–279.

Received August 3, 1994
Revised version received October 20, 1994

Regulation of intracellular pH in J774 murine macrophage cells: H^+ extrusion processes

LESLIE C. McKINNEY AND ARIE MORAN
Department of Physiology, Armed Forces Radiobiology Research Institute, Bethesda, Maryland 20889-5603; and Department of Physiology, Ben Gurion University of the Negev, Beersheba, Israel

McKinney, Leslie C., and Arie Moran. Regulation of intracellular pH in J774 murine macrophage cells: H^+ extrusion processes. *Am. J. Physiol.* 268 (*Cell Physiol.* 37): C210–C217, 1995.—Mechanisms of intracellular pH (pH_i) regulation were characterized in the murine macrophage cell line J774.1, using 2′,7′-bis(carboxyethyl)-5(6)-carboxyfluorescein to measure pH_i. Under nominally HCO_3^--free conditions, resting pH_i of nonadherent J774.1 cells was 7.53 ± 0.02 (n = 86), and of adherent cells was 7.59 ± 0.02 (n = 97). In the presence of HCO_3^-/CO_2, pH_i values were reduced to 7.41 ± 0.02 (n = 12) and 7.40 ± 0.01 (n = 28), respectively. Amiloride, an inhibitor of Na^+/H^+ exchange, did not affect resting pH_i. Inhibitors of a vacuolar type H^+-ATPase [bafilomycin A_1, *N*-ethylmaleimide (NEM), 7-chloro-4-nitrobenz-2-oxa-1,3-diazide (NBD), and *p*-chloromercuriphenylsulfonic acid (pCMBS)] reduced pH_i by at least 0.2 pH units. Inhibitors of other classes of H^+-ATPases (oligomycin, azide, vanadate, and ouabain) were without effect. Inhibition of H^+ efflux, measured by the change in extracellular pH of a weakly buffered cell suspension, followed the same pharmacological profile, indicating that the reduction of pH_i was due to inhibition of H^+ extrusion. Mechanisms of recovery from an imposed intracellular acid load were also investigated. In NaCl-Hanks' solution, pH_i recovered exponentially to normal within 2 min. The initial rate of recovery was inhibited >90% by amiloride or by replacement of extracellular Na^+ concentration by *N*-methylglucamine. Inhibitors of the vacuolar H^+-ATPase also inhibited recovery. NEM and NBD nonspecifically inhibited all recovery. Bafilomycin A_1 and pCMBS did not inhibit the initial amiloride-sensitive portion of recovery, but they did inhibit a late component of recovery when pH_i was above 7.0. We conclude that the Na^+/H^+ exchanger is primarily responsible for recovery from an acid load but does not regulate resting pH_i. Conversely, a vacuolar H^+-ATPase regulates the resting pH_i of J774 cells but contributes little to recovery from acidification.

pH regulation; proton-adenosinetriphosphatase; sodium/proton exchange; proton transport

MACROPHAGES, LIKE OTHER mammalian cells, have a resting membrane potential between −50 and −80 mV (11) and maintain intracellular pH (pH_i) above the equilibrium potential for H^+ (~6.5) by extruding H^+ equivalents via plasma membrane ion pumps and exchangers. These include both Na^+-dependent and Na^+-independent Cl^-/HCO_3^- exchangers and an amiloride-inhibitable Na^+/H^+ exchanger (12, 30). It has recently been shown that primary tissue macrophages may use mechanisms of pH_i regulation not commonly used by other cell types. For example, both thioglycolate-elicited murine peritoneal macrophages (28) and murine alveolar macrophages (2) express a vacuolar type H^+-ATPase on their plasma membrane that extrudes H^+ equivalents and contributes to recovery from an intracellular acid load. In these cells, Na^+/H^+ exchange is a secondary pathway for H^+ extrusion and contributes little to recovery from acidification. Another study in unelicited peritoneal macrophages confirmed these findings, and also indicated that the vacuolar H^+-ATPase might contribute to resting pH_i (30, 31).

The goal of this study was to determine whether the Na^+/H^+ exchanger and/or the vacuolar H^+-ATPase regulate pH_i in the J774 murine macrophage-like cell line and to compare these results with those obtained in primary cells. J774 cells have been used extensively in other studies of ion transport (18) and macrophage function (27). pH_i was measured by 2′,7′-bis(carboxyethyl)-5(6)-carboxyfluorescein (BCECF) fluorescence. Corresponding measurements of H^+ efflux were used to verify that changes in pH_i were due to transport of H^+ equivalents. Inhibitors of H^+ transport were used to distinguish between the various classes of H^+ extrusion processes and to dissect out their relative contributions to pH_i regulation. We found that Na^+/H^+ exchange was primarily responsible for recovery from an acid load and did not contribute to resting pH_i. A transporter sensitive to *p*-chloromercuriphenylsulfonic acid (pCMBS) and bafilomycin A_1, presumably a vacuolar H^+-ATPase, contributed significantly to resting pH_i and also to a late phase of recovery from acidification that was distinct from the earlier amiloride-sensitive phase. Thus cultured J774.1 macrophages use different methods for pH_i regulation than primary cells use.

METHODS

Cell Culture

J774 (J774A.1) cells were obtained from American Type Culture Collection (Rockville, MD) and maintained in spinner culture for no longer than 2 mo. Culture medium (RPMI 1640; GIBCO, Grand Island, NY) was supplemented with 5% fetal calf serum, 4 mM glutamine, and 100 U/ml penicillin-streptomycin. Cells were fed at least 12 h before each experiment.

pH_i Measurements

The fluorescent pH indicator BCECF was used to measure pH_i. Fluorescence was measured on an SLM-8000C fluorimeter (SLM Instruments, Urbana, IL). Fluorescence of BCECF at 529 ± 4 nm was measured for excitation at 497 ± 4 and 437 ± 4 nm and was expressed as the ratio of the two measurements.

Measurements were made on both nonadherent (suspended) and adherent cells in cuvettes containing 2 ml of a continuously stirring test solution at 37°C. Adherent cells were plated on 9 × 35-mm coverslips at least 24–48 h before the experiment. Loading with 3 μM BCECF-acetoxymethyl ester (AM) was carried out in media or in NaCl-Hanks' solution plus 5 mM glucose for 30–45 min at 37°C. After

loading, nonadherent cells were centrifuged and resuspended in NaCl-Hanks' solution plus glucose; adherent cells were rinsed several times. Cells were kept at 37°C 10–15 min to allow complete hydrolysis of BCECF. Coverslips of adherent cells were then mounted on a Teflon holder and placed in the cuvette at an ~30° angle to the incident light beam. Nonadherent cells were centrifuged again immediately before placement in the cuvette, which reduced extracellular fluorescence to ~10% of the total fluorescence in the cells plus supernatant. Additional washes did not significantly reduce the amount of extracellular dye. No correction was made for extracellular fluorescence when calculating pH_i. Background autofluorescence of J774 cells was negligible.

Calibration

The fluorescence signal was calibrated using a variation of the method of Thomas et al. (32). BCECF-loaded cells were exposed to 145 mM KCl Hanks' solutions of varying pH plus 3 μM nigericin and 3 μM valinomycin for 10–15 min, which resulted in the equilibration of pH_i and extracellular pH, and fluorescence ratios were obtained at each pH. Adherent and nonadherent cells were calibrated separately. The resulting calibration curve was fitted by a sigmoid equation of the form $y = A + \{B/[1 + e^{-(x-C)/D}]\}$, where A and $A + B$ correspond to the theoretical minimum and maximum values of the curve, C corresponds to the apparent pK_a for BCECF, and D represents the slope of the curve. These parameters were used to calculate pH_i from observed fluorescence ratios. In some experiments, we calibrated each individual coverslip using the one-point calibration method of Boyarsky et al. (7). Although this method reduced the day-to-day variability of the pH_i measurements, it did not qualitatively affect the results.

Leak Measurements

In J774 cells, fluorescent dyes such as Lucifer yellow and fura 2 are both extruded across the plasma membrane and sequestered into intracellular vacuoles via a probenecid-sensitive anion transporter (9, 16). Therefore, we examined J774 cells for evidence of BCECF leak and/or sequestration. Adherent cells were exposed to BCECF-AM for 30–120 min in media or in NaCl-Hanks' solution plus glucose and albumin, washed, and maintained at 37°C for various time periods, then examined using digital video microscopy. Morphology of BCECF-loaded cells appeared normal. BCECF was distributed homogeneously throughout the cytoplasm in >95% of the several dozen cells examined, and no sequestration was observed up to 1.5 h after loading. In only a few cells were large vacuoles (2–5 μM) observed that showed low levels of fluorescence, indicating either exclusion of the dye or low pH. Thus BCECF should accurately report cytoplasmic pH in J774 cells.

Measurement of the rate of leak of BCECF from nonadherent J774 cells was made by loading cells with BCECF, washing them, then repelleting them at various times after loading was complete, and measuring the fraction of fluorescence remaining in the cell pellet vs. supernatant with time. Leak of BCECF from J774 cells followed an exponential time course, with a rate coefficient at 37°C of 0.016 ± 0.001 min^{-1} (SE; $n = 6$). A similar value was obtained for adherent cells. The rate of leak was reduced by 80 and 87% for cells cooled to 25 or 4°C, respectively. The rate of BCECF leak was reduced to only 46 ± 4% of control ($n = 3$) by 2.5 mM probenecid, which inhibits fura 2 leak from J774 cells (16); 5 mM probenecid did not produce further inhibition (51%, $n = 2$). Because the rate of leak from J774 cells was high, continuous fluorescence measurements on suspended cells were restricted to ~6 min to avoid error from the accumulation of extracellular dye. Longer duration measurements could be made on adherent cells, which were transferred to new cuvettes containing fresh solution if measurements exceeded 10 min.

Functional Assays

Because the by-products of intracellular deesterification of BCECF are toxic, cell viability after loading with BCECF was measured by trypan blue exclusion. J774 cells were loaded with 1 or 10 μM BCECF, washed and plated, and maintained either at room temperature in NaCl-Hanks' solution plus glucose or in media at 37°C. J774 cells were >90% viable up to 4 h after loading with BCECF. Phagocytosis of chromium-labeled opsonized red blood cells (21) was measured at 0 and 2 h after loading with 1 μM BCECF and was not inhibited compared with nonloaded controls.

Measurement of Recovery from Acidification

J774 cells were acidified using the ammonium prepulse technique (5). Cells were first alkalinized by exposure to NH_4Cl containing Hanks' solution for 15 min at 37°C, then acidified by a 2-min exposure to Na^+-free Hanks' solution. Recovery from acidification over time was then followed in Na^+-containing or Na^+-free Hanks' solution ± test drug. In NaCl-Hanks' solution, control recovery of pH_i over time followed a roughly exponential time course. The initial rate of recovery was measured by carrying out a linear least-squares fit to the first 30 s of the tracing. The rates of subsequent phases of recovery were measured over times specified for a given experiment.

Measurement of Buffering Power

Measurements of intracellular buffering power (β) were carried out over the range 7.4–7.6 by adding small aliquots of NH_4Cl (final concn, 10 mM) to a suspension of BCECF-loaded J774 cells, and measuring the resultant change in pH_i. β was calculated from the equation $\beta = \delta[NH_4^+]_i/\delta pH_i$ (25). $[NH_4^+]_i$ was calculated from the Henderson-Hasselbach equation: $[NH_4^+]_i = [NH_3]_i \times 10^{pK_a - pH_i}$, assuming $[NH_3]_i = [NH_3]_o$ and where $[NH_3]_o$ is extracellular NH_3 concentration and was calculated from the known amount of NH_4Cl added to the solution. pK_a of NH_4Cl = 9.49 at 37°C (15). Over the pH_i range 7.38–7.57, β was found to be 28 ± 2 mM ($n = 7$).

Measurement of H^+ Efflux

Extrusion of H^+ equivalents from nonadherent cells (2 ml of 2×10^6 cells/ml) was monitored in a continuously stirred cuvette at 37°C by measuring the change in pH of a weakly buffered [500 μM *N*-2-hydroxyethylpiperazine-*N'*-2-ethanesulfonic acid (HEPES)] NaCl-Hanks' solution between the pH range of 7.4–7.2. Control rates of efflux, measured repetitively, were stable for at least 20 min. Ion transport inhibitors were added directly to the cuvette. Control experiments showed that drug carriers dimethyl sulfoxide and ethanol did not affect H^+ efflux. The rate of H^+ extrusion was calculated from the following relationship: H^+ flux = β × δpH, where β was the buffering power of the bathing solution, which was determined by titration to be 0.98 mM.

Solutions and Reagents

NaCl-Hanks' solution consisted of (in mM) 145 NaCl, 4.5 KCl, 1.6 $CaCl_2$, 1.2 $MgCl_2$, and 10 HEPES, pH 7.4. KCl-Hanks' solution was made by replacing NaCl with KCl. For Na^+ substitution experiments, Na^+ was replaced with an equimolar amount of *N*-methylglucamine (NMG). NH_4Cl-Hanks' solution contained 30 mM NH_4Cl replacing an equimolar amount

of NaCl. Bicarbonate containing NaCl-Hanks' solution was made by replacing HEPES with 21 mM $NaHCO_3^-$. When equilibrated with 5% CO_2 at 37°C, pH was 7.4. All solutions contained 5 mM glucose. Some also contained 0.02% bovine serum albumin (BSA), which was without effect on pH_i measurements. For calibration curves, KCl-Hanks' solutions were buffered with piperazine-*N*,*N*'-bis(2-ethanesulfonic acid) between pH 6 and 6.9, HEPES between pH 7 and 8, and *N*-tris(hydroxymethyl)methyl-3-aminopropane sulfonic acid above pH 8. Na^+ and K^+ content of each solution was determined with an Instrumentation Laboratory 943 flame photometer (Lexington, MA). Osmolarity was measured with a vapor pressure osmometer (Wescor, Logan, UT) and averaged 290 mosM.

BCECF was obtained from Molecular Probes (Eugene, OR). Bafilomycin A_1 was a generous gift of Dr. K. Altendorf, University of Osnabruck, Germany. Because the available quantity of bafilomycin A_1 was small, experiments with it were limited. All other drugs and reagents were obtained from Sigma Chemical (St. Louis, MO).

Statistical Methods

Mean values were considered to be significantly different if $P < 0.05$ using Student's *t*-test. Curve fits were carried out on a VAX 11/750, using the RS1 statistical package (BBN Software Products, Cambridge, MA).

RESULTS

Measurement of Resting pH_i

The pH_i of nonadherent J774 cells in nominally HCO_3^--free HEPES-buffered NaCl-Hanks' solution (+ glucose and BSA) at 37°C was 7.53 ± 0.02 (n = 86). Maintaining the cells under adherent culture conditions, which has previously been shown to dramatically affect membrane potential (17), did not affect pH_i. The pH_i of cells that were adherent for 24 h was 7.59 ± 0.02 (n = 97). These unusually alkaline resting pH_i values were reduced only slightly in the presence of HCO_3^-/CO_2 to 7.41 ± 0.02 (n = 12) and 7.40 ± 0.01 (n = 28) for nonadherent and adherent cells, respectively, indicating that HCO_3^--independent processes are largely responsible for maintaining pH_i. Therefore, using inhibitors, we focused on characterizing the roles of the Na^+/H^+ exchanger and the ATP-dependent H^+ pump in setting resting pH_i in these cells.

Effect of Inhibitors of Na^+/H^+ Exchange and the H^+-ATPase on Steady-State pH_i and H^+ Efflux

Table 1 lists the inhibitors of H^+ extrusion used to distinguish between the activity of the Na^+/H^+ exchanger and the various classes of H^+-ATPases, including their sites of action and concentrations. Figure 1*A* shows the effect of these agents on resting pH_i in J774 cells, expressed as the change in pH_i after exposure to the drug. Amiloride did not affect resting pH_i at concentrations up to 1 mM for exposures up to 30 min. In contrast, inhibitors of H^+-ATPase activity all resulted in a reduction in pH_i. Bafilomycin A_1 (13 μM) caused an 0.2 pH unit reduction, whereas pCBMS (100 μM), 7-chloro-4-nitrobenz-2-oxa-1,3-diazide (NBD; 100 μM), and *N*-ethylmaleimide (NEM; 1 mM) resulted in larger reductions (0.4 to 0.7 pH units). The effects of these four

Table 1. *Ion transport inhibitors*

Agent	Concn	Target
Amiloride	100 μM	Na^+/H^+ exchanger
Bafilomycin A_1	13–26 μM	Vacuolar H^+-ATPase
pCMBS	125 μM	Vacuolar H^+-ATPase
NBD	100 μM	Vacuolar H^+-ATPase
NEM	1 mM	Vacuolar H^+-ATPase
Oligomycin	2 μM	Mitochondrial H^+-ATPase
Na azide	1 mM	Mitochondrial H^+-ATPase
Vanadate	100 μM	Na^+ or H^+-K^+-ATPase
Ouabain	100 μM	Na^+-K^+-ATPase

pCMBS, *p*-chloromercuribenzene sulfonic acid; NBD, 7-chloro-4-nitrobenz-2-oxa-1,3-diazole; NEM, *N*-ethylmaleimide.

agents began within seconds, but the full effect was achieved only after 5–10 min. The reduction of pH_i by bafilomycin A_1 was reversible, but the effects of pCMBS and NBD were not. Amiloride, when applied after bafilomycin, produced no further reduction in pH_i (n = 4). Oligomycin (1 μM), azide (100 μM), vanadate (100 μM), and ouabain (100 μM) did not affect resting pH_i for exposures up to 20 min. Similar results were found on nonadherent cells (data not shown). Use of trypan blue exclusion as a measure of cell viability verified that none of the drugs that induced a drop in pH_i affected viability of the cells for up to 2 h. However, morphological changes (e.g., rounding and disattachment) were noted for cells exposed to NBD. To rule out the possibility that the drug-induced changes in pH_i were due to direct effects on BCECF fluorescence, the ability of each agent to quench a 1.5 μM solution of BCECF acid over 10–20 min was measured. Only NBD produced a small effect, which was insufficient to account for the observed drop in cellular pH_i.

To determine whether the drop in pH_i was due to inhibition of transport of H^+ equivalents across the plasma membrane, the effect of each drug on steady-state H^+ efflux was also measured (Fig. 1*B*). Efflux of H^+ equivalents was estimated by measuring the rate of pH change of a suspension of J774 cells in a weakly buffered NaCl-Hanks' solution. The results, which are expressed as percent control H^+ efflux, show a good correlation between drugs that reduced pH_i (bafilomycin A_1, pCMBS, NBD, and NEM) and those that inhibited H^+ efflux. Bafilomycin A_1, which produced the smallest decline in pH_i, also produced the smallest decrease in H^+ efflux. The actual value for control steady-state H^+ efflux, calculated as described in METHODS, was 9–25 $nM \cdot min^{-1} \cdot 10^6$ cells^{-1} across several different batches of cells.

To determine whether the observed inhibition of H^+ efflux by bafilomycin A_1 could account for the bafilomycin-induced reduction in pH_i, we calculated the δpH_i expected to result from the measured bafilomycin-induced reduction in H^+ efflux from the equation $\delta pH_i \times \beta = \delta H^+$ efflux, where β is intracellular buffering power (28 mM; see METHODS). Since H^+ efflux was measured per 10^6 cells/min, we estimated the volume of 10^6 cells to adjust β to the appropriate cell volume. Assuming an average cell diameter of 20 μM (17), the volume of 10^6 cells was estimated to be 4.2 μl. Bafilomycin A_1 reduced

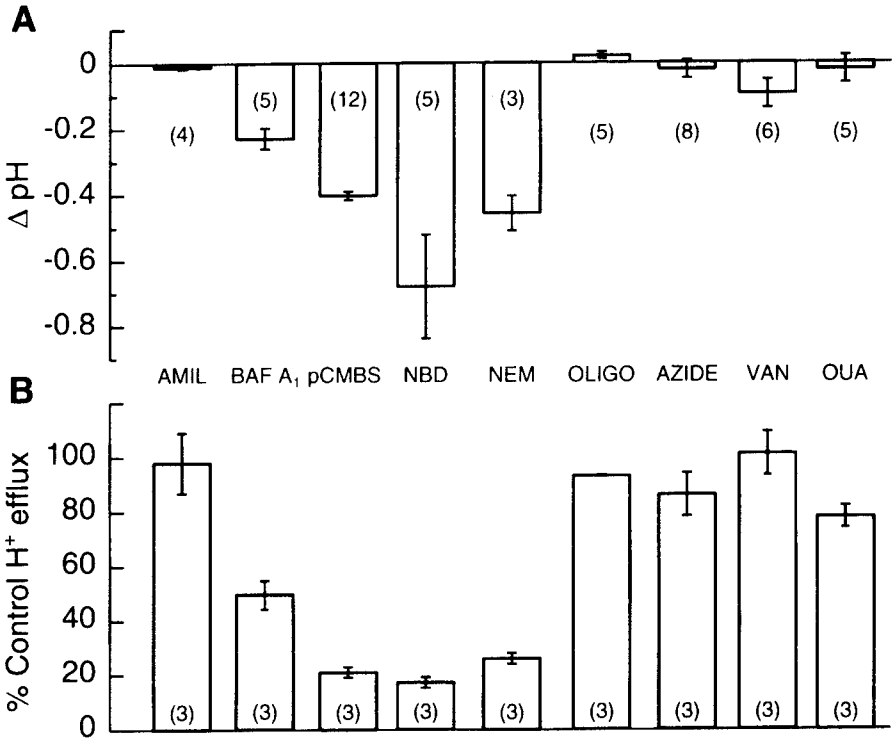

Fig. 1. *A*: effect of H^+ transport inhibitors on resting intracellular pH (pH_i) of adherent J774 cells. *B*: H^+ transport inhibitors on steady-state H^+ efflux from nonadherent J774 cells. Number of observations are in parentheses. AMIL, amiloride; BAF A, bafilomycin A; pCMBS, *p*-chloromercuriphenylsulfonic acid; NBD, 7-chloro-4-nitrobenz-2-oxa-1,3-diazide; NEM, *N*-ethylmaleimide; OLIGO, oligomycin; VAN, vanadate; and OUA, ouabain.

resting flux by ~50%, or an average of 8 $nM \cdot 10^6$ $cells^{-1} \cdot min^{-1}$, which yield a predicted drop of 0.07 pH units/min. This is very near the observed rate of decrease in pH_i induced by bafilomycin A_1 (the average 0.2 pH unit drop was observed over 2–4 min). Thus the inhibition of H^+ efflux induced by bafilomycin A_1 can account for the observed change in pH_i.

Recovery From Intracellular Acidification

Characterization of Na^+/H^+ exchange. J774 cells acidified to a pH_i of ~6.5 by ammonium prepulse recover by extruding H^+ equivalents. In NaCl-Hanks' solution, the time course of recovery is exponential and is 90% complete within 2 min for both adherent (Fig. 2, *trace a*) and nonadherent cells. The replacement of external Na^+ by NMG (Fig. 2, *trace b*) or the addition of 500 μM amiloride inhibited the initial rate of recovery by ~90% (Fig. 2, *trace c*). The rate of recovery was dependent on pH_i, being faster at lower pH_i.

Figure 3, *A* and *B*, show the dose dependence for Na^+ and amiloride. To obtain the data in Fig. 3*A*, cells were acidified and allowed to recover in solutions containing various concentrations of Na^+, and the initial rate of recovery was plotted vs. $[Na^+]_o$. The results were fit by a Michaelis-Menten equation yielding an apparent Michaelis-Menten constant for Na^+ of 79 ± 13 mM. Inhibition of recovery by amiloride was measured by acidifying the cells and allowing them to recover in the presence of NaCl-Hanks' solution plus varying concentrations of amiloride. The initial rate of recovery as a percent of control is plotted vs. amiloride concentration in Fig. 3*B*. An apparent 50% inhibition ($K_{½}$) of 2 ± 0.7 μM was obtained. Maximal inhibition of recovery (≈90%) in the presence of 100 μM amiloride was approximately the same as was observed in Na^+-free solution. Thus these data indicate that, in J774 cells, Na^+/H^+ exchange is the primary mechanism of recovery from intracellular acidification under bicarbonate-free conditions.

Characterization of an amiloride-insensitive component of recovery. Although recovery was significantly reduced by inhibiting Na^+/H^+ exchange, Figure 2, *traces b* and *c*, shows that, under Na^+-free conditions or in the presence of amiloride, a small component of recovery

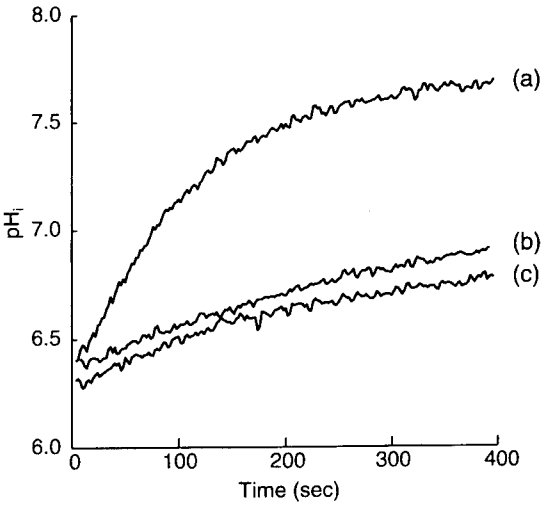

Fig. 2. Graph of pH_i vs. time for nonadherent cells showing recovery of acidified cells in NaCl-Hanks' solution (*trace a*), inhibition of recovery in Na^+-free Hanks' (*trace b*), and inhibition of recovery by 500 μM amiloride (*trace c*). Amiloride was added directly to cuvette at *time zero*. In this figure and subsequent figures of recovery, *time zero* is the time at which cells were exposed to recovery solution after preexposure to NH_4Cl (15 min) and Na^+-free Hanks' solution (2 min).

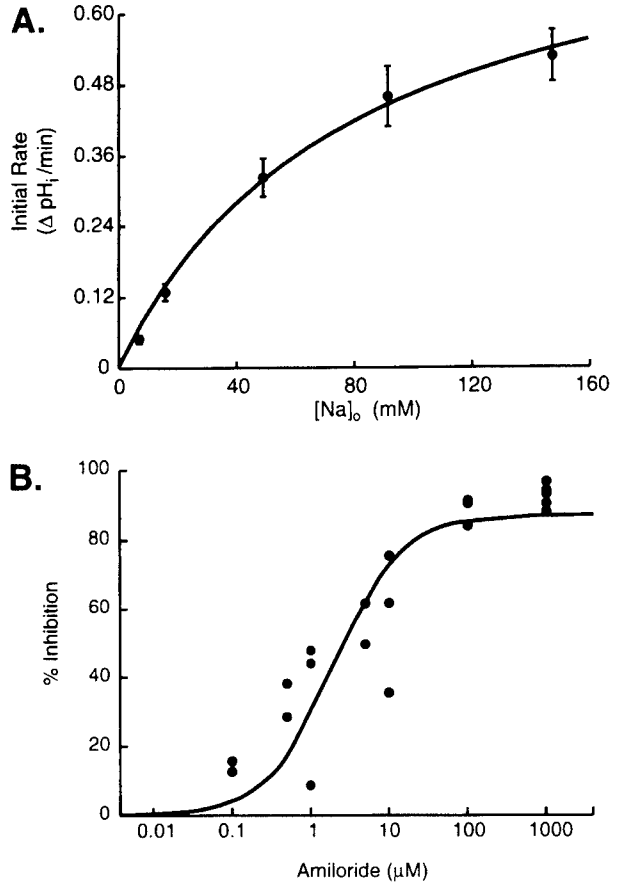

Fig. 3. *A*: graph of initial rate of recovery vs. extracellular Na^+ concentration ($[Na^+]_o$). Data were fit by the Michaelis-Menten equation with 2 free parameters, maximum velocity (V_{max}) and Michaelis-Menten constant (K_m) as follows: $V = V_{max} \cdot [Na^+]_o/(K_m + [Na^+]_o)$. *B*: graph of %inhibition of initial rate of recovery vs. amiloride concentration. Initial rates in presence of varying concentrations of amiloride were expressed as a percentage of control. Data were fit using a modified Michaelis-Menten equation of the form: %inhibition = %maximal inhibition·[AMIL]/($K_{½}$ + [AMIL]). Experiments were carried out on nonadherent cells. $K_{½}$, 50% inhibition.

remained. To determine whether this component of recovery was mediated by the H^+-ATPase, the effects of the H^+-ATPase inhibitors NBD, NEM, and pCMBS were tested. Figure 4 shows the effect of NBD. The amiloride-insensitive component is evident in Fig. 4, *trace a*, which shows recovery in NaCl-Hanks' solution with 100 μM amiloride present throughout. Figure 4, *trace b*, shows recovery in the presence of NaCl-Hanks' solution, with amiloride added at ~75 s. Recovery was attenuated but, by 400 s, was proceeding at the same rate as in Fig. 4, *trace a*. When 100 μM NBD was added at this juncture, recovery was completely inhibited. However, the effect of NBD was not selective for the amiloride-insensitive component. Cells that were exposed to NBD before being placed in NaCl-Hanks' solution for recovery showed no ability to recover from acidification (Fig. 4, *trace c*), indicating that NBD inhibited the amiloride-sensitive component of recovery as well.

NEM inhibited recovery from acidification similarly to NBD (Fig. 5). Figure 5, *trace a*, shows control

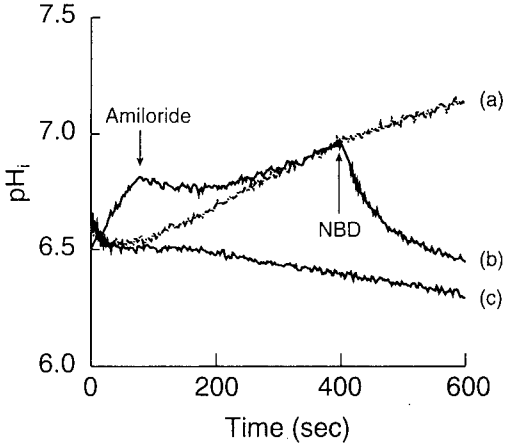

Fig. 4. Graph of pH_i vs. time showing effect of NBD on recovery from intracellular acidification. Recovery from acidification in NaCl-Hanks' solution plus 100 μM amiloride (*trace a*). Recovery in NaCl-Hanks' solution (*trace b*). At arrow, 100 μM amiloride was added. Recovery was attenuated, but not fully inhibited. At 400 s, 100 μM NBD was added, and amiloride-sensitive component of recovery was inhibited. Recovery in NaCl-Hanks' solution plus 100 μM NBD (*trace c*). Both amiloride-sensitive and amiloride-insensitive components of recovery are completely inhibited. Cells were preexposed to NBD for 20 min before recovery, i.e., at the time that they were exposed to NH_4Cl. Adherent cells were used.

recovery in NaCl-Hanks' solution. Figure 5, *trace b*, shows recovery in the absence of Na^+ and represents the amiloride-insensitive component of recovery, since Na^+/H^+ exchange does not occur in the absence of external Na^+. This amiloride-insensitive component was completely inhibited by 1 mM NEM (Fig. 5, *trace c*). However, like NBD, the effect of NEM was nonspecific; i.e., NEM also significantly inhibited the amiloride-sensitive component of recovery as well (Fig. 5, *trace d*).

The effects of pCMBS on the amiloride-insensitive component of recovery were ambiguous. pCMBS did not fully inhibit this component as NEM and NBD did. Because inhibition by pCMBS was partial at best, it was necessary to measure the rate of recovery for cells bathed in Na^+-free Hanks' solution plus 100 μM amiloride with or without 100 μM pCMBS, and compare the means of many traces. Values for the mean rates of

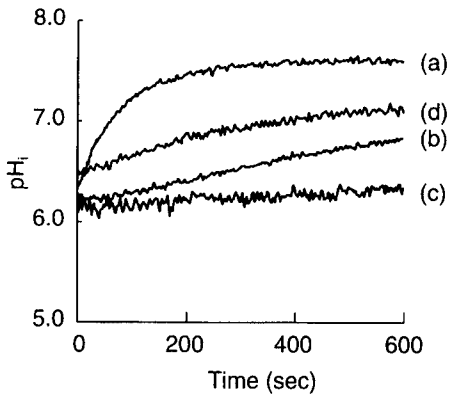

Fig. 5. Graph of pH_i vs. time showing effect of NEM on the recovery from acidification. Control recovery in NaCl-Hanks' solution (*trace a*). Recovery in Na^+-free Hanks' solution (*trace b*). Recovery in Na^+-free Hanks' solution plus 1 mM NEM (*trace c*). Recovery in Na^+-Hanks' plus 1 mM NEM (*trace d*).

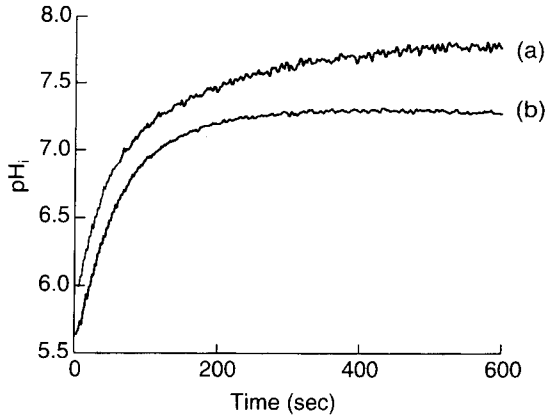

Fig. 6. Graph of pH_i vs. time showing effect of pCMBS on recovery from intracellular acidification. Recovery in NaCl-Hanks' solution (*trace a*). Recovery in NaCl-Hanks' solution plus 100 μM pCMBS (*trace b*). Cells were exposed to pCMBS for 20 min before recovery, i.e., at the time when the cells were exposed to NH_4Cl.

recovery for control and pCMBS-treated cells were $1.17 \pm 0.15 \times 10^{-3}$ pH units/s ($n = 10$) vs. $9.35 \pm 1.81 \times 10^{-4}$ pH units/s ($n = 8$), respectively, and were not significantly different. No other H^+-ATPase inhibitors (azide, oligomycin, vanadate, or ouabain; $n = 3$ each) affected the amiloride-insensitive component of recovery. Bafilomycin A_1 was not tested due to limited supply of the drug.

Since the amiloride-insensitive process that mediated recovery was not definitively identified, there remained the possibility that the slow component of recovery was an artifact of BCECF leak from the acidic intracellular compartment to the more alkaline external solution. The effect of probenecid on the rate of recovery was therefore measured. Cells that were acidified and allowed to recover in Na^+-free Hanks' plus amiloride showed nearly identical rates of recovery in the presence or absence of 2.5 mM probenecid ($1.40 \pm 0.05 \times 10^{-3}$ vs. $1.36 \pm 0.07 \times 10^{-3}$ pH_i/s; $n = 5$ each). Thus it is unlikely that this component of recovery was due to BCECF leak.

Characterization of a late phase of recovery. After acidification, the Na^+/H^+ exchanger alkalinizes J774 cells but is clearly not active at the resting pH_i of 7.5. Figure 2 demonstrated that in this pH range, only inhibitors of vacuolar H^+-ATPase activity can reduce resting pH_i. Could the H^+-ATPase inhibitors also prevent the final phase of recovery after acidification to pH_i 7.5? Figure 6, *trace a*, shows an example of recovery in the presence of NaCl-Hanks' solution, whose time course is clearly biphasic and was best fit by a biexponential function (data not shown). One hundred micromoles per liter pCMBS (Fig. 6, *trace b*) effectively inhibited only the late phase and not the early amiloride-sensitive phase of recovery. To quantitate the effect of pCMBS, linear least-squares fits to early (0–30 s) and late (400–600 s) portions of the curve were carried out. Table 2 shows that pCMBS inhibited only the late phase. Bafilomycin produced similar inhibition of the late phase of recovery, without affecting the early phase (data not shown). No other H^+-ATPase inhibitor tested (oligomycin, azide, vanadate, or ouabain) inhibited either phase of recovery. In the presence of pCMBS, the early phase of recovery remained sensitive to amiloride (Fig. 7). Figure 7, *traces a* and *b*, illustrates the time course of recovery in the presence of NaCl-Hanks' solution with or without 100 μM pCMBS. In Fig. 7, *trace b*, amiloride was added at ~30 s, and attenuation of recovery was observed, further demonstrating that pCMBS did not affect Na^+/H^+ exchange and selectively inhibited only the late phase of recovery.

Table 2. *Effect of pCMBS on recovery from acidification*

Recovery Rate, ΔpH/s	Control	pCMBS	%Control
Initial (0–30 s)	$2.0 \times 10^{-2} \pm 4.2 \times 10^{-4}$	$2.4 \times 10^{-2} \pm 1.1 \times 10^{-4}$	122
n	4	7	
Final (400–600 s)	$4.2 \times 10^{-4} \pm 1.1 \times 10^{-4}$	$1.9 \times 10^{-5} \pm 4.8 \times 10^{-6}$	4.5
n	7	7	

Values are means ± SE.

DISCUSSION

This study demonstrates that J774 cells regulate pH_i under nominally HCO_3^--free conditions using at least two H^+ extrusion mechanisms: a conventional amiloride-sensitive Na^+/H^+ exchanger and a transporter sensitive to bafilomycin A_1 and other agents that inhibit vacuolar type H^+-ATPases. The resting pH_i of nonadherent J774 cells under HCO_3^--free conditions was found to be 7.53, which is more alkaline than the resting pH_i values of 7.1–7.3 reported for primary macrophages from mouse and rabbit (3, 29), but is not unusually high for a tumor cell line (10, 22, 23, 26). Resting pH_i could be lowered to 7.4 by exposure to HCO_3^-/CO_2 buffer. This may indicate the presence of a Na^+-independent Cl^-/HCO_3^- exchange mechanism, which acidifies cells when there is an inward gradient for Cl^- (12). The pH_i of a population of nonadherent J774 cells was not significantly different from adherent cells (7.59 pH units). Others, using video microscopy of single cells, have observed a slight (0.1 pH unit) adherence-induced alkalinization in fibroblasts (26) and endothelial cells (14).

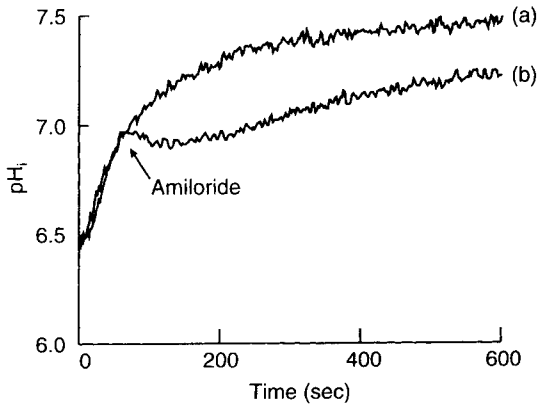

Fig. 7. Effect of amiloride on recovery from acidification in the presence of pCMBS. Recovery in NaCl-Hanks' solution (*trace a*). Recovery in 100 μM pCMBS (*trace b*). At ~50 s, 100 μM amiloride was added, and recovery was attenuated.

It is unlikely that resting pH_i values were influenced by nonuniform distribution of BCECF inside the cell. Although J774 cells are known to sequester other anionic fluorescent dyes such as Lucifer yellow (16) and fura 2 (9) into large vesicles, we found no visual evidence for sequestration and could effect only partial inhibition of BCECF leak with 5 mM probenecid. Thus the anion transport mechanism responsible for sequestration and efflux of fura 2 and Lucifer yellow apparently does not effectively transport BCECF in these cells.

Resting pH_i was unaffected by inhibitors of Na^+/H^+ exchange or of P-type or F_1F_0-ATPases (Fig. 1*A*). Inhibitors of the vacuolar H^+-ATPase reduced pH_i by varying amounts (0.2–0.7 pH units). The most potent and specific inhibitor, bafilomycin A_1 (6, 34), reduced pH_i the least and is probably the truest measure of the contribution of a vacuolar H^+-ATPase to the resting pH_i of J774 cells. The other three vacuolar ATPase inhibitors, NEM, NBD, and pCMBS, are all sulfhydryl reagents that covalently modify protein structure, and although they inhibit the vacuolar ATPase in many preparations (1, 13, 24, 33), they are both less potent and less specific.

We verified that the reduction in pH_i by H^+-ATPase inhibitors was due to an inhibition of H^+-equivalent extrusion (Fig. 1*B*) and was not due to cytotoxicity of the drugs or artifactual quenching of BCECF. The absolute level of steady-state H^+ efflux (9–25 $nM \cdot 10^6$ $cells^{-1} \cdot min^{-1}$) in J774 cells was higher than that reported for primary pulmonary macrophages (2.75 $nM \cdot 10^6$ $cells^{-1} \cdot min^{-1}$; Ref. 3), which also have a lower resting pH_i of 7.24. The source(s) of this steady-state H^+ efflux have not been identified, and could include organic as well as inorganic acids. It should be noted that bafilomycin A_1 inhibited only about one-half of the total steady-state H^+ efflux. The amount of inhibition produced by bafilomycin A_1 was sufficient to account for the observed bafilomycin-induced drop in pH_i. After exposure to bafilomycin, resting pH_i remained in the range of 7.2, and exposure to amiloride did not further reduce it. Thus it appears that even after the H^+-ATPase was inhibited, some process other than Na^+/H^+ exchange was able to maintain resting pH_i well above equilibrium.

Recovery from an imposed acid load was essentially complete within 2 min and could be inhibited by removal of external Na^+ or exposure to amiloride (100 μM; Figs. 2 and 3), indicating that it was mediated by a Na^+/H^+ exchanger. The low dissociation constant for amiloride (2 μM; Fig. 3*A*) is similar to that observed in other myeloid cells, including HL-60 cells and human neutrophils (8). The amiloride-sensitive portion of recovery was also nonspecifically inhibited by NBD and NEM (Figs. 4 and 5), but not by pCMBS (Figs. 6 and 7), bafilomycin A_1, or any of the other ATPase inhibitors. It is therefore unlikely that a H^+-ATPase contributes much to this early (0–60 s), rapid phase of recovery.

The late phase of recovery (400–600 s), which covered the pH_i range above 7.0, could be selectively inhibited by pCMBS (Fig. 6). In the presence of pCMBS, amiloride sensitivity was preserved (Fig. 7), indicating that the pCMBS-sensitive process was distinct from Na^+/H^+ exchange. It is likely that the same H^+ extrusion process responsible for maintaining an alkaline resting pH_i contributes to the late phase of recovery from an acid load.

The slow component of recovery observed in the presence of amiloride or the absence of external Na^+ (Fig. 2) was fully inhibited by NEM and NBD (Figs. 4 and 5), but not by pCMBS or any of the other H^+-ATPase inhibitors (bafilomycin A_1 was not tested). Definitive identification remains to be completed.

In summary, our results indicate that J774 cells, like other primary macrophages, express a vacuolar H^+-ATPase in their plasma membrane that can contribute to pH_i regulation. Under nominally bicarbonate-free conditions, this vacuolar H^+-ATPase contributes significantly to the maintenance of an unusually alkaline resting pH_i. Unlike primary macrophages, J774 cells do not use the H^+-ATPase for recovery from an acid load, using instead a conventional Na^+/H^+ exchanger. It is not yet clear whether the H^+-ATPase serves other functions besides pH_i regulation. At least one type of macrophage-like cell, the osteoclast, uses a H^+-ATPase specifically to acidify its microenvironment, which aids in the breakdown of bone matrix (4). It is possible that external acidification may enhance the activity of cytotoxic products that are secreted by activated macrophages during pathogen killing. Finally, it is possible that the high level of activity of the H^+-ATPase in J774 cells is correlated with their mitotic state. Treatment of J774 cells with lipopolysaccharide or radiation, which causes cessation of cell division, results in a 0.2–0.3 pH unit reduction of resting pH_i after several days (McKinney, unpublished observations). Further studies will determine which of the above is true.

We thank Dr. Joel Lowy for help with digital video microscopy, Spencer Green for carrying out functional assays, and Jeanine Faw for excellent technical assistance. Dr. Elaine Gallin kindly reviewed the manuscript.

Portions of this work have been published in abstract form (19, 20).

Address for reprint requests: L. C. McKinney, Dept. of Physiology, AFRRI, 8901 Wisconsin Ave., Bethesda, MD 20889-5603.

Received 30 December 1993; accepted in final form 18 July 1994

REFERENCES

1. **Al-Awqati.,** Q. Proton-translocating ATPases. *Annu. Rev. Cell Biol.* 2: 179–199, 1986.
2. **Bidani, A., and S. E. S. Brown.** ATP-dependent pH_i recovery in lung macrophages: evidence for a plasma membrane H^+-ATPase. *Am. J. Physiol.* 259 (*Cell Physiol.* 28): C586–C598, 1990.
3. **Bidani, A., S. E. S. Brown, T. A. Heming, R. Gurich, and T. D. Dubose, Jr.** Cytoplasmic pH in pulmonary macrophages: recovery from acid load is Na^+ independent and NEM sensitive. *Am. J. Physiol.* 257 (*Cell Physiol.* 26): C65–C76, 1989.
4. **Blair, H. C., S. L. Teitelbaum, R. Ghiselli, and S. Gluck.** Osteoclastic bone resorption by a polarized vacuolar proton pump. *Science Wash. DC* 245: 855–857, 1989.
5. **Boron, W. F., and P. DeWeer.** Intracellular pH transients in squid giant axons caused by CO_2, NH_3, and metabolic inhibitors. *J. Gen. Physiol.* 67: 91–112, 1976.
6. **Bowman, E. J., A. Siebers, and K. Altendorf.** Bafilomycins: A class of inhibitors of membrane ATPases from microorganisms, animal cells, and plant cells. *Proc. Natl. Acad. Sci. USA* 85: 7972–7976, 1988.
7. **Boyarsky, G., M. B. Ganz, R. B. Sterzel, and W. F. Boron.** pH regulation in single glomerular mesangial cells. I. Acid extrusion in absence and presence of HCO_3^-. *Am. J. Physiol.* 255 (*Cell Physiol.* 24): C844–C856, 1988.

8. **Clark, J. D., and L. E. Limbird.** Na^+/H^+ exchanger subtypes: a predictive review. *Am. J. Physiol.* 261 (*Cell Physiol.* 30): C945–C953, 1991.
9. **DiVirgilio, F., T. H. Steinberg, and S. C. Silverstein.** Inhibition of Fura-2 sequestration secretion with organic anion transport blockers. *Cell Calcium* 11: 57–62, 1990.
10. **Doppler, W., R. Jaggi, and B. Groner.** Induction of v-*mos* and activated H-*ras* oncogene expression in quiescent 3T3 cells causes intracellular alkalinisation and cell cycle progression. *Gene* 54: 147–153, 1987.
11. **Gallin, E. K., and L. C. McKinney.** Monovalent ion transport and membrane potential changes during activation in phagocytic leukocytes. In: *Mechanisms of Leukocyte Activation. Current Topics in Membranes and Transport*, edited by S. Grinstein and O. Rotstein. New York: Academic, 1990, vol. 35, p. 127–152.
12. **Grinstein, S., C. J. Swallow, and O. D. Rotstein.** Regulation of cytoplasmic pH in phagocytic cell function and dysfunction. *Clin. Biochem.* 24: 241–247, 1991.
13. **Hilden, S. A., and N. E. Madias.** Effect of sulfhydryl compounds on ATP-stimulated H^+-transport and Cl^- uptake in rabbit renal cortical endosomes. *J. Membr. Biol.* 124: 139–149, 1991.
14. **Ingber, D. E., D. Prusty, J. V. Frangioni, E. J. Cragoi, Jr., C. Lechene, and M. A. Schwartz.** Control of intracellular pH and growth by fibronectin in capillary endothelial cells. *J. Cell Biol.* 110: 1803–1811, 1990.
15. **Jacques, J. A., J. W. Poppell, and R. Jeltsch.** Solubility of ammonia in human plasma. *J. Appl. Physiol.* 14: 255–258, 1959.
16. **Lipman, B. J., S. C. Silverstein, and T. H. Steinberg.** Organic anion transport in macrophage membrane vesicles. *J. Biol. Chem.* 265: 2142–2147, 1990.
17. **McKinney, L. C., and E. K. Gallin.** Effect of adherence, cell morphology, and lipopolysaccharide on potassium conductance and passive membrane properties of murine macrophage J774.1 cells. *J. Membr. Biol.* 116: 47–56, 1990.
18. **McKinney., L. C., and E. K. Gallin.** G protein activators induce a potassium conductance in murine macrophages. *J. Membr. Biol.* 130: 265–276, 1992.
19. **McKinney, L. C., and A. Moran.** Characterization of Na^+/H^+ exchange in the murine macrophage cell line J774.1 (Abstract). In: *Bicarbonate, Chloride, and Proton Transport Systems*, edited by J. H. Durham and M. A. Hardy, 1989, vol. 574, p. 388–389. (Annu. Meet. NY Acad. Sci., New York, Jan. 19–21, 1989)
20. **McKinney, L. C., and A. Moran.** Intracellular pH regulation in J774.1 murine macrophages (Abstract). *J. Gen. Physiol.* 100: 25a, 1992.
21. **Metcalf, J. A., J. I. Gallin, W. M. Nauseef, and R. K. Root.** *Laboratory Manual of Neutrophil Function.* New York: Raven, 1986.
22. **Ober, S. S., and A. B. Pardee.** Intracellular pH is increased after transformation of Chinese hamster embryo fibroblasts. *Proc. Natl. Acad. Sci. USA* 84: 2766–2770, 1987.
23. **Perona, R., and R. Serrano.** Increased pH and tumorigenicity of fibroblasts expressing a yeast proton pump. *Nature Lond.* 334: 438–440. 1988.
24. **Randall, S. K., and H. Sze.** Probing the catalytic subunit of the tonoplast H^+-ATPase from oat roots. *J. Biol. Chem.* 262: 7135–7141, 1987.
25. **Roos, A., and W. F. Boron.** Intracellular pH. *Physiol. Rev.* 61: 296–434, 1981.
26. **Schwartz, M. A., G. Both, and C. L. Lechene.** Effect of cell spreading on cytoplasmic pH in normal and transformed fibroblasts. *Proc. Natl. Acad. Sci. USA* 86: 4525–4529, 1989.
27. **Snyderman, R., M. C. Pike, D. G. Fischer, and H. S. Koren.** Biologic and biochemical activities of continuous macrophage cell lines P388D1 and J774.1. *J. Immunol.* 119: 2060–2066, 1977.
28. **Swallow, C. J., S. Grinstein, and O. D. Rotstein.** A vacuolar type H^+-ATPase regulates cytoplasmic pH in murine macrophages. *J. Biol. Chem.* 265: 7645–7654, 1990.
29. **Swallow, C. J., S. Grinstein, and O. D. Rotstein.** Regulation of cytoplasmic pH in resident and activated peritoneal macrophages. *Biochim. Biophys. Acta* 1022: 203–210, 1990.
30. **Tapper, H., and R. Sundler.** Cytosolic pH regulation in mouse macrophages. Characteristics of HCO_3^--dependent mechanisms. *Biochem. J.* 281: 239–244, 1992.
31. **Tapper, H., and R. Sundler.** Cytosolic pH regulation in mouse macrophages. Proton extrusion by plasma-membrane-localized H^+-ATPase. *Biochem. J.* 281: 245–250, 1992.
32. **Thomas, J. A., R. N. Buchsbaum, A. Zimniak, and E. Racker.** Intracellular pH measurements in Ehrlich ascites tumor cells utilizing spectroscopic probes generated in situ. *Biochemistry* 18: 2210–2218, 1979.
33. **Uchida, E., Y. Ohsumi, and Y. Anraku.** Characterization and function of catalytic subunit *a* of H^+-translocating adenosine triphosphatase from vacuolar membrane of *Saccharomyces cerevisiae*. A study with NBD. *J. Biol. Chem.* 263: 45–51, 1988.
34. **Werner, G., and H. Hagenmaier.** Metabolic products of microorganisms: bafilomycins, a new group of macrolide antibiotics. *J. Antibiot. Tokyo* 37: 110–117, 1984.

EFFECTS OF S-2-(3-METHYLAMINOPROPYLAMINO)-ETHYLPHOSPHOROTHIOIC ACID (WR-3689), ALONE OR COMBINED WITH CAFFEINE, ON CATECHOLAMINE CONCENTRATION OF MOUSE ADRENALS

D. L. Palazzolo and K. S. Kumar

Radiation Biochemistry Department, Armed Forces Radiobiology Research Institute, Bethesda, Maryland, USA

S-2-(3-Methylaminopropylamino)ethylphosphorothioic acid (WR-3689), a radioprotective drug, can alter behavior (as determined by locomotor activity). Since catecholamines are known to modulate locomotor activity, it is possible that WR-3689-induced alterations in behavior are due to changes in catecholamine metabolism. A recent article reported that caffeine can ameliorate WR-3689-induced alterations in behavior; therefore the aim of this study is to determine whether ip injections of WR-3689, caffeine, or a combination of the two drugs affect adrenal catecholamine concentrations. Mice were administered saline (control), WR-3689 (100 or 200 mg/kg), caffeine (20 or 40 mg/kg), or the combined drugs (200 mg/kg WR-3689 and 40 mg/kg caffeine). Adrenals were excised at 0, 1, 2, 4, and 8 h after injections. The concentrations of epinephrine (EPI), norepinephrine (NE), and dopamine (DA) were determined using high-performance liquid chromatography (HPLC). The concentration of EPI increased, 1 h after treatment with 200 mg/kg WR-3689, from 1178 ± 174 ng/mg to 1784 ± 179 ng/mg ($p < .02$), while NE increased from 597 ± 52 ng/mg to 892 ± 118 ng/mg ($p < .04$). The concentration of EPI decreased, 4 h after treatment with 100 mg/kg WR-3689, from 1178 ± 61 ng/mg to 852 ± 122 ng/mg ($p < .04$); NE decreased, 4 h after injection of 100 and 200 mg/kg WR-3689, from 664 ± 50 ng/mg to 396 ± 59 ng/mg ($p < .02$) and 437 ± 80 ng/mg ($p < .03$) respectively. In comparison to controls, WR-3689 had no effect on adrenal DA levels. The concentrations of EPI and NE increased, 1 h after treatment

Received 22 April 1994; accepted 12 July 1994.

This work was supported by the Armed Forces Radiobiology Research Institute, Defense Nuclear Agency, under Work Unit 00162. Research was conducted according to the Guide for the Care and Use of Laboratory Animals prepared by the Institute of Laboratory Animal Resources, National Research Council. We are grateful to W. A. McLean for technical assistance and to Modeste Greenville for editorial assistance.

Address correspondence to Dr. Dominic L. Palazzolo, Nova Southeastern University, Health Professions Division, Basic Sciences Department, 1750 NE 167 Street, North Miami Beach, FL 33162-3017.

with 40 mg/kg caffeine, from 1178 ± 174 ng/mg and 597 ± 52 ng/mg to 1845 ± 193 ng/mg ($p < .01$) and 973 ± 158 ng/mg ($p < .03$), respectively. In comparison to controls, caffeine had no effect on adrenal DA levels. Combined administration of WR-3689 and caffeine increased EPI from 1178 ± 174 to 1871 ± 285 ng/mg ($p < .04$) and NE from 597 ± 52 to 902 ± 143 ng/mg ($p < .05$) 1 h after treatment and abolished the decrease observed in NE 4 h after treatment with WR-3689 alone. This combination also elevated DA from control values of 28 ± 5, 24 ± 4, and 20 ± 3 ng/mg to 45 ± 8 ($p < .05$), 37 ± 4 ($p < .03$), and 40 ± 8 ng/mg ($p < .04$) at 1, 2, and 4 h after treatment, respectively. These results indicate that WR-3689 alters adrenal catecholamine concentrations and that simultaneous administration of WR-3689 and caffeine may offset the NE decrease induced by WR-3689 alone.

Although phosphorothioates are effective radioprotectors (Giambarresi & Jacobs, 1987), they are also known to have toxic effects on mammalian physiology and behavior. For example, one such phosphorothioate, *S*-2-(3-aminopropylamino)ethylphosphorothioic acid (WR-2721), is known to reduce locomotor activity in mice (Landauer et al., 1988), diminish the ability of rats to maintain balance on an accelerod (Bogo et al., 1985), induce hypothermia in rats (Kandasamy et al., 1988), and curtail the ability of monkeys to visually discriminate between tasks (Bogo et al., 1988). In humans, WR-2721 is reported to induce emesis, hypotension, hypocalcemia, and mild somnolence (Kligerman et al., 1984; Glover et al., 1987, 1988). These impairments suggest that phosphorothioates may be centrally and/or peripherally neurotoxic, and could be a result of alterations in the metabolism of neurotransmitter systems, in particular the catecholaminergic system, since catecholamines are known to be involved in the modulation of such activities as sleep, temperature regulation, emesis, and locomotion.

Ideally, radioprotectors should provide a clear measure of radioprotection without affecting performance (Walker, 1988). If phosphorothioates are to be used as a prophylactic treatment for individuals exposed to high levels of radiation, a decrement in performance cannot be tolerated. In the past, a number of various derivatives of WR-2721 were synthesized in hopes that alterations in behavior could be reduced without disrupting the desirable radioprotective efficacy (Sweeney, 1979). One compound that was developed was *S*-2-(3-methylaminopropylamino)ethylphosphorothioic acid (WR-3689), a methylated derivative of WR-2721. It was shown to be less toxic and in some respects superior to WR-2721 (Brown et al., 1988; McDonough et al., 1992). Although WR-3689 appears to be less toxic than the other phosphorothioates, the level of toxicity (as determined by locomotor activity) produced by this compound at radioprotective doses is still unacceptable. In an attempt to reduce this toxicity, caffeine, a central nervous system stimulant,

was administered in combination with WR-3689. It was found that caffeine, when administered simultaneously with WR-3689, ameliorated the decrement in locomotor activity of mice observed when WR-3689 was administered alone (Landauer et al., 1992). In addition, caffeine did not appear to alter the radioprotective efficacy of WR-3689 (Kumar et al., 1990). In a recent study investigating the central effects of WR-3689 alone or in conjunction with caffeine, we found that the combination of WR-3689 and caffeine attenuated the caffeine-induced increase in the hypothalamic content of two catecholamines, norepinephrine (NE) and dopamine (DA), although WR-3689 by itself had no effect (Palazzolo & Kumar, 1993). In this report, we investigate the peripheral effects of WR-3689 on catecholamine concentrations and determine if caffeine can attenuate the WR-3689-induced effects (if any) on catecholamine metabolism.

MATERIALS AND METHODS

Animals

Male CD2F1 mice (Charles River Laboratories, Boston, MA), 8–10 wk old, were housed five per cage in a climate-controlled facility (21 ± 1°C, 50 ± 10% relative humidity, lights on from 0600 to 1800) accredited by the American Association for Accreditation of Laboratory Animal Care. Food and water were provided ad libitum, and the mice were maintained for at least 2 wk before use in the experiments. All work involving animals was conducted in accordance with the Guide for the Care and Use of Laboratory Animals prepared by the Institute of Laboratory Animal Research, National Research Council.

Chemicals

WR-3689 was obtained from the Drug Synthesis and Chemistry Branch, Division of Cancer Treatment, National Cancer Institute (Bethesda, MD). Anhydrous caffeine was purchased from Sigma Chemical Co. (St. Louis, MO).

Experimental Procedures

The experimental procedures outlined below were repeated on 8 separate days to give an n value of 8 for each time point within each treatment group. The procedures were as follows. The night before the experiments were to take place, six groups of mice (five mice per group) were moved to a nearby room to acclimatize them to new surroundings. Beginning at 0830 on the following day, neutralized saline (control;

group 1), WR-3689 (100 and 200 mg/kg; groups 2 and 3), caffeine (20 and 40 mg/kg; groups 4 and 5), or the combination of WR-3689 (200 mg/kg) and caffeine (40 mg/kg) (group 6) was administered ip. One mouse per group was sacrificed by quick cervical dislocation at the time of injection, and the remaining four mice in each group were sacrificed at 1, 2, 4, and 8 h after injection. Immediately after sacrifice, the adrenal glands were excised, the cortical tissue was gently rubbed off onto a paper towel, and the remaining medullary tissue was weighed and placed in 200 μl of .05 *M* perchloric acid ($HClO_4$). The medullary tissue was then sonicated (30 s) using a Heat Systems-Ultrasonics sonicator (Farmingdale, NY) and centrifuged (3 min) using an Eppendorf microcentrifuge (Hamburg, Germany). The supernatant was stored at −80°C until the time of catecholamine analysis.

Analysis

Adrenal catecholamine concentrations were determined using high-performance liquid chromatography (HPLC) with electrochemical detection (Bioanalytical Systems, West Lafayette, IN) (Palazzolo & Quadri, 1989, 1990). Briefly, the HPLC system consisted of an LC-4B electrochemical detector; a 10-cm, Phase II, 3-μm octadecasilane reversed-phase column; and a glassy carbon working electrode. The mobile phase (pH 3.1) was made using pyrogen-free water filtered through a Milli-Q purification system (Millipore Co., Bedford, MA) and consisted of monochloroacetic acid (14.15 g/L), sodium hydroxide (4.675 g/L), disodium EDTA (150 mg/L), octanesulfonic acid (300 mg/L), and 1% acetonitrile. The mobile phase was circulated through the HPLC system with a Beckman 112 solvent delivery pump (Fullerton, CA) at a flow rate of 1.3 ml/min. Detector sensitivity and working electrode potential were set at 100 nA full scale and .65 V (with respect to a Ag/AgCl reference electrode), respectively. Standard and sample injections were made with a Rheodyne 7125 syringe-loading injection valve (Cotati, CA). The column and working electrode were maintained at 30°C inside a Shimadzu CTO-6A column oven (Columbia, MD). Epinephrine (EPI), NE, and DA standards were prepared in 0.05 *M* $HClO_4$. Standard curves, ranging from 12.5 to 2500 ng per 50 μl injection, were generated for each catecholamine. Sample injections (50 μl) consisted of 10 μl of adrenal medullary supernatant plus 40 μl of 0.05 *M* $HClO_4$. The data were collected using a Shimadzu CR-4A chromatopac (Columbia, MD). Mean values (±SE) are expressed as nanograms per milligram wet weight of adrenomedullary tissue. Differences between treatment groups at each time point were determined using Student's *t*-test, where $p < .05$ indicates significance.

RESULTS

The effects of WR-3689, caffeine, or the combination of WR-3689 and caffeine on the adrenal concentrations of EPI, NE, and DA are shown in Table 1. The effects of WR-3689 on adrenal catecholamine concentrations were as follows. Treatment with 100 mg/kg WR-3689 did not alter EPI levels in comparison to control values 1 and 2 h after treatment. This same dose of WR-3689 decreased EPI levels from a control value of 1178 ± 61 ng/mg to 852 ± 122 ng/mg ($p < .04$) 4 h after treatment, but they returned to control levels 8 h after treatment. Treatment with 200 mg/kg WR-3689 increased EPI from a control value of 1178 ± 174 ng/mg to 1784 ± 179 ng/mg ($p < .02$) 1 h after treatment, returned to control levels 2 h after treatment and remained at control levels for the remaining time points. A similar profile was observed for NE. Treatment with 100 mg/kg WR-3689 did not alter NE content in comparison to control values 1 h after treatment. At 2 and 4 h after treatment, this same dose of WR-3689 decreased NE levels from control values of 624 ± 43 and 664 ± 50 ng/mg to 491 ± 44 (not significant) and 396 ± 59 ng/mg ($p < .03$), respectively. Eight hours after treatment with 100 mg/kg WR-3689, NE returned to control levels. Treatment with 200 mg/kg WR-3689 increased NE levels from a control value of 597 ± 52 ng/mg to 892 ± 118 ng/mg ($p < .04$) 1 h after treatment; they returned to control values 2 h after treatment, continued to decrease from a control value of 664 ± 50 to 437 ± 80 ng/mg ($p < .02$) 4 h after treatment, and returned to control levels 8 h after treatment. Treatment with 100 mg/kg WR-3689 did not alter DA levels from control values at any time point. Treatment with 200 mg/kg WR-3689 did not significantly alter DA levels from control values, but in comparison to the 100 mg/kg WR-3689 treatment group, DA levels increased from 25 ± 6 to 37 ± 5 ng/mg ($p < .05$) 1 h after treatment and increased from 18 ± 4 to 31 ± 6 ng/mg ($p < .05$) 4 h after treatment.

The effects of caffeine on adrenal catecholamine concentrations were as follows. In comparison to controls, the 20-mg/kg caffeine treatment had no effect on EPI, NE, and DA at any time point. The 40-mg/kg caffeine treatment increased EPI and NE 1 h after treatment; that is, caffeine increased EPI from a control value of 1178 ± 174 ng/mg to 1845 ± 193 ng/mg ($p < .01$) and increased NE from a control value of 597 ± 52 ng/mg to 973 ± 158 ng/mg ($p < .03$). Concentrations of EPI and NE returned to control levels 2 h after treatment and remained at control levels throughout the remaining time points. Treatment with 40 mg/kg caffeine had no effect on DA levels.

The effects of the combination of WR-3689 and caffeine on adrenal catecholamine concentrations are detailed next. One hour after the combination was administered, EPI increased from a control level of 1178

Table 1. Effect of WR-3689 (100 or 200 mg/kg), caffeine (20 or 40 mg/kg), and the combination of WR-3689 (200 mg/kg) and caffeine (40 mg/kg) on epinephrine, norepinephrine, and dopamine concentrations in mouse adrenals

Parameter and Treatment	Time Postinjection				
	0 h	1 h	2 h	4 h	8 h
Epinephrine (ng/mg)					
Control	1303 ± 257 (5)	1178 ± 174 (5)	1301 ± 128 (8)	1178 ± 61 (6)	1361 ± 177 (7)
WR-3689 (100 mg/kg)	1383 ± 159 (7)	1306 ± 185 (7)	1173 ± 172 (6)	852 ± 122 (6)[a]	1370 ± 208 (7)
WR-3689 (200 mg/kg)	1270 ± 216 (8)	1784 ± 179 (8)[a,b]	1148 ± 164 (7)	1152 ± 160 (7)	1010 ± 188 (5)
Caffeine (20 mg/kg)	1204 ± 98 (7)	1702 ± 272 (6)	1182 ± 305 (5)	1328 ± 195 (8)	1376 ± 104 (8)
Caffeine (40 mg/kg)	1501 ± 111 (6)	1845 ± 193 (5)[a]	1620 ± 220 (8)	1211 ± 166 (7)	1251 ± 244 (4)
Combination	1036 ± 105 (4)	1871 ± 285 (6)[a]	1280 ± 136 (6)	1253 ± 187 (8)	1149 ± 117 (6)
Norepinephrine (ng/mg)					
Control	615 ± 101 (5)	597 ± 52 (5)	624 ± 43 (8)	664 ± 50 (6)	654 ± 81 (7)
WR-3689 (100 mg/kg)	587 ± 76 (7)	581 ± 51 (7)	491 ± 44 (6)	396 ± 59 (6)[a]	581 ± 46 (7)
WR-3689 (200 mg/kg)	599 ± 70 (8)	892 ± 118 (8)[a,b]	556 ± 66 (7)	437 ± 80 (7)[a]	557 ± 116 (5)
Caffeine (20 mg/kg)	573 ± 38 (7)	736 ± 83 (6)	639 ± 118 (5)	673 ± 98 (8)	697 ± 86 (8)
Caffeine (40 mg/kg)	645 ± 61 (6)	973 ± 158 (5)[a]	800 ± 103 (8)	629 ± 58 (7)	646 ± 92 (4)
Combination	538 ± 78 (4)	902 ± 143 (6)[a]	595 ± 55 (6)	644 ± 114 (8)	545 ± 74 (6)
Dopamine (ng/mg)					
Control	31 ± 3 (5)	28 ± 5 (5)	24 ± 4 (8)	20 ± 3 (6)	20 ± 3 (7)
WR-3689 (100 mg/kg)	28 ± 4 (7)	25 ± 6 (7)	26 ± 6 (6)	18 ± 4 (6)	28 ± 8 (7)
WR-3689 (200 mg/kg)	26 ± 5 (8)	37 ± 5 (8)[b]	32 ± 4 (7)	31 ± 6 (7)[b]	22 ± 6 (5)
Caffeine (20 mg/kg)	24 ± 4 (7)	35 ± 5 (6)	25 ± 8 (5)	20 ± 5 (8)	24 ± 4 (8)
Caffeine (40 mg/kg)	32 ± 3 (6)	34 ± 10 (5)	30 ± 6 (8)	18 ± 3 (7)	25 ± 11 (4)
Combination	23 ± 4 (4)	45 ± 8 (6)[a,b]	37 ± 4 (6)[a]	40 ± 8 (8)[a,b,c]	28 ± 6 (5)

Note. Values are given as mean ± SE (n = sample size).
[a]Significantly different from the control group, $p < .05$.
[b]Significantly different from the WR-3689 (100 mg/kg) treatment group, $p < .05$.
[c]Significantly different from the caffeine (40 mg/kg) treatment group, $p < .05$.

± 174 to 1871 ± 285 ng/ml ($p < .04$). Two hours after this treatment, EPI levels returned to control levels and remained at control levels for the remaining time points. Similarly, 1 h after the drug combination was administered, NE increased from a control level of 597 ± 52 to 902 ± 143 ng/ml ($p < .05$), but 2 h after treatment, NE levels returned to control levels and remained at control levels for the remaining time points. This combined treatment of WR-3689 and caffeine abolished the decrease in NE observed 4 h after treatment with WR-3689 (200 mg/kg) alone. Dopamine levels, after simultaneous administration of WR-3689 and caffeine, increased from control levels of 28 ± 5, 24 ± 4, and 20 ± 3 ng/ml to 45 ± 8 ($p < .05$), 37 ± 4 ($p < .03$), and 40 ± 8 ng/ml ($p < .04$) after 1, 2, and 4 h, respectively.

DISCUSSION

This study indicates that WR-3689 alters adrenal catecholamine concentrations such that their profiles reflect an early increase (in EPI and NE within 1 h after treatment with the 200 mg/kg dose of WR-3689), followed by a later decrease (in EPI within 4 h after treatment with the 100 mg/kg dose of WR-3689 and in NE within 4 h after treatment with the 100 and 200 mg/kg doses of WR-3689) in catecholamine levels. It is interesting to note that 4 h after treatment, our results showed that the 100-mg/kg dose of WR-3689 is more effective in decreasing the content of NE and EPI than is the 200-mg/kg dose. The reason for this is probably due to the fact that 1 h after treatment with the 200 mg/kg dose of WR-3689, NE and EPI increased above control levels enough to counter the WR-3689-induced decrease 4 h later.

It is not clear why WR-3689 should increase adrenal NE and EPI concentrations within the first hour after treatment, but since phosphorothioates are known to cause a decrease in cytosolic Ca^{2+} intrusion (Polla et al., 1990), and Ca^{2+} is essential for the release of neurotransmitters and neuropeptides (Douglas & Poisner, 1964), the possibility exists that WR-3689 blocks the release of catecholamines, which in turn could lead to an increase in their adrenomedullary stores.

While it is not clear why WR-3689 should increase adrenal NE and EPI concentrations, there are several modes of action that could explain the decreases in NE and EPI concentrations 4 h after treatment. One explanation for these decreases is that WR-3689 inhibits the activity of dopamine β-hydroxylase (DBH), the enzyme responsible for conversion of DA to NE. The active form of WR-3689 is a sulfhydryl compound, and it is well known that sulfhydryl compounds have a profound inhibiting effect on DBH (Nagatzu, 1973; Terry & Craig, 1985). Evidence for a WR-3689-induced inhibition of this enzyme is seen in the decreases in NE and EPI contents that occur concomitantly with an accumulation

in the concentration of DA. Although DA levels are not significantly elevated above control levels, these data suggest that WR-3689 may decrease the concentration of EPI and NE as a consequence of WR-3689-induced decrease in DBH activity. Another explanation for the observed decreases in NE and EPI concentrations was reported by Vujnov et al. (1990), who found a decrease in the adrenal concentration of EPI and an increase in the plasma concentration of EPI 3 h after treatment with approximately 250 mg/kg WR-2721. They believe the increase in plasma EPI concentration is due to the WR-2721-induced increase in adrenal release, which in effect could deplete the adrenomedullary stores of this catecholamine and thus explain the WR-3689-induced decrease we observed in the adrenal content of NE and EPI. A third possibility for the observed WR-3689-induced decreases in adrenal NE and EPI can be explained by the hypoxia-inducing nature of phosphorothioates. Tyrosine hydroxylase (TH) activity and hence catecholamine synthesis are dependent on molecular oxygen. Since phosphorothioates are known to reduce oxygen tension (Purdie et al., 1983; Allanunis-Turner et al., 1989), it is possible that the decrease we observed in the adrenal content of NE and EPI may be partially due to a WR-3689-induced decrease in the synthesis of catecholamines. To further understand the mechanistic actions of WR-3689 on adrenal catecholamine metabolism, work is currently underway in our laboratory investigating the effects of WR-3689 on adrenal catecholamine synthesis (using L-DOPA accumulation as an index of synthesis) and release (using plasma levels of catecholamines as an index of release).

It is generally agreed upon that methylxanthines increase the synthesis and release of adrenomedullary catecholamines in a number of species. Snider and Waldeck (1974) reported a caffeine-induced increase in adrenal catecholamine synthesis. They found the rat adrenal concentration of NE and EPI to be unchanged but demonstrated an 80% increase in the adrenal concentration of DA after ip administration of 20 mg/kg caffeine. Minana and Grisolia (1986) reported similar results after long-term treatment of rats with caffeine (2–8 g/L) in drinking water. Peach (1972) noted that theophylline increased the release of catecholamines from perfused cat adrenals. Poisner (1973) observed that aminophylline increased the release of catecholamines from bovine adrenal glands in a dose-dependent manner. Robertson et al. (1978) indicated that caffeine increases the levels of plasma catecholamines in humans.

The caffeine-induced increase in catecholamine synthesis probably occurs via inhibition of cyclic nucleotide phosphodiesterase, resulting in an accumulation of adenosine 3′,5′-cyclic monophosphate (cAMP) (Snider & Waldeck, 1974; Rall, 1985). In turn, cAMP is known to enhance catecholamine production by stimulating TH, the rate-limiting

enzyme in catecholamine synthesis (Porter et al., 1991). New evidence indicates that caffeine increases mobilization of intracellular Ca^{2+}, resulting in increased concentrations of cytosolic free Ca^{2+} (Yamada et al., 1988, 1989), which leads to increased catecholamine secretion. The results of this study are in agreement with the aforementioned studies, indicating caffeine-induced increases in the adrenal concentrations of NE and EPI. Although caffeine was unable to increase DA concentrations, the possibility exists that an increase in DA synthesis is offset by an equivalent increase in DA release, resulting in little or no change in adrenal DA concentration. Another reason for the caffeine-induced increases in concentrations of NE and EPI and no change in the concentration of DA could be explained by caffeine's ability to stimulate DBH activity. Minana and Grisolia (1986) demonstrated that chronic administration of caffeine increases DBH activity in the hypothalamus, striatum, and serum of rats, but they were unable to find any alterations in the adrenal. In another experiment, performed in 10 healthy human subjects, it was reported that theophylline induced an increase in the amount of DBH released into the circulation and that the maximum increase occurred 1 h following treatment (Aunis et al., 1975). Interestingly enough, this 1-h time period coincides with the caffeine-induced increase we observed in the adrenal content of NE and EPI.

Our results indicate that when administered in combination with WR-3689, caffeine compensates for the WR-3689-induced decrease in the adrenal content of NE that occurs 4 h after treatment. There are a number of mechanisms that could explain this compensatory effect.

1. Since phosphorothioates are known to decrease cytosolic Ca^{2+} intrusion (Polla et al., 1990), which is essential for catecholamine release, and caffeine is known to mobilize intracellular Ca^{2+}, which stimulates catecholamine release (Yamada et al., 1988, 1989), it is possible that caffeine negates the inhibitory effect that WR-3689 has on catecholamine release.
2. Phosphorothioates are known to reduce oxygen tension (Purdie et al., 1983; Allalunis-Turner et al., 1989). WR-3689 could theoretically inhibit the activity of TH by limiting the availability of molecular oxygen needed for the activity of this enzyme, and could consequently reduce catecholamine synthesis. On the other hand, caffeine is known to stimulate the activity of TH, presumably through the action of cAMP (Porter et al., 1991), and hence to increase catecholamine synthesis.
3. Phosphorothioates have been shown to inhibit cAMP formation (Weaver et al., 1987). In contrast, caffeine induces cAMP accumulation through cyclic nucleotide phosphodiesterase inhibition.

4. The active form of WR-3689 is a sulfhydryl compound, and sulfhydryls are known to inhibit DBH activity (Nagatzu, 1973; Terry & Craig, 1985), resulting in decreased levels of NE and EPI, while caffeine is known to stimulate the activity of DBH (Minana & Grisolia, 1986), resulting in increased levels of NE and EPI.

These observations could explain why caffeine offsets the WR-3689-induced decrease in the adrenal content of NE.

The results of this study indicate that WR-3689 alters adrenal catecholamine concentrations and that simultaneous administration of WR-3689 and caffeine may offset the NE decrease induced by WR-3689 alone. In addition, it is tempting to speculate that WR-3689-induced alterations in catecholamine metabolism are at least partially responsible for the WR-3689-induced changes in behavior.

REFERENCES

Allalunis-Turner, M. J., Walden, T. L., and Sawich, C. 1989. Induction of marrow hypoxia by radioprotective agents. *Radiat. Res.* 118:581–586.

Aunis, D., Mandel, P., and Miras-Portugal, M. T. 1975. Changes of human plasma dopamine-β-hydroxylase activity after intravenous administration of theophylline. *Br. J. Pharmacol.* 53:425–427.

Bogo, V., Jacobs, A. J., and Weiss, J. F. 1985. Behavioral toxicity and efficacy of WR-27221 as a radioprotectant. *Radiat. Res.* 104:182–190.

Bogo, V., Franz, C. G., Jacobs, A. J., Weiss, J. F., and Young, R. W. 1988. Effects of ethiofos (WR-2721) and radiation on monkey visual discrimination performance. In *Perspectives in radiprotection,* eds. J. F. Weiss and M. G. Simic, pp. 93–95. New York: Pergamon Press.

Brown, D. Q., Grahm, W. J., MacKenzie, L. J., Pittock, J. W., and Shaw, L. M. 1988. Can WR-3689 be improved upon? In *Prospectives in radioprotection,* eds. J. F. Weiss and M. G. Simic, pp. 157–168. New York: Pergamon Press.

Douglas, W. W., and Poisner, A. M. 1964. Stimulus-secretion coupling in a neurosecretory organ: The role of calcium in the release of vasopressin from the neurohypophysis. *J. Physiol.* 172:1–18.

Giambarresi, L., and Jacobs, A. J. 1987. Radioprotectants. In *Military radiobiology,* eds. J. J. Conklin and R. I. Walker, pp. 265–301. New York: Academic Press.

Glover, D., Riley, L., Carmichael, K., Spar, B., Glick, J., Kligerman, M. M., Agus, Z. S., Slatopolsky, E., Attie, M., and Goldfarb, S. 1987. Hypocalcemia and inhibition of parathyroid hormone secretion after administration of WR-2721 (a radioprotective and chemoprotective agent). *N. Engl. J. Med.* 309:1137–1141.

Glover, D., Fox, K. R., Weiler, C., Kligerman, M. M., Turris, A., and Glick, J. H. 1988. Clinical trials of WR-2721 prior to alkylating agent chemotherapy and radiotherapy. In *Perspectives in radioprotection,* eds. J. F. Weiss and M. G. Simic, pp. 3–7. New York: Pergamon Press.

Kandasamy, S. B., Kumar, K. S., Hunt, W. A., and Weiss, J. F. 1988. Opposite effects of WR-2721 and WR-1065 on radiation-induced hypothermia: Possible correlation with oxygen uptake. *Radiat. Res.* 114:240–247.

Kligerman, M. M., Glover, D. J., Andrew, T. T., Norfleet, A. L., Yuhas, J. M., Coia, L. R., Simone, C., Glick, J. H., and Goodman, R. L. 1984. Toxicity of WR-2721 administered in single and multiple doses. *Int. J. Radiat. Oncol. Biol. Phys.* 10:1773–1776.

Kumar, K. S., Weiss, J. F., McLean, W. A., Kendrick, J. M., and Landauer, M. R. 1990. Radioprotection by combinations of WR-3689 and caffeine. *Abstr. Thirty-Eighth Annu. Meet. Radiation Research Society,* p. 193.

Landauer, M. R., Davis, H. D., Dominitz, J. A., and Weiss, J. F. 1988. Comparative behavioral toxicity of four sulfhydryl radioprotective compounds in mice: WR-2721, cysteamine, diethyldithiocarbamate, and *n*-acetylcysteine. In *Perspectives in radioprotection,* eds. J. F. Weiss and M. G. Simic, pp. 97–100. New York: Pergamon Press.

Landauer, M. R., Davis, H. D., Kumar, K. S., and Weiss, J. F. 1992. Behavioral toxicity of selected radioprotectors. *Adv. Space Res.* 12:273–283.

McDonough, J. H., Mele, P. C., and Franz, C. G. 1992. Comparison of behavioral and radioprotective effects of WR-2721 and WR-3689. *Pharmacol. Biochem. Behav.* 42:233–243.

Minana, M. D., and Grisolia, S. 1986. Caffeine ingestion by rats increases noradrenaline turnover and results in self-biting. *J. Neurochem.* 47:728–732.

Nagatzu, T. 1973. *Biochemistry of catecholamines,* pp. 71–73. Baltimore, MD: University Park Press.

Palazzolo, D. L., and Kumar, K. S. 1993. Effects of *S*-2(3-methylaminopropylamino)ethylphosphorothioic acid (WR-3689), alone or combined with caffeine, on catecholamine content of mouse hypothalamus. *Proc. Soc. Exp. Biol. Med.* 203:304–310.

Palazzolo, D. L., and Quadri, S. K. 1989. Reduced variation in retention times of biogenic amines by temperature control in liquid chromatography with electrochemical detection. *J. Chromatogr.* 479:216–219.

Palazzolo, D. L., and Quadri, S. K. 1990. Optimal conditions for the long term storage of biogenic amines for subsequent analysis by column chromatography with electrochemical detection. *J. Chromatogr.* 518:258–263.

Peach, M. J. 1972. Stimulation of release of adrenal catecholamines by adenosine 3′:5′-cyclic monophosphate and theophylline in the absence of extracellular Ca^{2+}. *Proc. Natl. Acad. Sci. USA* 69:834–836.

Poisner, A. M. 1973. Direct stimulant effect of aminophylline on catecholamine release from the adrenal medulla. *Biochem. Pharmacol.* 22:469–476.

Polla, B. S., Donati, Y., Kondo, M., Tochon-Danguy, H. J., and Bonjour, J. P. 1990. Protection from cellular oxidative injury and calcium intrusion by *N*-(2-mercaptoethyl)-1,3-propanediamine, WR-1065. *Biochem. Pharmacol.* 40:1469–1475.

Porter, J. C., Aguila-Mansilla, N., Ramin, S. M., Kozlowski, G. P., and Kedzierski, W. 1991. Tyrosine hydroxylase expression in hypothalamic cells: Analysis of the roles of adenosine 3′,5′-monophosphate- and Ca^{2+}/calmo-

dulin-dependent protein kinases in the action of pituitary cytotropic factor. *Endocrinology* 129:2477–2485.

Purdie, J. W., Inhaber, E. R., Schneider, H., and Labelle, J. L. 1983. Interaction of cultured mammalian cells with WR-2721 and its thiol, WR-1065: Implications for mechanisms of radioprotection. *Int. J. Radiat. Biol.* 43:517–527.

Rall, T. W. 1985. Central nervous system stimulants (continued), the methylxanthines. In *The pharmacological basis of therapeutics,* 7th ed., eds. A. G. Gilman, L. S. Goodman, T. W. Rall, and F. Murad, pp. 589–603. New York: Macmillan.

Robertson, D., Frolich, J. C., Carr, R. K., Watson, J. T., Hollifield, J. W., Shand, D. G., and Oates, J. A. 1978. Effects of caffeine on plasma renin activity, catecholamines and blood pressure. *N. Engl. J. Med.* 298:181–186.

Snider, S. R., and Waldeck, B. 1974. Increased synthesis of adrenomedullary catecholamines induced by caffeine and theophylline. *Naunyn Schmiedebergs Arch. Pharmacol.* 281:257–260.

Sweeney, T. R. 1979. A Survey of Compounds from the Antiradiation Drug Development Program of the U.S. Army Medical Research and Development Command. Washington, DC: Walter Reed Army Institute of Research.

Terry, L. C., and Craig, R. 1985. Cysteamine effects on monoamines, dopamine-β-hydroxylase and the hypothalamic-pituitary axis. *Neuroendocrinology* 41:467–475.

Vujnov, S., Simovic, M., Cvetkovic, M., and Savic, J. 1990. Effects of gammaphos and labetol on adrenaline level in the adrenals, plasma, and urine of rats subjected to irradiation injury. *Iugosl. Physiol. Pharmacol. Acta.* 26:411–418.

Walker, R. I. 1988. Requirements of radioprotectors for military and emergency needs. In *Perspectives in radioprotection,* eds. J. F. Weiss and M. G. Simic, pp. 13–20. New York: Pergamon Press.

Weaver, M. E., Morrissey, J., McConkey, C., Goldfarb, S., Slatapolsky, E., and Martin, K. 1987. WR-2721 inhibits parathyroid adenylate cyclase. *Am. J. Physiol.* 252:E197–E201.

Yamada, Y., Teraoka, H., Nakazato, Y., and Ohga, A. 1988. Intracellular Ca^{2+} antagonist TMB-8 blocks catecholamine secretion evoked by caffeine and acetylcholine from perfused cat adrenal glands in the absence of extracellular Ca^{2+}. *Neurosci. Lett.* 90:338–342.

Yamada, Y., Nakazato, Y., and Ohga, A. 1989. The mode of action of caffeine on catecholamine release from perfused adrenal glands of cat. *Br. J. Pharmacol.* 98:351–356.

RADIATION RESEARCH 141, 336–341 (1995)

Whole-Body Irradiation Transiently Diminishes the Adrenocorticotropin Response to Recombinant Human Interleukin-1α

Robert S. Perlstein,* Neerav R. Mehta,* Edward H. Mougey,‡ Mark H. Whitnall† and Ruth Neta*

*Department of Experimental Hematology and †Department of Physiology, Armed Forces Radiobiology Research Institute, Bethesda, Maryland 20889-5603; and ‡Neuroendocrinology and Neurochemistry Branch, Department of Medical Neurosciences, Walter Reed Army Institute of Research, Washington, D. C. 20307-5100

Perlstein, R. S., Mehta, N. R., Mougey, E. H., Whitnall, M. H. and Neta, R. Whole-Body Irradiation Transiently Diminishes the Adrenocorticotropin Response to Recombinant Human Interleukin-1α. *Radiat. Res.* **141**, 336–341 (1995).

Recombinant human interleukin-1α (rhIL-1α) has significant potential as a radioprotector and/or treatment for radiation-induced hematopoietic injury. Both IL-1 and whole-body ionizing irradiation acutely stimulate the hypothalamic-pituitary-adrenal axis. We therefore assessed the interaction of whole-body irradiation and rhIL-1α in altering the functioning of the axis in mice. Specifically, we determined the adrenocorticotropin (ACTH) and corticosterone responses to rhIL-1α administered just before and hours to days after whole-body or sham irradiation. Our results indicate that whole-body irradiation does not potentiate the rhIL-1α-induced increase in ACTH levels at the doses used. In fact, the rhIL-1α-induced increase in plasma ACTH is transiently impaired when the cytokine is administered 5 h after, but not 1 h before, exposure to whole-body irradiation. The ACTH response may be inhibited by elevated corticosterone levels after whole-body irradiation, or by other radiation-induced effects on the pituitary gland and hypothalamus.

INTRODUCTION

Recombinant human interleukin-1α (rhIL-1α) has significant potential as a radioprotector (*1–3*) and/or treatment (*2, 3*) for radiation-induced hematopoietic injury. It has also been demonstrated that IL-1 acutely stimulates the hypothalamic-pituitary-adrenal axis (*4–6*). The resulting increase in the circulating glucocorticoid levels has multiple effects on the production and actions of cytokines (*7*), but its contribution to IL-1-induced radioprotection is not yet established.

Whole-body ionizing irradiation also activates the hypothalamic-pituitary-adrenal axis (*8–12*). Plasma corticosterone increased in a biphasic manner, peaking approximately 2 and 48 h after irradiation (*8–12*). The first phase was thought to be a "stress response" and the later phase a response to developing radiation sickness.

The mechanism of radiation-induced activation of the hypothalamic-pituitary-adrenal axis has not been established. It was shown previously that head-shielded (body- or adrenal-only) irradiation induced a corticosterone response similar to that seen after whole-body irradiation (*8, 13*). The response to all three of these forms of irradiation was eliminated when the pituitary gland or the hypothalamus was removed or lesioned, indicating that the structural integrity of the pituitary gland and the hypothalamus was essential for radiation to activate the hypothalamic-pituitary-adrenal axis and a direct stimulatory effect of irradiation on the adrenal gland was unlikely (*8, 10, 11, 13*). Consequently, it is possible that radiation induces the production of systemic, extra-central nervous system (CNS) mediators that activate the hypothalamic-pituitary-adrenal axis. For example, ionizing radiation stimulates the release of cytokines (*14–17*) which are known hypothalamic-pituitary-adrenal axis secretagogues (*4*). However, since head-only irradiation also stimulates the axis (*18*), CNS-derived factors may be operative as well.

We therefore assessed the interaction of whole-body irradiation and rhIL-1α in activating the hypothalamic-pituitary-adrenal axis. Specifically, the alterations in the plasma levels of adrenocorticotropin (ACTH) and corticosterone after the administration of rhIL-1α just before and hours to days after whole-body or sham irradiation were determined. The early-phase activation of the axis by whole-body irradiation was also re-evaluated.

Our results indicate that whole-body irradiation does not potentiate the rhIL-1α-induced increase in ACTH levels at the doses used. On the contrary, the rhIL-1α-induced increase in plasma ACTH is transiently reduced when the cytokine is administered 5 h after, but not 1 h before, exposure to whole-body irradiation.

0033-7587/95 $5.00

MATERIALS AND METHODS

Experimental Animals

Intact female C3H/HeN mice (10–16 weeks old) were purchased from the National Cancer Institute (Frederick, MD). The mice were kept on a light–dark cycle (0600–1800 h light) and given commercial rodent chow and acidified tap water *ad libitum*. Animal holding rooms were maintained at 70 ± 2°F with 50 ± 10% relative humidity using at least 10 air changes per hour of 100% conditioned fresh air. Adrenalectomized and sham-adrenalectomized C3H/HeN mice were purchased from Charles River Laboratories (Portage, MI). Surgery was performed by the supplier 7–10 days prior to the experiments. These mice were handled in the same way as intact mice except that they were given 0.9% saline rather than water as drinking fluid. All animal-handling procedures were performed in compliance with guidelines from the National Research Council and approved by the Animal Care and Use Committee of the Armed Forces Radiobiology Research Institute.

Gamma- and Sham-Irradiation Experiments

Mice were irradiated (whole body) in the bilateral γ-radiation field in the AFRRI ^{60}Co facility.[1] During irradiation, the animals were confined in well-ventilated Plexiglas restrainers. The midline tissue dose to animals was 8.5 Gy delivered at a dose rate of 40 cGy/min. The quantity of whole-body irradiation administered was similar to the amounts that had activated the hypothalamic-pituitary-adrenal axis in rodents in earlier experiments (*8*, *12*). The radiation field in the irradiation position was uniform to within ±3%. Prior to irradiations of the animals, the desired dose rate was established in an acrylic mouse phantom using a 0.5 cm^3 tissue-equivalent ionization chamber (calibration traceable to the National Institute of Standards and Technology). Dosimetric measurements were made in accordance with the American Association of Physicists in Medicine protocol for the determination of absorbed dose (*19*). Sham-irradiated control mice were treated similarly to the irradiated mice, except that the ^{60}Co source elements were not raised into the exposure "on" positions.

In the first set of experiments, groups of five intact mice were irradiated with 8.5 Gy γ radiation or sham-irradiated. Either 1, 2, 4 or 6 h later, unanesthetized mice were decapitated (model 130 Rodent Decapitator, Harvard Apparatus, South Natick, MA) with minimal stress to obtain plasma samples for the assay of ACTH and corticosterone.

In the second set of experiments, groups of five intact mice were injected intraperitoneally (ip) with vehicle (0.5 ml pyrogen-free normal saline) or 100 ng of rhIL-1α 1 h before or 5, 24 or 72 h after 8.5 Gy γ irradiation or sham irradiation. Vehicle or 100 ng of rhIL-1α was also administered to control (not irradiated or sham-irradiated) mice at every time. We have demonstrated previously that 100 ng of rhIL-1α is radioprotective (*1*, *2*) and elicits a submaximal increase in the level of ACTH (*5*). All animals were decapitated 2 h after the injections to obtain plasma samples for the assay of ACTH and corticosterone.

In the third set of experiments, groups of five adrenalectomized or sham-adrenalectomized mice were injected ip with vehicle or 100 ng rhIL-1α 5 h after 8.5 Gy γ irradiation or sham irradiation. At that time, vehicle or rhIL-1α was also administered to adrenalectomized mice which had not been irradiated or sham-irradiated. All animals were decapitated 2 h after the injections to obtain plasma samples for the determination of ACTH and corticosterone.

Animals were irradiated between 0900 and 1100 h.

[1]R. E. Carter and D. M. Verrelli, *AFRRI Cobalt Whole-Body Irradiator*. Technical Report 73-3, Armed Forces Radiobiology Research Institute, Bethesda, MD, 1973.

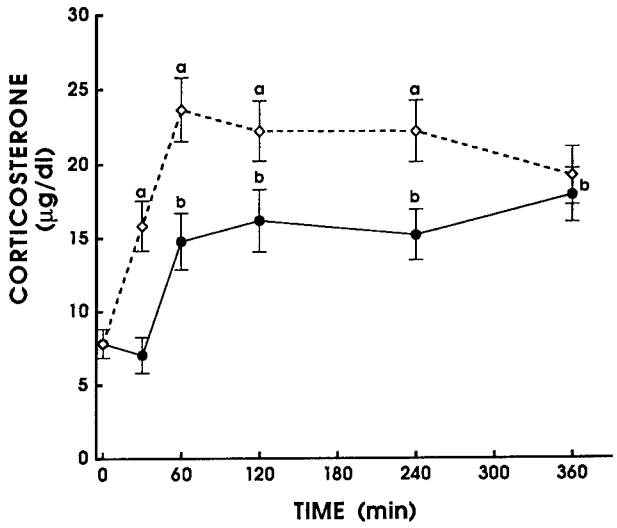

FIG. 1. Comparison of the time course of the increase in plasma corticosterone in C3H/HeN mice after (◇) 8.5 Gy γ irradiation or (●) sham irradiation. Each point represents the mean ± SEM of hormone determinations for 10–20 animals. a, $P < 0.05$ vs response after sham irradiation at the same time; b, $P < 0.05$ vs basal morning plasma corticosterone and the 30-min response after sham irradiation.

Cytokines

rhIL-1-α (117–271 Ro 24-5008; lot IL-1 2/88; specific activity 3×10^8 U/mg) was generously provided by Dr. Peter Lomedico, Hoffman LaRoche, Inc. (Nutley, NJ). It was diluted in 0.5 ml pyrogen-free saline on the day of injection.

Measurement of ACTH and Corticosterone in Plasma

ACTH was assayed in plasma from decapitated mice using an ^{125}I RIA kit (INCSTAR Corp., Stillwater, MN) as described previously (*5*). The ACTH antibody used in this assay is derived from rabbits immunized against $ACTH_{1\text{-}24}$, a region that is identical in human and murine ACTH. The threshold sensitivity of this assay was 8 pg/ml. Corticosterone was assayed in plasma as described previously (*20*).

Statistical Analysis

Evaluation of the results shown in Figs. 1–3 was carried out using analysis of variance followed by Fisher's protected least significant difference test.

RESULTS

Release of Corticosterone after 8.5 Gy γ Irradiation

Irradiation of mice with 8.5 Gy γ irradiation significantly increased plasma corticosterone at 30 (peak), 60, 120 and 240 min compared with the corticosterone levels at each of these times after sham irradiation (Fig. 1).

In addition, the plasma corticosterone levels 60-, 120-, 240- and 360 min after sham irradiation were significantly greater than the basal morning plasma corticosterone prior to any irradiation procedure or the 30-min response after sham irradiation. The values at earlier times (60 and 120 min) probably reflect a nonspecific stress response in the

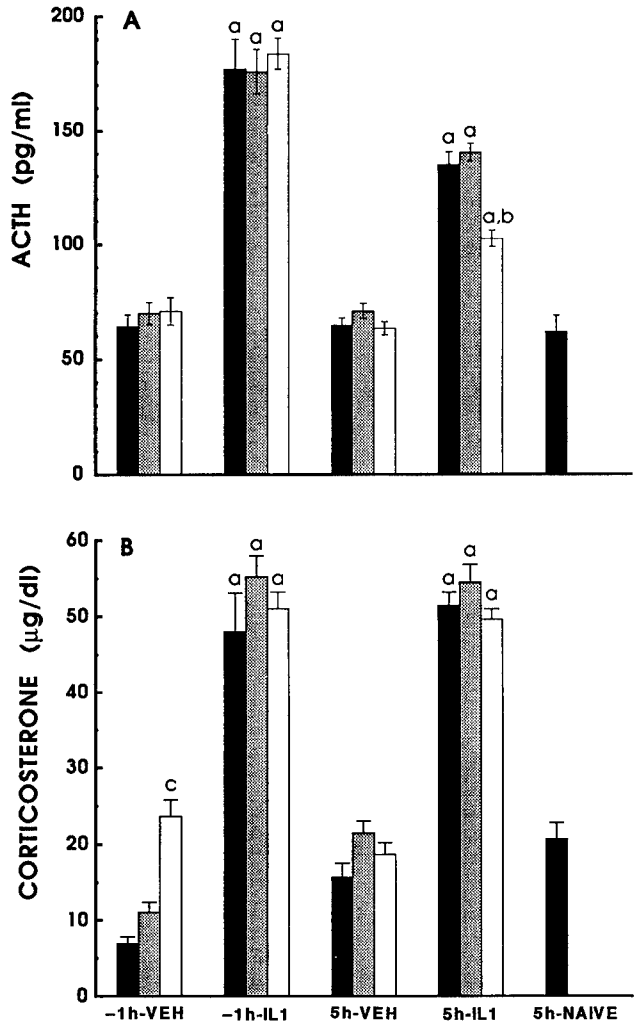

FIG. 2. Intact C3H/HeN mice received ip injections of 100 ng of rhIL-1α or vehicle 1 h before or 5 h after 8.5 Gy γ irradiation or sham irradiation. Control mice (not irradiated or sham-irradiated) received simultaneous injections of rhIL-1α or vehicle as well. Blood samples were obtained for ACTH (A) or corticosterone (B) 2 h after rhIL-1α or vehicle injections. Naive mice received no treatment, and blood samples were obtained at the same time as for the groups sacrificed 5 h after irradiation or sham irradiation. The results obtained from experiments in intact and sham-adrenalectomized mice were identical and therefore pooled. Each bar represents the mean ± SEM for 7–30 animals. a, $P < 0.05$ vs response to vehicle; b, $P < 0.05$ vs response to rhIL-1α in sham-irradiated or control mice (5 h mice); c, $P < 0.05$ vs response to vehicle in sham-irradiated or control mice (–1 h mice). (■) Control, (▩) sham-irradiated, (□) irradiated.

mice to handling and the irradiation procedure, while the values at later times (240 and 360 min) probably reflect the diurnal rhythm (*21*, *22*).

In contrast, we did not detect an increase in plasma ACTH levels at any of these times after irradiation or sham irradiation; i.e., the levels observed were not different from plasma ACTH levels in nonirradiated, non-sham-irradiated mice (58.6 ± 2.0 pg/ml) (data not shown).

Levels of ACTH after 8.5 Gy γ Irradiation and rhIL-1α in Intact and Sham-Adrenalectomized Mice

The data in Fig. 2A show the plasma ACTH levels 2 h after the injection of 100 ng of rhIL-1α or vehicle administered 1 h before or 5 h after 8.5 Gy γ irradiation or sham irradiation. The ACTH levels 2 h after the injection of rhIL-1α were determined simultaneously in control mice (not irradiated or sham-irradiated) as well. The results obtained from experiments in intact and sham-adrenalectomized mice were identical and therefore were pooled.

After the administration of rhIL-1α, a significant increase in the level of circulating ACTH was observed in all three groups at both times compared with the response in mice injected simultaneously with the vehicle (Fig. 2A). However, the administration of rhIL-1α 5 h after irradiation induced an ACTH response that was significantly less than the response observed in the sham-irradiated or control mice; i.e., the increase was blunted (Fig. 2A). In contrast, a blunted ACTH response was not observed when rhIL-1α was injected into mice 1 h before irradiation (Fig. 2A).

The administration of rhIL-1α 24 or 72 h after irradiation or sham irradiation resulted in similar levels of ACTH 2 h after the rhIL-1α injections in all three groups (data not shown).

Levels of Corticosterone after 8.5 Gy γ Irradiation and rhIL-1α in Intact and Sham-Adrenalectomized Mice

The data in Fig. 2B show the plasma corticosterone levels 2 h after the injection of 100 ng of rhIL-1α or vehicle administered 1 h before or 5 h after 8.5 Gy γ irradiation or sham irradiation. The corticosterone levels 2 h after the injection of rhIL-1α were determined simultaneously in control mice (not irradiated or sham-irradiated) as well. The results obtained from experiments in intact and sham-adrenalectomized mice were identical and therefore were pooled.

After the administration of rhIL-1α, a significant increase in circulating corticosterone was observed in all three groups at both times compared with the levels of corticosterone noted after the simultaneous injection of the vehicle (Fig. 2B). The magnitude of the rhIL-1α-induced corticosterone response in these animals (~50–55 μg %) was similar to published maximal corticosterone levels after stimulation of the hypothalamic-pituitary-adrenal axis in rodents (*23*) and data obtained previously in mice and rats in our laboratory (Perlstein, unpublished results). In contrast to the blunted increase in the ACTH level seen in Fig. 2A, the administration of rhIL-1α 5 h after irradiation induced an increase in plasma corticosterone which was not significantly less than the response observed in the sham-irradiated or control mice (Fig. 2B). In addition, the vehi-

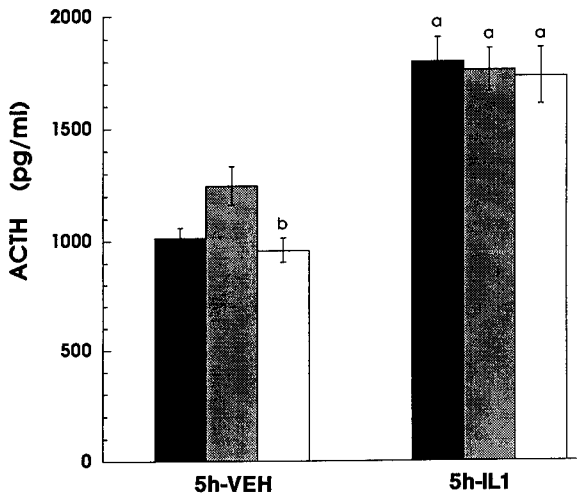

FIG. 3. Adrenalectomized C3H/HeN mice received ip injections of 100 ng of rhIL-1α or vehicle 5 h after 8.5 Gy γ irradiation or sham irradiation. Other adrenalectomized mice (not irradiated or sham-irradiated) received simultaneous injections of rhIL-1α or vehicle as well. Blood samples were obtained for ACTH 2 h after rhIL-1α or vehicle injections. Each bar represents the mean ± SEM for 10–30 animals. a, $P < 0.05$ vs response to vehicle; b, $P < 0.05$ vs response to vehicle in sham-irradiated mice. (■) Adrenalectomized, (▩) adrenalectomized + sham-irradiated, (□) adrenalectomized + irradiated.

cle-induced corticosterone levels 5 h after irradiation in all three groups were not different from the plasma corticosterone level at that time in naive mice (not irradiated, not sham-irradiated, not injected).

When the vehicle was administered 1 h prior to irradiation or sham irradiation, the plasma corticosterone level 2 h later was significantly greater in the irradiated mice compared with the sham-irradiated or control mice. The increased level of corticosterone more than likely reflects the 1-h response to irradiation (see Fig. 1) rather than a response to the vehicle. Although this resulted in a decrease in the *proportional* rhIL-1α-induced corticosterone response in irradiated mice compared with nonirradiated mice, the significance of this decrease was unclear since all rhIL-1α-induced corticosterone responses were maximal (see above).

The administration of rhIL-1α 24 or 72 h after irradiation or sham irradiation resulted in similar corticosterone levels 2 h after the injections in all three groups (data not shown).

Levels of ACTH after 8.5 Gy γ Irradiation and rhIL-1α in Adrenalectomized Mice

The data in Fig. 3 show the plasma ACTH levels 2 h after the injection of 100 ng of rhIL-1α or vehicle administered 5 h after 8.5 Gy γ irradiation or sham irradiation in adrenalectomized mice. In addition, the ACTH levels 2 h after injection of rhIL-1α or vehicle were determined simultaneously in adrenalectomized mice that were not irradiated or sham-irradiated.

After the administration of rhIL-1α, significant increases in circulating ACTH levels were observed in all three groups compared with the responses to simultaneously injected vehicle (Fig. 3). All of the responses were similar. Plasma corticosterone levels were absent or minimally detectable in all adrenalectomized animals (data not shown).

DISCUSSION

Our results demonstrate that (1) whole-body irradiation does not potentiate the rhIL-1α-induced increase in ACTH or corticosterone levels in the amounts administered; (2) in fact, the rhIL-1α-induced increase in plasma ACTH is transiently blunted when the cytokine is administered 5 h after, but not 1 h before, exposure to whole-body irradiation; and (3) there is a dissociation between the changes in the plasma levels of ACTH and corticosterone after whole-body irradiation.

When 100 ng of rhIL-1α was administered 1 h before whole-body irradiation, the plasma levels of ACTH and corticosterone 2 h after the injections (measured 1 h after irradiation) were not different from the responses to rhIL-1α observed in sham-irradiated or control animals. In earlier work, we showed that the same amount of rhIL-1α induces a submaximal increase in the plasma ACTH level and the combination of rhIL-1α and rhIL-6 synergistically stimulates the release of ACTH (*5*). Therefore, in contrast to other hypothalamic-pituitary-adrenal axis secretagogues administered simultaneously, whole-body irradiation and rhIL-1α, in the amounts administered, do not elicit a synergistic effect on ACTH levels (*22*).

In contrast, when rhIL-1α was injected 5 h after whole-body irradiation, the rhIL-1α-induced increase in plasma ACTH (but not the simultaneous increase in circulating corticosterone) was significantly blunted compared with the increase in sham-irradiated or control mice. It would appear that when the rhIL-1α-induced increase in the level of ACTH is initiated prior to irradiation, an impaired response does not occur. It is also conceivable that the diurnal rhythm of the responsivity of the hypothalamic-pituitary-adrenal axis (*24*) contributed to the difference in the effects of whole-body irradiation on the rhIL-1α-induced ACTH response at the two times. The persistence of the corticosterone response in the face of a blunted ACTH response can be explained by the fact that small amounts of ACTH can sustain sizable increases in plasma corticosterone (*25, 26*). Finally, rhIL-1α injected 24 or 72 h after whole-body irradiation elicited similar ACTH and corticosterone responses in the irradiated, sham-irradiated and control animals. These findings indicate that whole-body irradiation transiently interferes with the stimulation of the

release of ACTH by rhIL-1α administered several hours after irradiation.

The explanation for this blunting of the rhIL-1α-induced increase in plasma ACTH compared with control animals may be based on a short-lived, direct effect of radiation on the pituitary gland and/or hypothalamus. Such an effect is consistent with the impaired response of the hypothalamic-pituitary-adrenal axis to stimulation with acetylcholine and histamine 24 h after head-only irradiation in dogs (*27, 28*) as well as the established ability of radiation to produce hypopituitarism months to years after exposure (*29*). In contrast, we did not observe a blunting of rhIL-1α-induced increases in ACTH or corticosterone levels 24 h after whole-body irradiation, suggesting differential effects of whole-body irradiation and head-only irradiation, or differences between species.

The impaired rhIL-1α-induced ACTH response may be explained in another way. It is well known that elevated glucocorticoids exert feedback inhibition on the activity of the hypothalamic-pituitary-adrenal axis (*21, 22*). After 8.5 Gy whole-body γ irradiation, we observed a significant increase in plasma corticosterone in irradiated mice compared with sham-irradiated mice that appeared 30 min after whole-body irradiation, peaked at 1 h and gradually declined over the next few hours. This is similar to earlier observations in rodents (*8–12*) as well as our own recent findings in rats (Whitnall, unpublished results). Therefore, the activation of the axis by whole-body irradiation may have elicited a corticosterone response sufficient to interfere with subsequent stimulation of the axis by rhIL-1α. In this regard, it is well established that activation of the axis with one secretagogue can diminish the response to a second stressor (*21, 22, 30*).

In an attempt to distinguish between the above possibilities, we measured the rhIL-1α-induced ACTH responses in adrenalectomized or sham-adrenalectomized mice 5 h after whole-body irradiation or sham irradiation. We observed that the ACTH response to rhIL-1α was no longer blunted in irradiated adrenalectomized animals. This suggests that negative feedback by the radiation-induced corticosterone response could account for the blunted rhIL-1α-induced ACTH response observed in intact animals. However, since corticotrophic cells are hyper-responsive in adrenalectomized animals (*21, 22*), a direct effect of whole-body irradiation on the pituitary gland/hypothalamus that partially impaired responsivity could have been masked. Therefore, similar experiments in glucocorticoid-replaced adrenalectomized mice will be necessary to exclude that possibility more definitively.

In contrast to the corticosterone response, we did not observe an increase in plasma ACTH 30 to 360 min after whole-body irradiation in mice [or rats (Whitnall, unpublished results)]. This is consistent with the observations of Romashko, who reported that plasma ACTH levels, determined by bioassay, in rats after 6.5 Gy irradiation peak at 4 min and then rapidly decline to normal within 10 min (*31*). Minimal or no increases in the level of ACTH during significant increases in corticosterone are not uncommon (*26, 32*), and may be due to the short half-life of ACTH in the circulation, compared to that of corticosterone (*33*). Plasma corticosterone concentrations can remain elevated long after ACTH levels return to normal (*33*). In addition, it should be noted that small increases in ACTH can result in sizable and sustained increases in corticosterone levels, because of substantial amplification in the induction of release of corticosterone by ACTH in the adrenal cortex (*25, 26*). It is also possible that very small changes in plasma ACTH were not detected by our radioimmunoassay.

In contrast to our findings, Weidenfeld and coworkers reported that IL-1 failed to stimulate an increase in circulating ACTH in adrenalectomized rats (*34*). They postulated that IL-1 interferes with feedback inhibition by glucocorticoids on the hypothalamus and pituitary gland (*34*). On the other hand, Rivier and Vale (*35*) elicited a substantial increase in plasma ACTH in adrenalectomized rats after the administration of rhIL-1α, similar to our observations in adrenalectomized mice. In addition, Loxley *et al.* reported marked increases in corticotropin-releasing hormone when hypothalami from adrenalectomized rats were exposed to IL-1α or IL-1β *in vitro* (*36*). Taken together, these last findings suggest that glucocorticoid feedback is not necessary for IL-1-induced activation of the hypothalamic-pituitary-adrenal axis. The reason for these divergent findings is not known.

In summary, our results demonstrate that whole-body irradiation does not potentiate the rhIL-1α-induced increase in ACTH levels in the amounts administered. On the contrary, the rhIL-1α-induced increase in plasma ACTH is transiently blunted when the cytokine is administered 5 h after, but not 1 h before, whole-body irradiation. The ACTH response may be blunted because of feedback inhibition by elevated corticosterone levels elicited by whole-body irradiation, or other radiation-induced effects on the pituitary gland and hypothalamus.

ACKNOWLEDGMENTS

We thank Drs. T. J. MacVittie, G. D. Ledney and T. C. Pellmar for reviewing this manuscript critically; Dr. P. Lomedico for graciously providing us with rhIL-1α; and Petty Officer Sam Tom for his technical assistance. This research was supported by the Armed Forces Radiobiology Research Institute, Defense Nuclear Agency, under work units 00129 and 00105. Views presented in this paper are those of the authors; no endorsement by the Defense Nuclear Agency or the Department of Defense has been given or should be inferred. Research was conducted according to the principles enunciated in the Guide for the Care and Use of Laboratory Animals prepared by the Institute of Laboratory Animal Resources, National Research Council.

Received: June 13, 1994; accepted: September 1, 1994

REFERENCES

1. R. Neta, J. J. Oppenheim, R. D. Schreiber, R. Chizzonite, G. D. Ledney and T. J. MacVittie, Role of cytokines (interleukin-1, tumor necrosis factor and transforming growth factor-beta) in natural and lipopolysaccharide-enhanced radioresistance. *J. Exp. Med.* **173**, 1177–1182 (1991).
2. R. Neta, Radioprotection and therapy of radiation injury with cytokines. *Progr. Clin. Biol. Res.* **352**, 471–478 (1990).
3. R. Neta and J. J. Oppenheim, Radioprotection with cytokines—learning from nature to cope with radiation damage. *Cancer Cells* **3**, 391–396 (1991).
4. R. S. Perlstein, M. H. Whitnall, J. S. Abrams, E. H. Mougey and R. Neta, Synergistic roles of interleukin-6, interleukin-1 and tumor necrosis factor in the ACTH response to bacterial lipopolysaccharide *in vivo*. *Endocrinology* **132**, 946–952 (1993).
5. R. S. Perlstein, E. H. Mougey, W. E. Jackson and R. Neta, Interleukin-1 and interleukin-6 act synergistically to stimulate the release of adrenocorticotropic hormone *in vivo*. *Lymphokine Cytokine Res.* **10**, 141–146 (1991).
6. R. Neta, R. Perlstein, S. N. Vogel, G. D. Ledney and J. Abrams, Role of interleukin 6 (IL-6) in protection from lethal irradiation and in endocrine responses to IL-1 and tumor necrosis factor. *J. Exp. Med.* **175**, 689–694 (1992).
7. D. T. Boumpas, G. P. Chrousos, R. L. Wilder, T. R. Cupps and J. E. Balow, Glucocorticoid therapy for immune-mediated diseases: basic and clinical correlates. *Ann. Intern. Med.* **119**, 1198–1208 (1993).
8. J. M. A. Hameed and T. J. Haley, Plasma and adrenal gland corticosterone levels after X-ray exposure in rats. *Radiat. Res.* **23**, 620–629 (1964).
9. W. Eechaute, G. Demeester and I. Leusen, Irradiation totale aux rayons X et activitie surrenalienne. *Arch. Int. Pharmacodyn.* **135**, 235–248 (1962).
10. Z. M. Bacq, R. G. Smelik, M. Goutier-Pirotte and J. Renson, Effect of the destruction of hypothalamus on the suprarenal response of the rat to total-body irradiation. *Br. J. Radiol.* **33**, 618–621 (1960).
11. H. M. Patt, M. N. Swift, E. B. Tyree and R. L. Straube, X-irradiation of hypophysectomized rats. *Science* **108**, 475–476 (1948).
12. Z. Malatova, I. Ahlers and M. Praslicka, Effect of dexamethasone on pituitary-adrenocortical response to acute irradiation stress in rats. *Endocrinol. Exp.* **15**, 205–210 (1981).
13. K. Nakasone, Influence of X-irradiation of the adrenal gland on corticoid secretory activity in dogs. *Tohoku J. Exp. Med.* **106**, 83–87 (1972).
14. R. R. Weichselbaum, D. E. Hallahan, V. Sukhatme, A. Dritschilo, M. L. Sherman and D. W. Kufe, Biological consequences of gene regulation after ionizing radiation exposure. *J. Natl. Cancer Inst.* **83**, 480–484 (1991).
15. M. L. Sherman, R. Datta, D. E. Hallahan, R. R. Weichselbaum and D. W. Kufe, Regulation of tumor necrosis factor gene expression by ionizing radiation in human myeloid leukemia cells and peripheral blood monocytes. *J. Clin. Invest.* **87**, 1794–1797 (1991).
16. G. E. Woloschak, C-M. Chang-Liu, P. S. Jones and C. A. Jones, Modulation of gene expression in Syrian hamster embryo cells following ionizing radiation. *Cancer Res.* **50**, 339–344 (1990).
17. H. Ishihara, K. Tsuneoka, A. B. Dimchev and M. Shikita, Induction of the expression of the interleukin-1 beta gene in mouse spleen by ionizing radiation. *Radiat. Res.* **133**, 321–326 (1993).
18. T. Shimizu, M. Mieno and K. Yamashita, Responses of the hypothalamic-pituitary-adrenal and -gonadal systems to head X-irradiation. *Tohoku J. Exp. Med.* **109**, 155–161 (1973).
19. American Association of Physicists in Medicine (AAPM Task Group 21), A protocol for the determination of absorbed dose from high-energy photon and electron beams. *Med. Phys.* **10**, 741–771 (1983).
20. E. H. Mougey, J. L. Meyerhoff, L. L. Pennington, C. C. Kenion and G. J. Kant, Pituitary cyclic AMP and plasma hormone responses to epinephrine administration *in vivo*. *Life Sci.* **39**, 2305–2313 (1986).
21. M. E. Keller-Wood and M. F. Dallman, Corticosteroid inhibition of ACTH secretion. *Endocrinol. Rev.* **5**, 1–24 (1984).
22. M. F. Dallman, S. F. Akana, C. S. Cascio, D. N. Darlington, L. Jacobson and N. Levin, Regulation of ACTH secretion: Variations on a theme of B. *Recent Progr. Horm. Res.* **43**, 113–173 (1987).
23. L. Givalois, J. Dornand, M. Mekaouche, M. D. Solier, A. F. Bristow, G. Ixart, P. Siaud, I. Assenmacher and G. Barbanel, Temporal cascade of plasma level surges in ACTH, corticosterone, and cytokines in endotoxin-challenged rats. *Am. J. Physiol.* **266**, R164–R170 (1994).
24. M. J. Bradbury, C. S. Cascio, K. A. Scribner and M. F. Dallman, Stress-induced adrenocorticotropin secretion: diurnal responses and decreases during stress in the evening are not dependent on corticosterone. *Endocrinology* **128**, 680–688 (1991).
25. E. Papaikonomou, Rat adrenocortical dynamics. *J. Physiol. (London)* **265**, 119–131 (1977).
26. C. E. Wood, J. Shinsako, L. C. Keil, D. J. Ramsay and M. F. Dallman, Apparent dissociation of adrenocorticotropin and corticosteroid responses to 15 ml/kg hemorrhage in conscious dogs. *Endocrinology* **110**, 1416–1421 (1982).
27. K. Yamashita, T. Shimizu, M. Mieno and K. Kawao, The susceptibility of the hypothalamic-pituitary-adrenocortical axis to histamine after head X-irradiation. *Tohoku J. Exp. Med.* **110**, 161–166 (1973).
28. K. Yamashita, T. Shimizu, M. Mieno and E. Yamashita, Effects of exogenous acetylcholine upon adrenal 17-hydroxycorticosteroid secretion of intact and head x-irradiated dogs. *Neuroendocrinology* **27**, 39–45 (1978).
29. L. S. Constine, P. D. Woolf, D. Cann, G. Mick, K. McCormick, R. F. Raubertas and P. Rubin, Hypothalamic-pituitary dysfunction after radiation for brain tumors. *N. Engl. J. Med.* **328**, 87–94 (1993).
30. M. H. Whitnall, Regulation of the hypothalamic corticotropin-releasing hormone neurosecretory system. *Progr. Neurobiol.* **40**, 573–629 (1993).
31. O. O. Romashko, Adrenocorticotropic function of the hypophysis during irradiation. *Radiobiologiya* **11**, 153–158 (1971).
32. A. R. Gwosdow, M. S. A. Kumar and H. H. Bode, Interleukin 1 stimulation of the hypothalamic-pituitary-adrenal axis. *Am. J. Physiol.* **258**, E65–E70 (1990).
33. M. E. Keller-Wood, J. Shinsako and M. F. Dallman, Integral as well as proportional adrenal responses to ACTH. *Am. J. Physiol.* **245**, R53–R59 (1983).
34. J. Weidenfeld, O. Abramsky and H. Ovadia, Effect of interleukin-1 on ACTH and corticosterone secretion in dexamethasone and adrenalectomized pretreated male rats. *Neuroendocrinology* **50**, 650–654 (1989).
35. C. Rivier and W. Vale, Stimulatory effect of interleukin-1 on adrenocorticotropin secretion in the rat; is it modulated by prostaglandins? *Endocrinology* **129**, 384–388 (1991).
36. H. D. Loxley, A-M. Cowell, R. J. Flower and J. C. Buckingham, Modulation of the hypothalamo-pituitary-adrenocortical responses to cytokines in the rat by lipocortin 1 and glucocorticoids: a role for lipocortin 1 in the feedback inhibition of CRF-41 release? *Neuroendocrinology* **57**, 801–814 (1993).

RADIATION RESEARCH 141, 37–43 (1995)

Late Mitosis/Early G_1 Phase and Mid-G_1 Phase Are Not Hypersensitive Cell Cycle Phases for Neoplastic Transformation of HeLa × Skin Fibroblast Human Hybrid Cells Induced by Fission-Spectrum Neutrons

J. L. Redpath,* R. J. Antoniono,* C. Sun,* H. M. Gerstenberg† and W. F. Blakely†

*Department of Radiation Oncology, University of California Irvine, Irvine, California 92717; and †Radiation Biophysics Department, Armed Forces Radiobiology Research Institute, Bethesda, Maryland 20889-5603

Redpath, J. L., Antoniono, R. J., Sun, C., Gerstenberg, H. M. and Blakely, W. F. Late Mitosis/Early G_1 Phase and Mid-G_1 Phase Are Not Hypersensitive Cell Cycle Phases for Neoplastic Transformation of HeLa × Skin Fibroblast Human Hybrid Cells Induced by Fission-Spectrum Neutrons. *Radiat. Res.* **141**, 37–43 (1995).

A two- to threefold increase in the rate of neoplastic transformation in cells irradiated at a dose rate of 0.22 cGy/min with fission-spectrum neutrons compared to that at 10.7 cGy/min has been confirmed with the use of alkaline phosphatase chromogenic substrate Western Blue staining to detect foci of neoplastically transformed cells through their expression of a tumor-associated antigen, the end point of the HeLa × skin fibroblast human hybrid cell transformation assay. To investigate whether the inverse dose-rate effect is due to the existence of a period in the cell cycle in which cells are significantly more sensitive to neoplastic transformation than in the rest of the cell cycle, as has been postulated previously (Rossi and Kellerer, *Int. J. Radiat. Biol.* **50**, 353–361, 1986; Brenner and Hall, *Int. J. Radiat. Biol.* **58**, 745–758, 1990; Elkind, *Int. J. Radiat. Biol.* **59**, 1467–1475, 1991), we compared the sensitivity of late mitotic/early G_1-phase and mid-G_1-phase cells with that of asynchronous cells. The rationale for examining these particular cell cycle phases was based on the fact that mitosis has been hypothesized to be a candidate for the extremely sensitive period, and on a preliminary report that mid-G_1-phase C3H 10T1/2 cells may exhibit enhanced sensitivity for neutron-induced transformation. A nominal dose of 45 cGy of fission-spectrum neutrons was delivered at approximately 10 cGy/min. The data indicate that neither late mitotic/early G_1-phase nor mid-G_1-phase cells are significantly more sensitive than asynchronous cells. Further, the dependence on the phase of the cell cycle for neoplastic transformation of CGL1 cells induced by fission-spectrum neutrons is different from that previously demonstrated for γ radiation, where late-mitotic cells were approximately five times more sensitive than mid-G_1-phase and asynchronous cells (Redpath and Sun, *Radiat. Res.* **121**, 206–211, 1990).

INTRODUCTION

Several investigators (*1–13*) have observed an inverse dose-rate effect for neoplastic transformation *in vitro* and cancer induction *in vivo* at low doses or multiple fractions of low doses of certain high-LET (linear energy transfer) radiations. While there are exceptions (*14–17*), it is generally accepted that such an effect exists and may be of general importance. The magnitude of the effect is not thought to be as large as the factor of 9 originally reported for C3H 10T1/2 cells (*1, 2*); a factor of 2 to 3 would agree with most observations. Possible underlying mechanisms have been hypothesized, and perhaps the most plausible is that an extremely sensitive period exists in the cell cycle for neutron-induced neoplastic transformation (*18–23*).

Using the HeLa × skin fibroblast human hybrid cell neoplastic transformation assay, we previously demonstrated that cells in the late G_2 and mitotic phases of the cell cycle are 10 and 5 times, respectively, more sensitive to γ-radiation-induced transformation than either asynchronous cells or cells in the mid-G_1 phase of the cell cycle (*24*). Subsequently a similar finding was reported for C3H 10T1/2 cells by Cao *et al.* (*25*), who used γ irradiation; however, another group, also working with C3H 10T1/2 cells, did not find an enhanced sensitivity in X-irradiated mitotic cells but did observe an enhanced sensitivity in G_2-phase cells (*26*).

In the HeLa × skin fibroblast hybrid cell transformation assay, neoplastically transformed cells are detected by the expression of a tumor-associated antigen originally designated p75/150 (*27, 28*) but now identified as intestinal alkaline phosphatase, or IAP (*29, 30*). This human-derived neoplastic transformation assay has two practical advantages: a shorter postirradiation period of 21 days (*31–34*) compared with 6 weeks for the popular murine cell system C3H 10T1/2 and, as stated above, a specific molecular marker (p75/IAP expression) for neoplastic transformation (*27–30*).

0033-7587/95 $5.00

In this hybrid cell system, neoplastic transformation and IAP expression are associated with loss of a fibroblast chromosome 11 (*34–38*). The current understanding of the molecular mechanism underlying the neoplastic transformation process is that a tumor-suppressor gene located on both copies of the fibroblast chromosome 11 negatively trans-regulates the IAP gene and an as yet unidentified oncogene (*39*).

A new staining technique has recently been developed for this assay (*40*) which uses the alkaline phosphatase chromogenic substrate Western Blue (WB) for direct detection of cells expressing IAP. The WB method is simpler, faster and more sensitive to weakly positive foci than is the immunoperoxidase (IMPO) method used previously. Here, we report for the first time the use of the WB staining technique to (1) confirm the magnitude of the inverse dose-rate effect after exposure of asynchronous CGL1 cells to fission neutrons and (2) compare the sensitivity of late-mitotic/G_1 and mid-G_1 phases of the cell cycle to asynchronous cells for fission-neutron-induced transformation. The rationale for examining these particular cell cycle phases is based on the fact that mitosis has been hypothesized to be a candidate for the extremely sensitive period, and on a preliminary report that mid-G_1-phase C3H 10T1/2 cells may exhibit enhanced sensitivity for neutron-induced transformation (R. C. Miller, personal communication).

MATERIALS AND METHODS

General Experimental Procedure

Mitotic, mid-G_1-phase and asynchronous cells are harvested and frozen at the University of California Irvine. They are then express-mailed on dry ice to the Armed Forces Radiobiology Research Institute (AFRRI), where they are prepared for irradiation. After irradiation the cells are pelleted, resuspended in modified freezing medium, frozen and shipped back to Irvine for processing in the transformation assay. We previously demonstrated the validity of this freeze/thaw method in studies of radiation-induced neoplastic transformation (*41*) and of the inverse dose-rate effect (*6, 7*). Details of each step in the procedure are provided below.

Cell Lines and Culture Conditions

The derivations of the human hybrid (HeLa × skin fibroblast) cell lines CGL1 and CGL3 have been described (*35*). CGL1 is nontumorigenic when inoculated subcutaneously into nude mice and is IAP-negative (*27*). CGL3, an IAP-expressing, tumorigenic segregant, arose spontaneously in a mass culture of the original cell hybrid fusion (ESH5) after more than 200 population doublings (*35*). It is used as the IAP-positive control when cells in the radiation-induced transformation experiments are stained. Cells are routinely checked for the presence of mycoplasma.

Cells are grown in Minimum Essential Medium-Eagle Modified (Flow Labs, Inc.) supplemented with 5% calf serum (GIBCO), 2 m*M* glutamine (GIBCO), nonessential amino acids (GIBCO) and 100 IU/ml penicillin (Irvine Scientific). Sodium bicarbonate (20 m*M*) is added to the medium so that, upon incubation in humidified air at 37°C and 4.5% CO_2, the pH is maintained at 7.2. *In vitro* plating efficiencies of unirradiated and irradiated CGL1 cells are determined by standard methods as described previously (*30, 31*). Depending on the level of survival, 100 to 1000 CGL1 cells are plated into T-25 flasks containing 5 ml of growth medium and are incubated for 7–10 days to allow for colony formation.

Harvesting of Cells for Cell Cycle Studies

Up to 24 T-150 flasks containing 50 ml of complete medium are seeded with 8×10^6 cells. One day after seeding the cultures should have just attained confluence and contain approximately 1.1×10^7 cells. If no empty spaces are present the harvesting procedure can begin. It is important to avoid empty spaces since the subsequent trypsinization step will allow for the collection of nonmitotic cells. We have modified our collection procedure published previously (*24*) to include a light-trypsinization step, which improves the plating efficiency of the collected cells by a factor of 2 without reducing the mitotic index. This is a valuable improvement in view of the large numbers of cells required for transformation experiments. The medium is aspirated off the confluent cultures, which are then washed twice with 6 ml of serum-free medium. The cultures are then evenly coated with 4 ml of trypsin (0.625 mg/ml) in phosphate-buffered saline (PBS; Sigma stock is 10×) and put in a 37°C incubator for 2 min, after which the trypsin is aspirated off and gently replaced by 4 ml of ice-cold serum-free medium. The cells are then examined under the microscope to ensure that there are few floating cells. Mitotic cells are collected after the edge of the flask is hit once with the palm of the hand and the medium is aspirated into a sterile tube that is kept on ice. The cells in the culture flask are then *gently* washed twice with 4 ml of ice-cold complete medium containing 7.5% calf serum. These washes are pooled with the original aspirate for a total volume of 12 ml and a final serum concentration of 5%. With this procedure, four flasks can be handled in parallel to collect 48 ml. The pooled suspension is kept on ice while a cell count is made and a mitotic squash is prepared for determination of the mitotic index by standard procedures. This process will use about 2×10^5 cells. The mitotic indices for cells collected in this manner are typically in excess of 90% (150–200 cells scored) with a yield of approximately 2% or 2×10^5 cells/flask. If the yield is higher than 4%, the mitotic index will likely be <90% and the cells are discarded. For the experiments reported in this paper the mitotic indices of the harvested populations were in the range 90 to 96%. Based on the reports in the literature, this represents an excellent synchrony. Once the mitotic index is acceptable, a 0.5-ml aliquot is taken for determination of plating efficiency and the remaining collected cells are pelleted, resuspended in 1.8 ml of ice-cold modified freezing medium containing 90% fetal calf serum and 10% dimethyl sulfoxide, or DMSO (this modified freezing medium results in superior plating efficiencies), and frozen in liquid nitrogen at a final concentration of 5–7 $\times 10^5$ cells/vial. This collection procedure can be repeated 3 h later on the same set of flasks. If 24 flasks are initially set up, 12 vials can be collected in 1 day by an experienced worker.

The preparation of mid-G_1-phase cells follows the same procedures up to harvesting mitotic cells. At this point, the cells are plated out in a T-150 flask and placed in a 37°C incubator for 5 h, after which the cells are collected, pelleted and frozen in the same modified freezing medium at a concentration of approximately 2×10^6 cells/vial.

Asynchronous cells are collected in the standard fashion and frozen in 1.8 ml modified freezing medium also at a concentration of approximately 2×10^6 cells/vial.

Flow Cytometric Analysis of Cell Cycle Distribution

Cells are prepared for DNA analysis by flow cytometry using a modification of a rapid staining technique (*42*) which allows for the production of stained cell nuclei. The modification involves the lysing of $1–2 \times 10^6$ alcohol-fixed cells with a mixture of 0.5% Triton-X-100 and 2*N* HCl, following which the preparation is neutralized with sodium tetraborate. The cells are then stained with propidium iodide in PBS (5 μg/ml) and filtered through 0.52 μm Nytex mesh. The sample is then ready for analysis.

Sample Irradiation and Dosimetry

Fission-neutron irradiations from AFRRI's Mark F TRIGA nuclear reactor[1] were performed at two nominal dose rates to obtain a dose of 45 cGy. For low-dose-rate exposures attached cells were used, while for high-dose-rate exposures both attached and suspended cells were used. Different exposure configurations were used for the attached and suspended cells. The flasks with the attached cells were mounted by hand and centered in a large lead cave open at the front and facing a 15-cm lead shielding wall placed between the cave opening and the reactor core. The purpose of the lead cave was to enhance the sample neutron dose by selectively shielding the irradiated samples from the reactor's γ rays as well as the scattered radiation from the exposure room. The cave center was located 1.06 m from the reactor core center and the dose rates used were 0.2 and 10 cGy/min.

The samples with cells in suspension were shuttled between the setup area outside the exposure room and a large lead box through a curved aluminum extractor tube that penetrates the exposure room shielding wall. The lead box, similar to the lead cave described above, completely shielded the samples on all sides. The additional front wall of lead shielding used to close the cave was to enhance the neutron to γ-ray dose on the samples further. The extractor-tube delivery system minimizes the time between when the samples leave the setup area and when exposure is completed, an important factor in experiments with synchronized cell populations. For these exposures, the distance from the box to the core center was 1.76 m and the dose rate was 10 cGy/min.

Paired ion chambers, placed in sample tubes at the center of the sample array, were used to determine separately the dose due to γ and neutron radiation (*43*). The neutron to total-dose ratios were measured to be approximately 0.9 for the high-dose-rate exposures and to fall between 0.9 and 0.8 for the low-dose-rate exposures; the ratios, with decreasing dose rates, had measured uncertainties as large as ±20% for the exposures used in the experiments reported. Each run was actively monitored using fission and ionization chambers in the exposure room. The fluence-weighted mean neutron energy was determined to be 0.71 MeV for the lead cave and assumed to be the same for the lead box.[2] For the cave, rhodium foils were used to determine field uniformity across the array and was within ±7%. For the box, ion chambers were used and the uniformity was within ±3%.

Irradiation Procedures for Attached Asynchronous Cells

The preparation, irradiation and postirradiation protocols for fission-neutron irradiation of attached asynchronous CGL1 cells were as described previously (*7*). Briefly, 3 days before irradiation, exponentially growing CGL1 cells are seeded into T-25 cm^2 flasks at 1.25×10^5 cells per flask. Before irradiation, flasks containing cells are filled with complete medium, prewarmed to 37°C. Typically, 10 T-25 cm^2 flasks are placed in a holder that positions two rows of five T-25 cm^2 flasks each inside the above-described cave in which the air temperature is regulated by an air heater to 37°C. Sham-treated (0 Gy) samples are placed in an air-heated incubator in lieu of the irradiation facility.

After the irradiation interval, flasks containing cells are returned to the cellular laboratory where medium is removed via aspiration and replaced with fresh complete medium (37°C). Cells are permitted a postirradiation incubation interval of 2.5–6 h. This variation in postirradiation incubation period was due to logistical reasons; however, from our studies of γ-radiation effects (*32*), we do not anticipate that this variation would have any significant impact on the measured neoplastic transformation frequencies. After the incubation interval, cells are harvested by the conventional trypsin-induced detachment method. Typically, 1 million cells are recovered per T-25 cm^2 flask. Cells are pelleted by centrifugation, resuspended in 4°C modified freezing medium and transferred to 2-ml cryovials. Cells in cryovials are then subjected to a controlled-rate cell-freezing protocol using a liquid nitrogen cell-freezing apparatus (Cryo Med, MI).

Irradiation Procedures for Asynchronous, Mitotic or Mid-G_1-Phase Cells in Suspension

Vials of frozen asynchronous, mitotic or G_1-phase cells are rapidly thawed in a 37°C water bath and centrifuged to pellet cells; then the supernatant (modified freezing medium) is removed via aspiration, all within 9 min. Cells are resuspended with 4°C complete medium and transferred to 15- or 50-ml centrifuge tubes placed on ice in a test-tube holder. The holders are immediately carried to the fission-neutron irradiation facility and placed in the shuttle of the extractor tube. The shuttle is then transported rapidly through the extractor tube into the room-temperature lead box located in the exposure room. Aliquots of cells representing the sham treatment are also kept on ice outside the exposure room.

After the irradiation interval, centrifuge tubes containing the irradiated cells are promptly returned to the cellular laboratory and, along with the tubes containing the sham-treated aliquots, are centrifuged to pellets. The supernatant medium is removed via aspiration and cells are then resuspended in 4°C modified freezing medium and transferred to 2-ml cryovials. Cells in cryovials are then frozen as described previously. Typically, the maximum time from cell thawing until cell freezing is less than 40 min.

Standard Western Blue-Based Neoplastic Transformation Assay

The first step is to determine the plating efficiencies of the batches of frozen cells received from AFRRI. The cell-plating protocol used for this purpose yielded single-cell suspensions as judged by colony multiplicities <1.04 (*44*). The plating efficiencies of unirradiated cells are typically in the range 15 to 30% for mitotic cells and 30 to 60% for mid-G_1-phase and asynchronous cells. The surviving fractions are in the 50 to 70% range for irradiated cells and are independent of the cell cycle phase. Batches with very low plating efficiencies (e.g. <10% for irradiated mitotic cells and <20% for the rest) are discarded. Batches with acceptable plating efficiencies are then processed for the transformation assay. Based on the prior determinations of plating efficiency, cells are seeded into T-75 flasks each containing 15 ml of standard growth medium such that there are approximately 2×10^3 surviving cells per flask. After day 7 or 8, the cultures are fed two times per week. At 21 days the cultures are fixed with 2% paraformaldehyde/PBS for 20 min, rinsed with PBS and stained for the presence of foci of cells expressing IAP by adding 3 ml of WB reagent to each flask and allowing a 5-min incubation (*40*). The reagent is then suctioned off, the flasks are rinsed with PBS, and the blue foci are scored against a white background (*40*). The unirradiated control cultures are handled accordingly. Plating efficiencies for the irradiated and unirradiated cells are determined by standard methods. Data are scored by counting the total number of foci and their distribution within the flasks as well as the total number of cells surviving the treatment protocol. Neoplastic transformation frequencies are calculated by the null method (*45*).

Description of Western Blue Reagent and Staining Characteristics

Western Blue (Promega) contains 5-bromo-4-chloro-3-indolyl-phosphate (BCIP) and nitro blue tetrazolium (NBT) in a special buffer which is stable at room temperature for a year and requires no dilution. When the phosphate group of BCIP is cleaved by alkaline phosphatase, a hydrogen-donating intermediate is formed which interacts chemically with NBT, changing it into a water-insoluble purple/blue crystalline product.

[1]M. L. Moore and S. Elasser, The TRIGA Reactor Facility at the Armed Forces Radiobiology Research Institute: A Simplified Technical Description. Technical Report 86-1, AFRRI, Bethesda, MD, 1992.

[2]R. B. Schwartz and C. M. Eisenhauer, *Annual Progress Report to the Armed Forces Radiobiology Research Institute from the National Institute of Standards and Technology*, 1991.

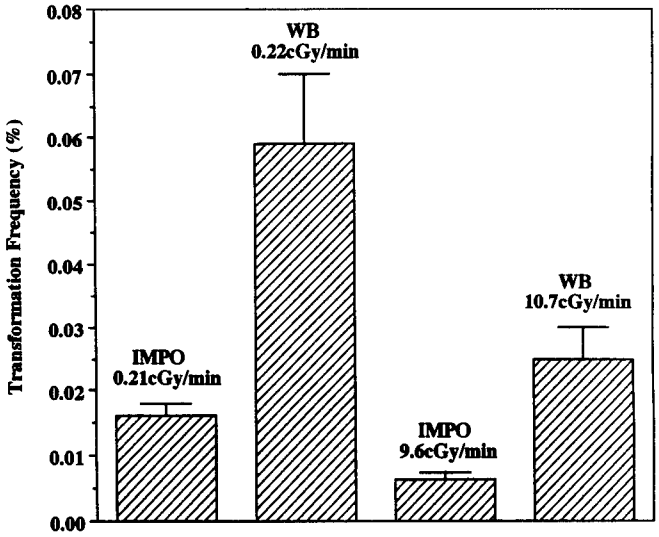

FIG. 1. A comparison of the IMPO and WB staining techniques used to study neoplastic transformation frequencies induced in HeLa × skin fibroblast human hybrid cells by a dose of 45 cGy of fission-spectrum neutrons delivered at nominal dose rates of 0.2 and 10 cGy/min. While the absolute values are greater with WB staining due to its increased sensitivity, the magnitude of the inverse dose-rate effect is the same with a value in the range 2.3 to 2.6.

RESULTS

For our experiments in which CGL1 cells were irradiated as attached asynchronous populations and stained using WB, an inverse dose-rate effect of almost identical magnitude, 2.3 ± 0.6, to that observed previously, 2.6 ± 0.7, using IMPO staining (*7*) was obtained (Fig. 1, Table I). Note that the absolute values of the neoplastic transformation frequencies were considerably higher for the WB-stained cells than those obtained using IMPO staining. This has been a consistent observation in our comparisons of these two staining procedures and principally reflect an increased ability of WB staining to pick up weakly positive foci of cells (*40*).

Mitotic CGL1 cells collected by our modified shake technique resulted in excellent synchrony as judged by mitotic indices >90%; in similar studies using C3H 10T1/2 cells, an 80% parity of mitotic cells has been reported (*26*). To characterize the purity of the synchronized populations of CGL1 cells used in this study further, we performed additional cell cycle parameter analyses, subsequent to a sham experimental protocol, using flow cytometry techniques. This was done by thawing a frozen vial of mitotic or mid-G_1-phase cells, preparing the cells as if for irradiation and then running the flow cytometry analysis. Our data (Fig. 2) show that, as a consequence of this procedure, the initial mitotic cell population progresses to a mixture of approximately 50% mitotic and 50% early G_1-phase cells at the time of fission-neutron irradiation. Since the irradiation occurred 10 to 15 min after thawing of the frozen mitotic cells, the G_1-phase fraction of this population had to be very early in the G_1 phase. The mid-G_1-phase cells were cells 5 h after mitosis and demonstrate a population containing 78% G_1-phase cells (compared to 40–45% for an asynchronous population).

The results of the neoplastic transformation experiments are detailed in Table II for late mitotic/early G_1-phase, mid-G_1-phase and asynchronous cells. For these studies cells were irradiated in suspension. These data represent the accumulation of four experiments with asynchronous and late mitotic/early G_1-phase cells and three experiments with mid-G_1 phase cells. The surviving fraction at the nominal dose of 45 cGy was not significantly different for any of the phases of the cell cycle and had a value of 0.63 ± 0.15. The analysis of neoplastic transformation frequency also indicates no significant difference between the transformation sensitivities of the three populations studied (Table II).

DISCUSSION

Using a new staining technique (*40*), we have confirmed our previous observations (*6*, *7*) of an inverse dose-rate effect on the order of 2.5 for the neoplastic transformation

TABLE I
The Influence of Dose Rate on Neoplastic Transformation of Nontumorigenic HeLa × Skin Fibroblast Human Cell Hybrids by TRIGA Reactor Fission-Spectrum Neutrons

Dose rate (cGy/min)	Dose (cGy)	Number of surviving cells ($\times 10^{-5}$)	N	n	$\lambda \pm$ SE	Transformation frequency[a] ± SE ($\times 10^4$)	95% confidence limits
0	0	0.93	50	47	0.062 ± 0.036	0.33 ± 0.19	0.00–0.71
0.22	44.6	0.82	50	19	0.97 ± 0.18	5.90 ± 1.10	3.70–8.10
0	0	2.10	45	38	0.17 ± 0.06	0.36 ± 0.14	0.08–0.64
10.7	45.1	1.62	50	22	0.82 ± 0.16	2.53 ± 0.49	1.55–3.51

Notes. N = total number of T-75 flasks, n = number of T-75 flasks without foci, λ = mean number of foci/flask = $-\ln(n/N) \pm \sqrt{\frac{1}{n} - \frac{1}{N}}$. SE = standard error of the mean.

[a]Transformants per surviving cell = $\lambda \cdot N/S$.

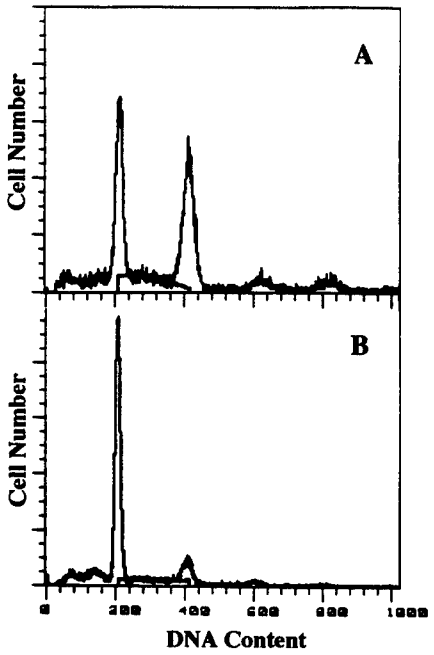

FIG. 2. Flow cytometric analysis of DNA from (A) cells harvested at mitosis (initial mitotic index >0.90) and (B) cells in mid-G_1 phase (i.e. 5 h after mitosis) under circumstances designed to mimic the condition of the cells at the time of irradiation. It is clear from the analysis of the mitotic cell population data that this population has undergone cell progression, resulting in cells in the G_1 phase of the cell cycle by the time irradiation is begun. This cell population is estimated to be composed of approximately 50% late mitotic cells and 50% early G_1-phase cells. The mid-G_1-phase population contains 78% G_1-phase cells. The analysis of cell cycle distributions was determined on data less than 580 DNA content units to avoid any bias from higher aggregates of DNA which are most likely due to nuclei clumping from the fixation and staining protocol.

of HeLa × skin fibroblast human hybrid cells by fission-spectrum neutrons. Furthermore, our results indicate that the cell cycle dependencies for γ-ray-induced and fission-neutron-induced neoplastic transformation of HeLa × skin fibroblast human hybrid cells are different. While mitotic cells showed an enhanced sensitivity (factor of 6) to 1 Gy γ radiation compared with asynchronous and mid-G_1-phase cells (*24*), there was no evidence of any significant difference between late mitotic/early G_1-phase, mid-G_1-phase and asynchronous cells to fission-neutron irradiation for this end point. The fact that cell populations that show great differences in sensitivity to γ radiation show similar sensitivities to fission neutrons in terms of both cell killing and neoplastic transformation is consistent with classical radiobiological dogma *vis à vis* low- vs high-LET radiation.

Evidence for the mid-G_1 phase as a potential sensitive window for monoenergetic (5.9 MeV, average LET = 40 keV/μm) neutron-induced neoplastic transformation of C3H 10T1/2 cells has been observed (R. C. Miller, private communication). The experiments reported here using fission neutrons show cells in mid-G_1 phase to be no more sensitive than either asynchronous or late mitotic/early G_1-phase cells at the $P = 0.05$ level. It has to be concluded, therefore, that mid-G_1 phase does not qualify as the radiosensitive window for this human hybrid cell line irradiated with fission-spectrum neutrons.

The two most recent considerations of a biophysical model to explain the inverse dose-rate effect (*22*, *23*) are both derived from an earlier model (*20*) that postulated that cells are especially sensitive to radiation-induced neoplastic transformation by fission neutrons during some unspecified period of the cell cycle. One of the major differences between these more recent analyses and the original model is with respect to the duration of this radiosensitive window. The original estimate of 7–12 min (*20*) has been extended to approximately 1 h (*22*, *23*). It should be noted that this latest estimate is close to an earlier estimate of 50 min for the duration of the process that results in enhanced transformation (*2*). These latest estimates of the period of enhanced sensitivity have led to the suggestion that this radiosensitive window may be in and around mitosis, i.e.

TABLE II

Comparison of the Sensitivities of Asynchronous, Late Mitotic/Early G_1-Phase and Mid-G_1-Phase Nontumorigenic HeLa × Skin Fibroblast Human Cell Hybrids to Neoplastic Transformation by TRIGA Reactor Fission-Spectrum Neutrons Delivered at a Dose Rate of 10.9 ± 0.7 cGy/min

Cell cycle phase	Mean dose ± SE (cGy)	Number of surviving cells ($\times 10^{-5}$)	N	n	λ ± SE	Transformation frequency[a] ± SE ($\times 10^4$)	95% confidence limits
Asynchronous	0	3.09	137	126	0.84 ± 0.024	0.37 ± 0.11	0.15–0.59
Late M/early G_1 phase	0	1.11	62	55	0.12 ± 0.045	0.67 ± 0.25	0.17–1.17
Mid-G_1 phase	0	1.13	70	61	0.14 ± 0.046	0.87 ± 0.28	0.31–1.43
Asynchronous	45.6 ± 1.2	4.42	208	117	0.58 ± 0.062	2.73 ± 0.29	2.15–3.31
Late M/early G_1 phase	44.9 ± 0.3	4.89	145	61	0.87 ± 0.097	2.56 ± 0.29	1.98–3.14
Mid-G_1 phase	44.9 ± 0.3	2.53	120	49	0.90 ± 0.11	4.27 ± 0.52	3.23–5.31

Notes. N = total number of T-75 flasks, n = number of T-75 flasks without foci, λ = mean number of foci/flask = $-\ln(n/N) \pm \sqrt{\frac{1}{n} - \frac{1}{N}}$. SE = standard error of the mean.

[a]Transformants per surviving cell = $\lambda \cdot N/S$.

late G_2-phase/early mitosis and/or late mitosis/early G_1 phase (*23*). The data in this paper rule out late mitosis/early G_1 and mid-G_1 phases as periods of enhanced sensitivity, at least for these cells. Nonetheless, these human hybrid cells consistently show an inverse dose-rate effect for neoplastic transformation at low doses of fission-spectrum neutrons. It is obviously necessary to examine additional positions of cells in the cell cycle before one can rule out the hypothesis based on an extra-sensitive period in the cell cycle. Late G_2 phase/early mitosis is an obvious period to examine based on the observed sensitivity of this phase of the cell cycle to neoplastic transformation by low-LET radiation (*24–26*).

ACKNOWLEDGMENTS

The authors thank Deborah M. Mosbrook (Radiation Biophysics Department, AFRRI) and the staffs of AFRRI's Reactor Division and Radiation Health Physics Division for their excellent technical support. We are also grateful to Dr. E. John Ainsworth for his support and encouragement in pursuing this research. This research was supported by American Cancer Society Grant DHP-71 and AFRRI under work unit 04640. The views presented in this paper are those of the authors and do not necessarily reflect those of AFRRI.

Received: March 23, 1994; accepted: September 1, 1994

REFERENCES

1. C. K. Hill, F. M. Buonagura, C. P. Myers, A. Han and M. M. Elkind, Fission-spectrum neutrons at reduced dose rates enhance neoplastic transformation. *Nature* **298**, 67–69 (1982).
2. C. K Hill, A. Han and M. M. Elkind, Fission-spectrum neutrons at a low dose rate enhance neoplastic transformation in the linear, low dose region (0–10 cGy). *Int. J. Radiat. Biol.* **46**, 11–15 (1984).
3. C. K. Hill, B. A. Carnes, A. Han and M. M. Elkind, Neoplastic transformation is enhanced by multiple low doses of fission-spectrum neutrons. *Radiat. Res.* **102**, 404–410 (1985).
4. C. A. Jones, B. A. Sedita, C. K. Hill and M. M. Elkind, Influence of dose rate on the transformation of Syrian hamster embryo cells by fission-spectrum neutrons. In *Low Dose Radiation—Biological Bases of Risk Assessment* (K. F. Baverstock and J. W. Stather, Eds.), pp. 539–546. Taylor & Francis, London, 1989.
5. R. C. Miller, D. J. Brenner, C. R. Geard, K. Komatsu, S. A. Marino and E. J. Hall, Oncogenic transformation by fractionated doses of neutrons. *Radiat. Res.* **114**, 589–598 (1988).
6. J. L. Redpath, C. K. Hill, C. A. Jones and C. Sun, Fission-neutron-induced expression of a tumor-associated antigen in human cell hybrids (HeLa × skin fibroblast): Evidence for increased expression at low dose rate. *Int. J. Radiat. Biol.* **58**, 673–680 (1990).
7. J. L. Redpath, C. Sun and W. F. Blakely, Effect of fission-neutron dose rate on the induction of a tumor-associated antigen in human cell hybrids (HeLa × skin fibroblast). *Radiat. Res.* **128**, S71–S74 (1991).
8. R. C. Miller, G. Randers-Pehrson, L. Heiber, S. A. Marino, M. Richards and E. J. Hall, The inverse dose-rate effect for oncogenic transformation by charged particles is dependent on linear energy transfer. *Radiat. Res.* **133**, 360–364 (1993).
9. D. J. Brenner, E. J. Hall, G. Randers-Pehrson and R. C. Miller, Mechanistic considerations on the dose-rate/LET dependence of oncogenic transformation by ionizing radiations. *Radiat. Res.* **133**, 365–369 (1993).
10. J. F. Thomson, F. S. Williamson, D. Grahn and E. J. Ainsworth, Life shortening in mice exposed to fission neutrons and gamma rays. II. Duration of life and long-term fractionated exposures. *Radiat. Res.* **86**, 573–579 (1981).
11. R. L. Ullrich and J. B. Storer, Life shortening and tumor induction after low doses of fission neutrons. *Radiat. Res.* **87**, 453 (1981). [Abstract]
12. H. H. Vogel, Jr. and H. W. Dickson, Mammary neoplasia following acute and protracted irradiation with fission neutrons and ^{60}Cobalt gamma-rays. *Radiat. Res.* **87**, 453–454 (1981). [Abstract]
13. R. L. Ullrich, Tumor induction in BALB/c mice after fractionated or protracted exposure to fission-spectrum neutrons. *Radiat. Res.* **97**, 587–597 (1984).
14. E. K. Balcer-Kubiczek, G. H. Harrison, G. H. Zeman, P. J. Mattson and A. Kunska, Lack of inverse dose rate effect on fission neutron induced transformation of C3H10T1/2 cells. *Int. J. Radiat. Biol.* **54**, 531–536 (1988).
15. E. K. Balcer-Kubiczek and G. H. Harrison, Lack of dose rate modification of fission neutron-induced neoplastic transformation in C3H10T1/2 cells. *Int. J. Radiat. Biol.* **59**, 1017–1026 (1991).
16. L. Hieber, G. Ponsel, H. Roos, S. Fenn, E. Fromke and A. M. Kellerer, Absence of a dose-rate effect in the transformation of C3H10T1/2 cells by alpha particles. *Int. J. Radiat. Biol.* **52**, 859–869 (1987).
17. M. Terzaghi-Howe, Induction of preneoplastic alterations by X rays and neutrons in exposed rat tracheas and isolated tracheal epithelial cells. *Radiat. Res.* **120**, 352–363 (1989).
18. P. R. Burch and M. S. Chesters, Neoplastic transformation of cells *in vitro* at low and high dose rates of fission neutrons: An interpretation. *Int. J. Radiat. Biol.* **49**, 495–500 (1986).
19. M. M. Elkind and C. K. Hill, Biophysical models for the role of intracellular repair in the anomalous enhancement of neoplastic transformation by low doses of fission-spectrum neutrons at low dose rates. Reply to the letter to the Editor by P. R. J. Burch and M. S. Chesters. *Int. J. Radiat. Biol.* **50**, 181–183 (1986).
20. H. H. Rossi and A. M. Kellerer, The dose rate dependence of oncogenic transformation by neutrons may be due to variation of response during the cell cycle. *Int. J. Radiat. Biol.* **50**, 353–361 (1986).
21. M. M. Elkind and C. K. Hill, Age dependent variations in cellular susceptibility to neoplastic transformation. Reply to the letter to the Editor by H. H. Rossi and A. M. Vellere. *Int. J. Radiat. Biol.* **50**, 1117–1122 (1986).
22. D. J. Brenner and E. J. Hall, The inverse dose rate effect for oncogenic transformation by neutrons and charged particles: A plausible interpretation consistent with published data. *Int. J. Radiat. Biol.* **58**, 745–758 (1990).
23. M. M. Elkind, Enhanced neoplastic transformation due to protracted exposures of fission spectrum neutrons: biophysical model. *Int. J. Radiat. Biol.* **59**, 1467–1475 (1991).
24. J. L. Redpath and C. Sun, Sensitivity of a human hybrid cell line (HeLa × skin fibroblast) to radiation-induced neoplastic transformation in G_2, M and mid-G_1 phases of the cell cycle. *Radiat. Res.* **121**, 206–211 (1990).
25. J. M. Cao, R. L. Wells and M. M. Elkind, Enhanced sensitivity to neoplastic transformation by 137-Cs gamma rays of cells in the G_2-/M-phase age interval. *Int. J. Radiat. Biol.* **62**, 191–199 (1992).
26. R. C. Miller, C. R. Geard, M. J. Geard and E. J. Hall, Cell-cycle-dependent radiation-induced oncogenic transformation of C3H 10T1/2 cells. *Radiat. Res.* **130**, 129–133 (1991).
27. C. J. Der and E. J. Stanbridge, A tumor-specific membrane phosphoprotein marker in human cell hybrids. *Cell* **26**, 429–438 (1981).

28. D. C. Bicknell, D. R. Sutherland, E. J. Stanbridge and M. F. Greaves, Monoclonal antibodies specific for a tumor-associated membrane phosphoprotein in human cell hybrids. *Hybridoma* **4**, 143–152 (1985).

29. K. M. Latham and E. J. Stanbridge, Identification of the HeLa tumor-associated antigen, p75/150, as intestinal alkaline phosphatase and evidence for its transcriptional regulation. *Proc. Natl. Acad. Sci. USA* **87**, 1263–1267 (1990).

30. K. M. Latham and E. J. Stanbridge, Examination of the oncogenic potential of a tumor-associated antigen, intestinal alkaline phosphatase, in HeLa × fibroblast hybrids. *Cancer Res.* **52**, 616–622 (1992).

31. J. L. Redpath, C. Sun, M. Colman and E. J. Stanbridge, Neoplastic transformation of human hybrid cells by irradiation: A quantitative assay. *Radiat. Res.* **110**, 468–472 (1987).

32. C. Sun, J. L. Redpath, M. Colman and E. J. Stanbridge, Further studies on the radiation-induced expression of a tumor-specific antigen in human cell hybrids. *Radiat. Res.* **114**, 84–93 (1988).

33. C. Sun, M. Colman and J. L. Redpath, Suppression of radiation-induced expression of a tumor-associated antigen in human cell hybrids by the protease inhibitor antipain. *Carcinogenesis* **9**, 2333–2335 (1988).

34. M. S. Mendonca, C. Sun and J. L. Redpath, Suppression of radiation-induced neoplastic transformation of human cell hybrids by long term incubation at low extracellular pH. *Cancer Res.* **50**, 2123–2127 (1990).

35. E. J. Stanbridge, R. R. Flandemeyer, D. W. Daniels and W. A. Nelson-Rees, Specific chromosome loss associated with expression of tumorigenicity in human cell hybrids. *Somat. Cell Genet.* **7**, 699–712 (1981).

36. E. S. Srivatsan, W. F. Benedict and E. J. Stanbridge, Implication of chromosome 11 in the suppression of neoplastic expression in human cell hybrids. *Cancer Res.* **46**, 6174–6179 (1986).

37. P. J. Saxon, E. S. Srivatsan and E. J. Stanbridge, Introduction of human chromosome 11 via microcell transfer controls tumorigenic expression of HeLa cells. *EMBO J.* **5**, 3461–3466 (1986).

38. M. Kaelbling and H. P. Klinger, Suppression of tumorigenicity in somatic cells. III. Cosegregation of human chromosome 11 of a normal cell and suppression of tumorigenicity in intraspecies hybrids of normal diploid × malignant cells. *Cytogenet. Cell Genet.* **41**, 67–70 (1986).

39. J. L. Redpath, M. Mendonca, C. Sun, R. Antoniono, M. Colman, K. M. Latham and E. J. Stanbridge, Tumor suppressor gene inactivation and radiation-induced neoplastic transformation *in vitro*: Model studies using human hybrid cells. In *Radiation Research: A Twentieth-Century Perspective*, Vol. 2 (W. C. Dewey, M. Edington, R. J. M. Fry, E. J. Hall and G. F. Whitmore, Eds.), pp. 342–347. Academic Press, San Diego, 1992.

40. M. S. Mendonca, R. J. Antoniono, C. Sun and J. L. Redpath, A simplified and rapid staining method for the HeLa × skin fibroblast human hybrid cell neoplastic transformation assay. *Radiat. Res.* **131**, 345–350 (1992).

41. C. Sun and J. L. Redpath, Application of a freeze–thaw technique to studies of radiation-induced cell transformation. *Int. J. Radiat. Biol.* **54**, 825–827 (1988).

42. I. W. Taylor, A rapid single step staining technique for DNA analysis by flow microfluorimetry. *J. Histochem. Cytochem.* **28**, 1021–1024 (1980).

43. J-P. Meulders, Dosimetry in mixed n + γ fields. In *Ionizing Radiation: Protection and Dosimetry* (G. Paic, Ed.), pp. 203–216. CRC Press, Boca Raton, FL, 1988.

44. W. K. Sinclair and R. A. Morton, X-ray and ultraviolet sensitivity of synchronized Chinese hamster cells at various stages of the cell cycle. *Biophys. J.* **5**, 1–25 (1965).

45. A. Han and M. M. Elkind, Transformation of mouse C3H10T1/2 cells by single and fractionated doses of X-rays and fission-spectrum neutrons. *Cancer Res.* **39**, 123–130 (1979).

In: Dubois A, King GL, Livengood DR (eds)
Radiation and the Gastrointestinal Tract (1994).
Boca Raton, Fla.: CRC Press, Inc.

Chapter 15

NUTRITIONAL SUPPORT OF IRRADIATED INTESTINE

Venkataraman Srinivasan and Andre Dubois

I. NUTRITION AND GASTROINTESTINAL MUCOSA

Eating, digestion, and the presence of food within the intestinal lumen produce a series of complex physiological responses that result in the growth of gastrointestinal (GI) mucosa and the maintenance of gut mass.[1] Pancreaticobiliary secretion and hormones such as insulin and thyroxine as well as trophic hormones are known to substantially influence the GI tract morphology and function. The presence of food in the GI tract directly affects mucosal growth by contributing to villus exfoliation and by providing local nutrition (Figure 1). The indirect effects of the food in the GI tract include neuronal stimulation, increased motility, and release of several gastrointestinal peptides.[2]

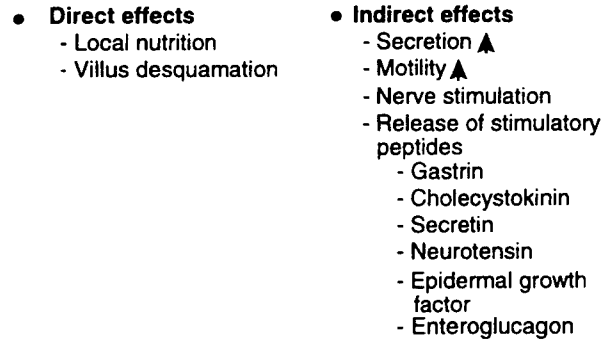

Figure 1. Influence of nutrition on GI structure.[1] (Redrawn with permission.)

During starvation the intestinal mass is significantly reduced with a concomitant decrease in the count of proliferating enterocytes, a prolongation of cell cycle and a delay in cell migration.[2] Similar changes have also been noted during gastrointestinal injury due to stress or surgery. The route of administration and the composition of the nutrients are also important in mucosal morphology.[3] Thompson et al. demonstrated that rats given total parenteral nutrition developed significant intestinal hypoplasia.[4] The activity of diamine oxidase, an intestinal mucosal enzyme which serves as a marker of cellular maturity and integrity, was also significantly reduced in these

intravenously-fed rats.[4] Similarly, it has been well documented in humans that long-term parenteral nutrition results in loss of integrity of the GI tract. In contrast, increased food intake during cold acclimatization results in increased food intake and adaptive hyperplastic growth of mucosa in experimental animals.[3] Therefore, there appears to be a correlation between the nutrient distribution in the GI tract and its normal structural profile.[5] Despite the recognition of a role for oral nutrient intake on the maintenance of gastrointestinal mucosa, the precise relationship between individual dietary components and the mucosal integrity has not been clearly established. Studies in jejunectomized rats indicate that intragastric administration of carbohydrates or proteins do not effectively prevent hypoplasia associated with total parenteral nutrition.[6] However, recent clinical and experimental studies show that administration or feeding of the amino acid glutamine is effective in preventing gastrointestinal injury. Furthermore, patients undergoing postoperative care as well as patients exposed to total body irradiation for bone marrow transplantation exhibit characteristic gastrointestinal injury that is significantly reduced by oral or parenteral administration of glutamine.[7] Therefore, glutamine is emerging as the single potential nutrient for the prevention of gastrointestinal injury under various experimental conditions. The role of glutamine in radiation-induced gastrointestinal injury will be described later.

The gut is a metabolically active tissue with enormous cellular surface accounted for by mucosal villi and microvilli. The specific nutritional needs of this organ to sustain normal structure and adequate function have been recognized.[8] The enterocytes and colonocytes covering this surface are in a constant state of rapid proliferation, and their increased demand for nutrients is met by the unique ability of the intestine to draw nutrients from both the blood and the intestinal lumen. Animal studies have shown that the amino acid glutamine acts as the preferred respiratory fuel for the GI tract.[9] The other major fuels of the GI tract are the ketone bodies β-hydroxy-butyrate and acetoacetate. However, use of these fuels appears to be species specific.[9] The ketone bodies are utilized by the rat enterocytes while the dog enterocytes do not utilize them. Colonocytes on the other hand utilize short chain fatty acids (SCFA), produced by bacterial fermentation of polysaccharides from the dietary fiber as well as from *n*-butyrate, glutamine, and ketone bodies as primary fuels. Structural and functional changes may occur in the colon by depletion of these nutrients.[10]

The relationship between functional aspects of the GI tract and nutrition have also been studied extensively. Starvation and malnutrition alter mucosal permeability, resulting in bacterial translocation and generalized bacteremia and death.[11] The immunological system of the GI tract, consisting of intestinal lymphocytes, macrophages, secretory IgA, and mesenteric lymph nodes, is critical in the prevention of bacterial translocation. Alverdy et al.[12] have shown that decreased secretion of intestinal IgA is inversely

related to increased bacterial translocation of cecal anaerobes. Furthermore, Ardawi and Newsholme[13] and Newsholme et al.[14] have demonstrated that lymphocytes and macrophages possess high glutaminase activity and utilize significant amount of glutamine. Finally, it was suggested that glutamine is essential for lymphocyte proliferation in response to antigenic challenge both as a precursor of nucleotide and as a major energy source (Figure 2).

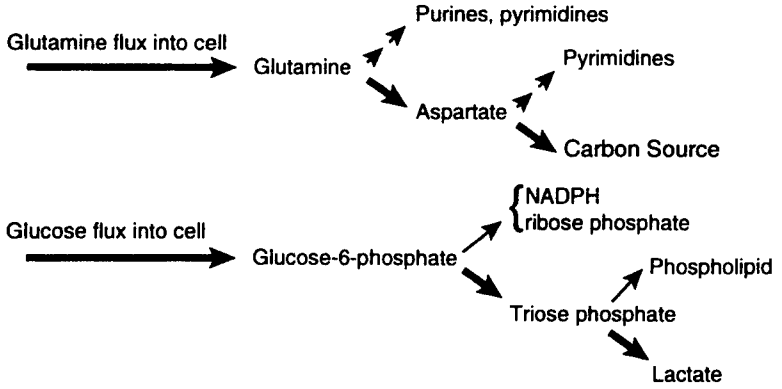

Figure 2. Glutamine utilization as a precursor for nucleotides and as a major energy source.[14] (Redrawn with permission.)

II. RADIATION-INDUCED GI INJURY

The degree of GI injury due to ionizing radiation depends on a variety of conditions. The acute, subacute and chronic effects of ionizing radiation on the digestive tract appear in a manner that is both dose- and time-dependent.[15,16] The relationship between dose-rate, fractionation, type of radiation with different linear energy transfer (LET) potential, and their influence on GI damage has been described.[17] Thus, neutron radiation is more destructive to intestinal cells than similar quantities of gamma photon irradiation. As discussed by Gunter-Smith elsewhere in this volume (Chapter 11), radiation causes early functional alterations of electrolytes transport[18] as well as subsequent structural damage. The GI injury that may appear one to three weeks after radiation is characterized by diminished replacement of epithelial cells that, when combined with normal sloughing of differentiated cells, leads to the depletion of mature intestinal surface epithelial cells. Such a subacute injury results in the breakdown of the intestinal luminal barrier and may be responsible in part for radiation-induced lethality. The alterations in the crypts and villi have been used as an index to assess GI damage following ionizing radiation. More recently, scanning and transmission electron microscopy have delineated the ultrastructural changes observed in the GI tract of animals exposed to X-radiation, either alone, or in combination with hyperthermia and neutron irradiation (Figure 3).[19,20]

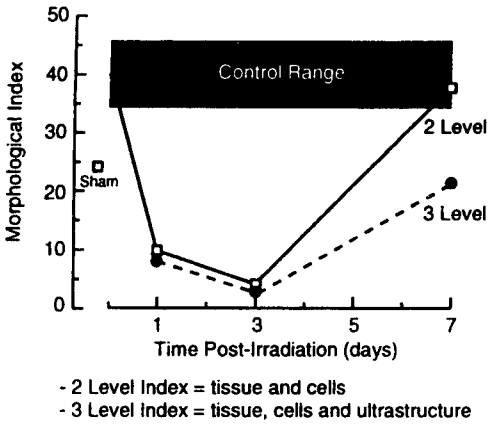

Figure 3. Multiple morphometric index range: summary of tissue, cell and ultrastructural scores.[20]

Thus, 20, 65, and 90% of all proliferating cells were inhibited after 2.5 Gy, 8 Gy, and 12 Gy of gamma irradiation, respectively.[20] In addition, different cell types and tissues of the mouse small intestine were modified by ionizing radiation (Figure 3, Table 1). Tissue indices showed a drop at day 1 and 3 and partial recovery of nerve cells and epithelial cells (not shown) while the muscle score continued to drop up to at least the last time point. Therefore, the electron microscopic studies[20] suggest that the conventional crypt/microcolony assay utilized by several investigators to describe changes in GI due to ionizing radiation does not totally describe the fine alterations induced by ionizing radiation in different cell types of the GI tract (Table 1).

Table 1. Comparison of Tissue Scores.[20]

Type	Day 1	Day 3	Day 7
Villus scores	↓	↓	↓↓
Muscle 3 level	↓	↓↓	↓↓↓
Nerve 3 level	↓*	↓↓*	↓↓↓
Cryptal cell-separation	↓	↓↓	↓↓↓
Connective tissue-vacuoles	↓	↓↓	↓↓↓

III. PROTECTION AGAINST RADIATION-INDUCED GI DAMAGE: ROLE OF NUTRITION

As discussed in Chapters 13 and 14, free radical scavengers such as WR-2721 as well as prostaglandins have been shown to minimize radiation-induced damage to stem cells in the crypts of the GI tract.[21] In this chapter, we will focus on the role of nutrients in GI radioprotection. Antioxidant nutrients such as vitamin E and selenomethionine have been shown to be effective radioprotectors when given either alone or in combination with phosphorothioate (WR compounds) radioprotectors such as WR-3689 and WR-2721.[22,23] Radioprotection by other nutrients such as selenium,[23] copper,[24] zinc,[25] and vitamin A[26] have also been demonstrated in experimental animals, whereas vitamin C has been shown to have no radioprotective characteristics in vivo.[27] Furthermore, injection of ascorbate together with cysteamine (ß-mercaptoethylamin or MEA) partially reversed the radioprotective action of MEA and suppressed the action of MEA on RNA synthesis in bone marrow cells in mice.[28] The concept of combining different radioprotective compounds in achieving a better protection has been considered by many investigators and has been reviewed by Weiss et al.[29] For example, significant radioprotection was achieved in rodents by using a combination of non-nutrient compounds: a low dose of WR-3689 (50 mg/kg), a dose with minimal behavioral toxicity, plus eicosanoids (misoprostol and iloprost) and the immunomodulator 3D-MPL.[30]

In addition, various lines of evidence indicate that the antioxidants nutrients may exert their radioprotective effect by influencing the immune system in addition to acting as radical scavengers. We have shown, for example, that vitamin E and WR-2721 significantly reversed immunosuppression induced by ionizing radiation as measured by delayed hypersensitivity response reflecting a T lymphocyte function.[31] Furthermore, Roy and Petrella[32] determined serum hemagglutination titers (HA) to sheep red blood cells in mice subjected to irradiation and maintained on vitamin E deficient diets for 8 weeks. Vitamin E injection increased IgG titers and partially reversed radiation-induced depression of lymphocyte response.

This radioprotection against the hemopoietic system may be used as a model for GI radioprotection. Paulus et al. compared the hematopoietic stem cells to the stem cell equivalent (crypts) of the digestive tract, demonstrating that the regulatory processes were very similar in the two systems.[33] More recently GI mucosal injury due to oxidative stress in experimental animals was shown to be prevented by vitamin E administration.[34] Further, Empey et al.[35] have shown in their experiments with local irradiation of the abdomen that vitamin E administration preserved the GI structure.

In recent years, the importance of diet therapy in the treatment of gastrointestinal diseases has become better defined.[36] A number of elemental diets containing predigested proteins and various amounts of

carbohydrates and fats have been shown to alleviate various clinical conditions.[37] However, hypoplasia of the small bowel mucosa and loss in functional integrity has been noted during prolonged feeding of an elemental diet.[38] Further, increased bacterial translocation have also been documented. Recent evidence indicates that the increased bacterial translocation attributable to elemental diet therapy can be controlled by incorporation of dietary fiber or by treatment with hormones such as bombesin or somatostatin.[39]

The effectiveness of elemental diet protection against radiation-induced intestinal injury was studied in experimental animals. It was observed that elemental diet facilitated mucosal healing by maintenance of glycocalyx and its normal content of disaccharides.[40] However, the nutritional management of patients with chronic radiation enteropathy depends on a variety of factors such as the degree of damage, the functionality, the region affected, etc. Many metabolic changes such as malabsorption of protein, fat soluble vitamins and micronutrients might ensue after irradiation. Clinical studies reveal that continuous feeding of elemental diets starting three days before irradiation and continued after irradiation significantly minimized mucosal damage attributable to radiation.[41] Furthermore, other investigators have also shown the beneficiary effects of elemental diet in the prevention of acute and delayed radiation enteropathy as well as in Crohn's disease.[42] To summarize, the approach of using elemental diets to minimize or prevent GI damage caused by various agents such as chemicals or ionizing radiation appears promising and should be pursued in greater detail.

IV. ROLE OF GLUTAMINE IN THE PROTECTION AGAINST RADIATION-INDUCED GI DAMAGE

The GI tract is the major organ of glutamine utilization. Glutamine is taken up by the epithelial cells that line the intestinal villi. There are dietary and arterial supplies of glutamine to the intestinal mucosa. Historically, the role of glutamine in ammonia metabolism was first demonstrated in kidneys by Sir Hans Krebs in 1935. Glutamine was shown to be essential for mammalian cells in culture by Eagle in 1955.

Studies in rats have shown that the rate of utilization of glutamine in the jejunum is comparable when the glutamine is derived from the lumen or from the arterial blood.[43] After a protein meal, the dietary source of glutamine is in the form of oligopeptides. Metabolic studies indicate that glutamine dipeptide is absorbed as such and is then hydrolyzed intracellularly.[44] Further, parenteral administration of either glutamine or glutamine dipeptide brings about similar metabolic effects.[45]

The importance of dietary glutamine in reversing the hypoplasia of GI tract in glutamine-deficient rats has been established.[46] Further, glutamine feeding resulted in adaptive hyperplasia after partial intestinal resection in experimental animals.[50] The mucosal atrophy observed in experimental

animals on total parenteral nutrition solution correlates with the deficiency of glutamine. In addition, changes in tissue glutamine concentrations have also been shown to correlate with net protein turnover. The mechanism of this effect of glutamine is unclear. Recent in vitro data suggest that, although epidermal growth factor (EGF) directly activates the early growth response genes that encode nuclear transcription factors, glutamine is a necessary cofactor for the actual synthesis of nucleic acids and proteins.[47] Glutamine also plays an important role in regulating the metabolism during the catabolic state. It is released from muscle and is utilized by the kidney, macrophages, and lymphocytes as well as by intestinal mucosal cells. Recent studies have shown that glutamine may be a conditionally essential nutrient and that its requirement may increase two- to threefold during postoperative conditions.[48] During stress and organ failure, the GI tract is severely challenged, and its support requires particular attention. Several authors have compared the protective effect of arginine, xylitol, growth hormone, glutamine, and branched chain amino acids.[14] They found that glutamine appeared to be the most effective agent in protecting the GI tract. Glutamine supplementation has also been shown to be beneficial in rats during septic shock[49] and in dogs after small bowel resection.[50] Therefore, glutamine or glutamine peptides appear to play an important role in GI mucosal integrity.

The beneficial effect of glutamine in combination with an elemental diet was demonstrated in the sarcoma rat model.[51] In this model, the toxicity of methotrexate was reduced, and its tumoricidal effectiveness was enhanced by glutamine administration. In contrast, Xu et al.[52] were unable to demonstrate the effectiveness of glutamine in reversing the increased bacterial translocation observed after prolonged feeding of an elemental diet. Further, these authors were unable to demonstrate the beneficial effect of glutamine on immunosuppression observed after feeding elemental diet.

Souba et al[53] demonstrated the role of nutrients such as glutamine in preventing subacute GI tissue damage due to ionizing radiation. Bacterial translocation was studied in rats exposed to 10 Gy X-radiation (dose rate 2.27 Gy/min) to the abdomen, with the thorax, head, gonads and extremities shielded. Glutamine was provided through drinking water. The animals receiving glutamine showed lower culture positive lymph nodes (20%) as compared to a greater culture positive lymph nodes (89%) in unsupplemented animals. The predominance of gram negative rods (*Escherichia coli*) in the culture positive lymph nodes indicated that the bacterial flora of the gut was involved in translocation and that such a translocation was inhibited by glutamine administration. The protective effect of oral glutamine after abdominal radiation (10 Gy) was studied in experimental animals.[53] The survival rate was 100% in animals receiving glutamine when compared with 45% in animals receiving glycine. Glutamine ingestion diminished bloody diarrhea and the incidence of bowel perforation. Another study evaluated the

effect of glutamine along with elemental diet on the intestinal mucosal growth and function.[54] 10 Gy of X-irradiation were delivered to the abdomen of rats which were given 4 days of either glutamine-enriched or glutamine-free elemental diet. After irradiation, all animals received a glutamine-free diet. Four days later, animals fed the glutamine-enriched elemental diet had a significant increase in the number and height of jejunal villi compared to animals fed the glutamine-free diet. This protection of the small bowel mucosa appeared to be mediated by a glutamine-induced increase in crypt cell proliferation. Recently, Klimberg et al.[55] have shown that glutamine given with elemental diet before radiation significantly increased the jejunal villous number, villous height, and number of metaphase mitosis per crypt.

Nutritional support has been considered to play a key role in preventing metabolic failure.[56] The catabolic states resulting from trauma, sepsis or surgery are associated with net skeletal muscle breakdown. The positive role of glutamine-enriched parenteral nutrition in improving nitrogen balance has been documented in postoperative patients[7,57] (Table 2). The purpose of these studies was to improve nitrogen retention and reduce hospital stay in patients who undergo radiotherapy for bone marrow transplantation. Results revealed that nutrient intake was comparable between control and glutamine-supplemented groups. However, nitrogen balance was improved significantly in the glutamine-treated group. The clinical infection rate was also significantly reduced although the number of antibiotic days was similar. The hospital stay was reduced from an average of 36 days in the control group to 29 days in the glutamine-supplemented group. Recently, Schloerb and Amare[58] following the same protocol of glutamine administration in BMT patients subjected to radiotherapy confirmed the earlier observations of Zeigler et al[7]. A significant reduction in days of hospitalization was again noted in patients on glutamine-supplemented total parenteral nutrition. Glutamine supplementation also benefitted patients with solid tumors undergoing BMT. However, hospitalized patients receiving standard total parenteral nutrition for reasons other than bone marrow transplantation did not significantly benefit from incorporation of glutamine in the parenteral solution.[58] These results suggest that, although the potential benefits induced by glutamine administration in TPN patients are apparent, additional studies are required to establish the conditions wherein the efficacy of glutamine is optimal.

Thus experimental and clinical evidence clearly demonstrates the beneficial effects of glutamine administration on GI protection under various conditions such as after exposure to ionizing radiation or after certain chemical or drug therapy. However, glutamine may not be effective under certain conditions as has been noted in the clinic.[45] Scott and Moellman[59] also observed that intravenous glutamine administration did not accelerate small bowel mucosal

indwelling catheters were inserted in the jugular veins of rats which subsequently received 10 Gy of abdominal irradiation. Isonitrogenous and isocaloric intravenous total parenteral nutrition containing either 0 or 2% glutamine was given for 5 days postirradiation. Irradiation caused a similar 40% decrement in both the villous height and the DNA content of intestinal segments in the two groups of animals.

Table 2.
Effect of Parenteral Nutrition with or without Glutamine on Various Parameters in Patients Subjected to Total Body Radiation for Bone Marrow Transplantation (After Ziegler et al.[7])

Variable	Standard Parenteral	Glutamine Supplemented
Number	21	24
Hospital stay	36 days	29 days*
Nitrogen bal	-4.2 g/D	-1.4 g/D
Total N bal	-29.6 g/7 D	-9.7 g/7 D*
No. positive culture	1	10*
+ stool culture	16	10*
+ throat culture	18	13*
Clin. infection	9	3
Total antibiotic	15 days	13 days

* Significantly different from standard

These contradictory observations indicate that the route of administration and the experimental conditions appear to modify the radioprotective effect exerted by glutamine on the GI tract. Scott and Moellman[59] showed that i.v. glutamine was ineffective in experimental conditions involving combined injury of radiation and surgery, while both experimental and clinical studies have demonstrated the beneficial effects of dietary glutamine.[54] Therefore it appears that additional investigations will be required to clarify the role of glutamine in the protection of GI structure and function during stress.

V. CONCLUSIONS

The role of nutrition on the GI structure and function has been clearly established by several investigators although in many instances it has not been possible to identify specific changes attributable to individual nutrients. Electron microscopic studies reveal that there are microscopic changes in different cell types of the intestine which should be taken into account while evaluating the alterations to the GI tract after exposure to ionizing radiation.

There is some indication that nutritional supplements may provide a low risk, cost effective intervention that could limit the adverse effects of ionizing radiation on the gut and reduce mortality due to ionizing radiation. Further, experimental and clinical studies indicate that the amino acid glutamine may be a promising nutrient in protecting the GI tract from the ill-effects of ionizing radiation. In many tissues, glutamine appears to serve as an ammonia scavenger and as a nitrogen donor for the biosynthesis of a number of important compounds such as nucleotides, aminosugars and amino acids. Recent clinical studies have aroused considerable interest in the role of glutamine in critical care situations. The results of parenteral administration of glutamine have shown the beneficial role of glutamine against the mucosal atrophy generally associated with total parenteral nutrition.[60,61] Finally, a recent review of the current status of glutamine in hospitalized patients indicates that glutamine supplementation may become a common practice in the near future.[62]

REFERENCES

1. Bragg LE, Thompson JS, Rikkers LF. Influence of nutrient delivery on gut structure and function. Nutrition 1991; 7:237-243.
2. Johnson LR. Regulation of gastrointestinal growth. In: Johnson LR. eds., Physiology of the gastrointestinal tract, 2nd Edition, New York: Raven Press, 1987; 299.
3. Greenberg GR. Nutrition and diet in management of diseases of the gastrointestinal tract: (c) Small intestine: Nutrient interactions with structure. In: Shils ME, Young VR. eds. Modern nutrition in health and disease, 7th Edition, Lea and Febiger, Philadelphia 1988; pp. 1135-1136.
4. Thompson JS, Vaughan WP, Forst CF, Jacobs DL, Weekly JS, Rikkers LF. The effect of the route of nutrient delivery on gut structure and diamine oxidase levels. J Parenter Enteral Nutr 1987; 11:28-32.
5. Karasov WH, Diamond JM. Adaptive regulation of sugar and amino acid transport by vertebrate intestine. Amer J Physiol 1983; 245:G443-G462.
6. Morin CI, Grey VL, Garofalo C. Influence of lipids on intestinal adaptation after resection. In: Mechanism of intestinal adaptation. Robinson JWL, Drowling RH, Riecken ED. eds., Lancaster, UK. MTP Press 1982; 175-184.
7. Ziegler TR, Lorraine SY, Benfell K, Scheltinga M, Hortos K, Bye R, Morrow FD, Jacobs DO, Smith RJ, Antin JH, Wilmore DW. Clinical and metabolic efficacy of glutamine-supplemented parenteral nutrition after bone marrow transplantation: A randomized, double-blind, controlled study. Ann Int Med 1992; 116:821-828.
8. Souba WW, Scott TE, Wilmore DW. Intestinal consumption of intravenously administered fuels. J Parenter Enteral Nutr 1985; 9:18-22.
9. Windmueller HG, Spaeth AE. Identification of ketone bodies and glutamine as the major respiratory fuels in vivo for postabsorptive rat small intestine. J Biol Chem 1978; 253:69-75.
10. Bristol JB, Williamson RCN. Nutrition, operations and intestinal adaptation. J Parenter Enteral Nutr 1988; 12:299-309.
11. Deitch EA. Bacterial translocation of the gut flora. J Trauma 1990; 30:S184-S189.
12. Alverdy JC, Aoys E, Moss, GS. Total parenteral nutrition promotes bacterial translocation from the gut. Surgery 1988; 104:185-190.
13. Ardawi MSM, Newsholme EA. Glutamine metabolism in lymphocytes of the rat. Biochem J 1983; 212:835-842.

14. Newsholme EA, Crabtree B, Ardawi MSM. Glutamine metabolism in lymphocytes: its biochemical, physiological and clinical importance. Quart J Exper Physiol 1985; 70:473-489.
15. Dubois A. Radiation injury to the gut In: *Bockus Gastroenterology*, Section 10. "The Colon and Rectum", Chapter 86., 5th Edition WB. Saunders 1994, in Press
16. Dubois A, Walker RL. Prospects for management of gastrointestinal injury associated with acute radiation syndrome. Gastroentrol 1988; 95:500-507.
17. Alpen EL. *Radiation Biophysics,* Alpen EL, eds., Prentice Hall, Englewood Cliffs, NJ 1990
18. Gunter-Smith PJ. Gamma radiation affects active electrolyte transport by rabbit ileum: Basal Na and Cl transport. Am J Physiol 1986; 250:G540-G545.
19. Dickson GR, Kamel HMH, Hume SP, Jaber M, Carr KE. Early effects on the morphology of the mouse small intestine of single or combined modality treatment of hyperthermia and X-irradiation. Scannning Microscopy 1992; 6:847-854.
20. Carr KE, McCullough JS, Nelson AC, Hume SP, Nunn S, Kamel HMH. Relationship between villous shape and mural structure in neutron irradiated small intestine. Scanning Microscopy 1992; 6:561-572.
21. Hanson WR. Radioprotection of murine intestine by WR-2721, 16-16 dimethyl prostaglandin E_2 and the combination of both agents. Radiat Res 1987; 111:361-373.
22. Srinivasan V, Weiss JF. Radioprotection by vitamin E; Injectable vitamin E administered alone or with WR-3689 enhances survival of irradiated mice. Int J Rad Oncol Biol Phys 1992; 24:841-845.
23. Weiss JF, Srinivasan V, Kumar KS, Landauer MR. Radioprotection by metals: Selenium. Adv in Space Research 1991; 12:223-231.
24. Sorenson JRJ. Bis(3,5-diisopropylsalicyoato)copper(II), a potent radioprotectant with superoxide dismutase mimetic activity. J Med Chem 1984; 27:1747-1749.
25. Floersheim GL, Bieri A. Further studies on selective radioprotection by organic zinc salts and synergism of zinc aspartate with WR-2721. Brit J Radiol 1990; 63:468-475.
26. Seifter E, Rettura G, Padawer J, Levenson, SM. Vitamin A and Beta-carotene as adjunctive therapy to tumor excision, radiation therapy, and chemotherapy. In: Prasad KN. ed. Vitamins, Nutrition, and Cancer. Karger, Basel 1984:1-19.
27. Bacq ZM. In: Kugelmass ed. Chemical Protection against Ionizing Radiation. Charles C. Thomas, Springfield IL. 1965.
28. Forsberg J, Harms-Ringdahi M, Ehrenberg L. Interaction of ascorbate with the radioprotective effect of mercaptoethylamin. An exploratory study in mice, whole animals and cell cultures Int J Radiat Biol 1978; 34:245-252.
29. Weiss JF, Kumar KS, Walden TL, Neta R, Landauer MR, Clark EP. Advances in radioprotection through the use of combined agent regimens. Int J Radiat Biol 1990; 57:709-722.
30. Kumar KS, Bogo V, Srinivasan V, Palazzolo DL, Landauer MR, Clark EP. Radioprotection at drug doses that do not disrupt motivated performance. Unpublished data.
31. Srinivasan V, Jacobs AJ, Simpson SA, Weiss JF. Radioprotection by vitamin E: effects on hepatic enzymes, delayed type hypersensitivity, and postirradiation survival of mice. In: Meyskens FL, Prasad KN. eds. Modulation and mediation of cancer by vitamins. Basel: Karger. 1983, pp 119-131.
32. Roy RM, Petrella M. Humoral immune response of mice injected with tocopherol after exposure to X-radiation. Immunopharmacol Immunotoxicol 1987; 9:47-70.
33. Paulus U, Potten CS, Loeffler M. A model of the control of cellular regeneration in the intestinal crypt after perturbation based solely on the local stem cell regulation. Cell Prolif 1992; 25:559-578.

34. Kurose I, Fakumara D, Miura S, Suematsu M, Suzuki M, Seikizuka E, Nagata H, Morishita T, Tsuchiya MJ. Fluorographic study on the oxidative process of gastric mucosal injury: attenuation effect of vitamin E. Gastroenterol Pathol 1993; 8:254-258.
35. Empey LR, Papp JD, Jewell LD, Fedorak RN. Mucosal protective effects of vitamin E and misoprostol during acute radiation-induced enteritis in rats. Dig Dis Sci 1992; 37:205-214.
36. Cerde JJ. Diet and gastrointestinal disease. Med Clin North Amer 1993; 77:881-887.
37. Bounous G. Elemental diets in the prophylaxis and therapy for intestinal lesions: an update. Surgery 1989; 105:571-575.
38. Hosoda N, Nishi M, Nakagawa M, Hiramatsu Y, Hioki K, Yamamoto M. Structural and functional alterations in the gut of parenterally or enterally fed rats. J Surg Res 1989; 47:129-133.
39. Haskel Y, Xu D, Lu Q, Dietch E. Elemental diet-induced bacterial translocation can be hormonally modulated. Ann Surg 1993; 217:634-642.
40. McArdle AH, Wittnich C, Freeman CR, Duguid WP. Elemental diet as prophylaxis against radiation injury: Histological and ultrastructural studies. Arch Surg 1985; 120:1026-1032.
41. McArdle AH, Reid EC, Laplante MP, Freeman CR. prophylaxis against radiation injury: The use of elemental diet prior to and during radiotherapy for invasive bladder cancer and in early postoperative feeding following radical cystectomy and ileal conduit. Arch Surg 1986; 121:879-884.
42. Bounous G, Lebel E, Shuster J, Gold P, Tahan WT, Bastin E. Dietary protection during radiation therapy. Strahlentherpie 1975; 149:476-483.
43. Windmueller HG, Spaeth AE. Intestinal metabolism of glutamine and glutamate from the lumen as compared to glutamine from blood. Arch Biochem Biophys 1975; 17:662-672.
44. Minami H, Morse EL, Adibi SA. Characteristics and mechanism of glutamine-dipeptide absorption in human intestine. Gasteroenterol 1992; 103:3-11.
45. Jiang ZM, Wang LJ, Qi Y, Liu TH, Qiu MR, Yang NF, Wilmore DW. Comparison of parenteral nutrition supplemented with L-glutamine or glutamine dipeptides. J Parenter Enteral Nutr 1993; 17:134-141.
46. Plattel C, McCauley R, McCulloch R, Hall J. Influence of glutamine and branched amino acids on the jejunal atrophy associated with parenteral nutrition. J Gastroenterol Hepatol 1991; 6:345-349.
47. KO TC, Beauchamp RD, Townsend CM Jr, Thompson JC. Glutamine is essential for epidermal growth factor-stimulated intestinal cell proliferation. Surgery 1993; 114:147-154.
48. Smith RJ, Wilmore DW. Glutamine nutrition and requirements. J Parenter Enteral Nutr 1990; 14:94s-99s.
49. Ardawi MSM. Effects of xylitol- and/or glutamine -supplemented nutrition on septic rats. Clin Sci 1992; 82:419-427.
50. Gouttebel MC, Astre C, Girardot PM, Saint Aubert B, Joyeux H. Clinical, biological, and histological follow-up during intestinal adaptation after small-bowel resection in the dog. Eur Surg Res 1991; 23:333-340.
51. Klimberg VS, Nwokedi E, Hutchins LF, Pappas AA, Lang NP, Broadwater JR, Read RC, Westbrook KC. Glutamine facilitates chemotherapy while reducing toxicity. J Parenter Enteral Nutr 1992; 16:83S-87S.
52. Xu DQL, Thirstrup C, Berg R, Deitch EA. Elemental diet-induced bacterial translocation and immunosuppression is not reversed by glutamine. J Trauma 1993; 35:821-824.
53. Souba WW, Klimberg VS, Hautamaki RD, Mendenhall WH, Bova PC, Howard RJ, Bland KI, Copeland EM. Oral glutamine reduces bacterial translocation following abdominal radiation. J Surg Res 1990; 48:1-5.

54. Klimberg-VS, Souba WW, Dolson DJ, Salloum RM, Hautamaki RD, Plumley DA, Mendenhall WM, Bova FJ, Khan SR, Hacket RL et al. Prophylactic glutamine protects the intestinal mucosa from radiation injury. Cancer 1990; 66:62-68.
55. Klimberg VS, Souba WW, Dolson DJ, Salloum RM, Hautmaki RD, Plumley DA, Mendenhall WM, Bova FJ, Khan SR, Hackett RL, Bland KI, Copeland EM III. Prophylactic glutamine protects the intestinal mucosa from radiation injury. Cancer 1990; 66:62-68.
56. Baue AE. Nutrition and metabolism in sepsis and multisystem organ failure. Surg Clin North Am 1991; 71:549-565.
57. Hammarqvist F, Wernerman J, Ali R, Von der Decken A, Vinners W. Addition of glutamine to total parenteral nutrition after elective abdominal surgery spares free glutamine in muscle, counteracts the fall in muscle protein synthesis, and improves nitrogen balance. Ann Surg 1989; 209:455-61.
58. Schloerb PR, Amare M. Total parenteral nutrition with glutamine in bone marrow transplantation and other clinical applications (a randomized, double -blind study) J Parenter Enteral Nutr 1993; 17:407-413.
59. Scott TE, Moellman JR. Intravenous glutamine fails to improve gut morphology after radiation injury. J Parenter Enteral Nutr 1992; 16:440-444.
60. Grant JP, Snyder PJ. Use of L-glutamine in total parental nutrition. J Surg Res 1988; 44:506-513.
61. O'Dwyer ST, Smith RJ, Hwang TL, Wilmore DW. Maintenance of small bowel mucosa with glutamine-enriched parenteral nutrition. J Parenter Enteral Nutr 1989; 13:579-585.
62. Souba WW. Total parenteral nutrition with glutamine in bone marrow transplantation and other clinical applications (editorial). J Parenter Enteral Nutr 1993; 17:403.

In: Dubois A, King GL, Livengood DR (eds)
Radiation and the Gastrointestinal Tract (1994).
Boca Raton, Fla.: CRC Press, Inc.

Chapter 7

NITRIC OXIDE AND SMOOTH MUSCLE RELAXATION IN THE INTESTINE. CHEMICAL AND RADIATION EFFECTS MEASURED BY EPR/SPIN TRAPPING

Linda Steel-Goodwin and Alasdair J. Carmichael

I. INTRODUCTION

Electron paramagnetic resonance (EPR)/spin trapping was used to compare the effects of the ganglionic blocking agent, hexamethonium bromide (Hex), and γ-radiation on the small intestine. The intestine is an organ containing smooth muscle layers which are continually contracting and relaxing in a spontaneous manner. These spontaneous contractions and relaxations are altered by Hex and ionizing radiation. Exposure to Hex or ionizing radiation will cause the motion to become rhythmical and and cause the contractions and relaxations to increase significantly in amplitude and frequency.[1] The mechanism of the Hex and ionizing radiation induction of this regular pattern of contraction and relaxation is not clear. However, the work of Kagnoff and Kivy-Rosenberg[1] has not excluded the possibility that application of Hex to the intestine results in the removal of some form of ganglionic regulation over postganglionic structures. It could also be possible that Hex directly affects the intestinal smooth muscle. In irradiated animals it is possible that the intestinal ganglia are functionally altered resulting in the regularized pattern. Hex is a quaternary ammonium salt and blocks acetylcholine nicotinic receptors.[2] Nicotine is associated with various cardiovascular diseases (hypertension, myocardial ischemia and infarction) and when added to cultured endothelial cells has been shown by Udeinya et al. to inhibit the release of endothelial derived relaxing factor (EDRF).[3] It has been suggested that nitric oxide ($NO^{\cdot}$) is EDRF.[4] In a recent report Steel-Goodwin et al. using spin trapping techniques showed the Hex-induced production of the free radical, $NO^{\cdot}$, in the small intestine (jejunum).[5,6] It was shown that N^{ω}-nitro-L-arginine (L-NOARG), a specific inhibitor of the $NO^{\cdot}$ generating enzyme nitric oxide synthase (NOS)[7], completely abolished the Hex effect suggesting that $NO^{\cdot}$ is directly involved in the Hex-induced intestinal motility. Since radiation injury occurs through free radical mechanisms and since radiation also induces increased intestinal motility, similar to Hex, it is important to determine the role of $NO^{\cdot}$ in the radiation effects in the intestine. $NO^{\cdot}$ is short-lived, rapidly produced, and diffuses over short distances.[8] Techniques such as spin trapping and chemiluminescence are available to measure $NO^{\cdot}$.[9] Spin trapping is a technique which involves the reaction of a short-lived free radical with a spin trap, usually a nitrone or a nitroso compound, forming a

longer lived nitroxide spin adduct which can be measured using EPR.[10,11] The measurement of NO· in mouse jejunum slices exposed to the chemical Hex or ionizing radiation was compared to nonexposed jejunum slices using the EPR/spin trapping analytical technique. Motility and histology measurements were made on the same tissues to relate the free radical effects to pathological changes.

II. PROCEDURES

Male CD2F1 strain mice (National Cancer Institute, Frederick, MD) weighing 20-25 g, were housed eight to a cage. They were fed a commercial diet (Wayne Rodent Lab Blox, Wayne Pet Food Division, Continental Grain Company, Chicago, IL) and acidified water (pH 2.7) ad libitum. A 12-h light-dark cycle (0700-1900 and 1900-0700, respectively) was used. Mice were placed in plastic containers approximately 15 minutes before total-body irradiation. They were sham irradiated or irradiated (whole body) in a bilateral γ-radiation field of the AFRRI ^{60}Co facility.[12] The midline tissue dose, delivered at a dose rate of 0.1 Gy/min, was 15 Gy. Prior to irradiation, the dose rate was established in an acrylic mouse phantom using 0.5 cc tissue-equivalent ionizing chamber (calibration factor traceable to the National Institute of Standards and Technology). The tissue-air ratio was 0.96 and the field was uniform to within ± 5%. Dosimetric measurements were made in accordance with AAPM protocol for the determination of absorbed dose from high-energy photon and electron beams.[13] Groups of mice were euthanized by cervical dislocation over a period of four days post irradiation. The intestine was immediately excised and washed with saline. Slices of jejunum were placed in incubation media for determination of free radicals and intestinal motility studies or in saline formalin fixative for light histology.

Free radicals were determined by the technique of EPR/spin trapping. The spin trap 3,5-dibromo-4-nitrosobenzenesulfonate (DBNBS) was used in the study. DBNBS was made using the technique developed by Kaur et al.[14] All spin traps were prepared in phosphate buffered saline (PBS) supplemented with 300 U/ml superoxide dismutase (SOD) as described previously by Steel-Goodwin et al.[6,15] The SOD was purchased from Sigma, St Louis, MO. For studies of chemical effects on nitric oxide the ganglionic blocking agent hexamethonium bromide (Hex, Sigma, St Louis, MO) was present in the incubation medium at a concentration of 1mM. The specific NOS inhibitor N^{w}-nitro-L-arginine (L-NOARG, Sigma, St Louis, MO) was added to the incubation media at various concentrations (0-10mM) in both the studies on the Hex-stimulated jejunum slices and the jejunum slices from the irradiated mice. The jejunum slices were preincubated at 37°C for 10 min in PBS supplemented with L-NOARG (0-10 mM) and then they were transferred to the EPR incubation media and incubated at 37°C for 20 to 90 min. Samples of incubate at 20, 40, 60 and 90 min periods were placed in quartz EPR flat

cells (Wilmad, Buena, N.J.). EPR spectra were recorded on a Varian E109 X-band spectrometer at 100 kHz field modulation. For the expanded and compressed spectra respectively: the magnetic field was set at 338.8 mT and 378.8 mT; scan range 10 mT; scan time 16 min for both; time constant 4 s for both; modulation amplitude 2 G and 40 G; microwave frequency 9.505 GHz for both; and microwave power 20 mW for both. The height of the compressed spectra was measured for each time point and normalized for intestinal protein concentration. The protein content of the slices were measured using the technique of Smith et al.[16] Linear regressions were performed on the normalized data using weighted least squares with weights equal to the inverse of variance. Recordings were made of the spontaneous motility of the isolated in vitro segments of jejunum using the methods reported by Kagnoff and Kivy-Rosenberg and by Freas et al.[1,17] Contractions and relaxations of 1 cm longitudinal slices of jejunum from sham-irradiated and irradiated mice were recorded with and without the NOS inhibitor L-NOARG present in the bathing fluid (37° C). For histology studies formalin-fixed jejunum from sham-irradiated and irradiated mice were embedded in paraffin wax, cut into four micron sections, stained in hematoxylin and eosin, and photographed.

III. CHEMICAL EFFECTS

A. EFFECT OF HEXAMETHONIUMBROMIDE

Addition of Hex to jejunum sections incubated in PBS containing the spin trap DBNBS caused a significant increase in DBNBS-spin adduct formation. The typical DBNBS-spin adduct EPR spectrum from these experiments has been described previously Steel-Goodwin et al.[5,6] Furthermore, the Hex effect on this spin adduct formation was abolished in the presence of the specific NOS inhibitor, N^{ω}-nitro-L-arginine (L-NOARG).[5,6] For example, Figure 1 shows the effect on the DBNBS spin adduct formation after addition of L-NOARG at various concentrations (0-10 mM) to hex-stimulated jejunum slices and incubation at 37 °C for 60 min. The results show that at L-NOARG concentrations between 1-10 μM the hex-induced DBNBS-spin adduct formation was reduced to control levels. Because L-NOARG is a specific NOS inhibitor, the results in Figure 1 strongly suggest that the Hex-induced DBNBS-spin adduct formation originated from the production of $NO^{\cdot}$.

L-NOARG is a potent inhibitor of the inducible and constitutive forms of NOS. Recent reports by Gross et al. and Lambert et al. have shown that the inhibition of the inducible NOS occurs at an L-NOARG concentration, [L-NOARG] ≥ 100 μM.[18,19] NOS is assumed in the present experiments to be in the myenteric plexi of the mouse as NOS has been immunologically detected in the myenteric plexi throughout the gut of the rat by Bredt et al.[20] Therefore, the results in Figure 1 also suggest that the L-NOARG inhibited

the constitutive form of NOS, since the Hex effect was virtually eliminated at an [L-NOARG] ~ 10 μM.

Kagnoff and Kivy-Rosenberg showed that *in vitro* stimulation of jejunum sections of rat with Hex caused an increase in rhythmical contractions and relaxations of the longitudinal smooth muscle.[1] This also occured with mouse jejunum and, in addition, Steel-Goodwin et al. showed that the Hex effect was abolished in the presence of L-NOARG.[6] These results strongly suggested that Hex induced the production $NO^{\cdot}$ in the myenteric plexus and this $NO^{\cdot}$ was subsequently involved in the relaxation phase in the jejunum sections. These experiments were consistent with and support the EPR/spin trapping results in Figure 1.

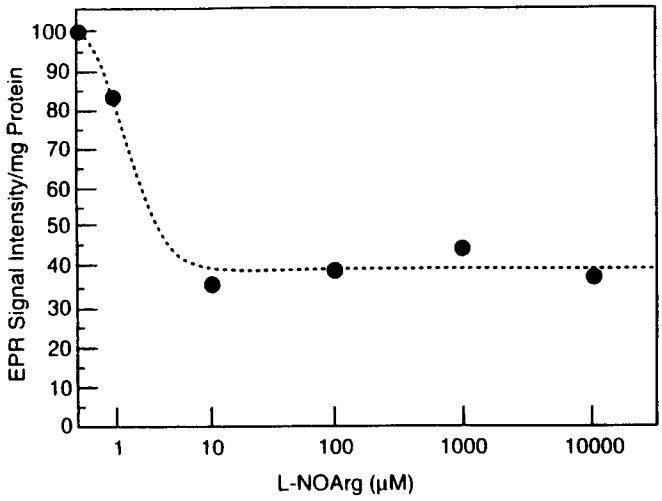

Figure 1. DBNBS spin adduct EPR signal intensity at various concentrations of the nitric oxide synthase inhibitor, L-NOARG, after addition of the inhibitor to incubations of jejunum sections (~ 1 cm) containing Hex and DBNBS. The EPR signal was measured at 60 min. incubation (37°C).

IV. RADIATION EFFECTS

A. EFFECT OF GAMMA-RADIOLYSIS

The intestine is a primary target of radiation injury. Therefore, it was of interest to determine free radical involvement in the deterioration of the gut following its exposure to ionizing radiation. As with Hex, spin adducts were also generated when sections of jejunum suffering radiation effects were

incubated in the PBS buffer in the presence of DBNBS. After exposure of mice to 15 Gy whole body γ-radiation, DBNBS spin adducts were generated by jejunum sections in the incubation media over a period of 4-5 days postradiation. Figure 2 shows a typical spin adduct EPR spectrum from the bathing solution following incubation (20 min., 37°C) of a jejunum section (~ 1 cm) in the presence of DBNBS (1 mM). This EPR spectrum consists of the superposition of several DBNBS spin adduct EPR spectra. It is similar to the DBNBS spin adduct EPR spectra obtained after incubation of jejunum sections with Hex.[6] Although the exact nature of the spin adducts is unknown, two are immediately recognized. One is a prominent triplet with a hyperfine coupling constant, a_N = 1.25 mT, similar to reported oxidation product of DBNBS.[21] The second is a triplet (arrows) with a hyperfine coupling constant, a_N = 0.959 mT, corresponding to the reported value for aqueous DBNBS solutions exposed to NO·.[22] No EPR spectra were obtained in the incubation media containing DBNBS in the absence of tissue. Also shown in Figure 2 is the compressed EPR spectrum yielding a single peak in which all the DBNBS spin adducts formed are included. This permits a more accurate calculation of the EPR spectral intensity and of the total DBNBS spin adduct yield.

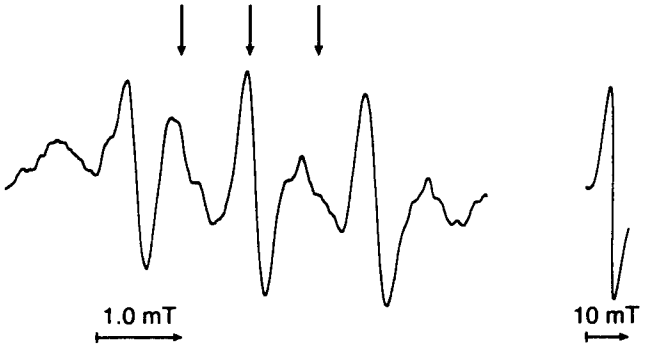

Figure 2. Typical DBNBS spin adduct EPR spectrum obtained from the bathing solution after incubating (37° C, 20-90 min) jejunum sections (~ 1 cm) from mice exposed to γ-radiation (15 Gy). Arrows indicate spectrum corresponding to the spin adduct obtained in the reaction between DBNBS and dissolved NO·.

The intensities of the compressed EPR spectra plotted as a function of incubation time are shown in Figure 3. These results were obtained following incubation of jejunum sections (~ 1 cm) from day one through day

four postradiation. Since the gut slowly deteriorated during this period, the EPR signal intensities were normalized for the quantity of protein in the jejunum section and plotted as EPR intensity per mg protein. EPR spectra were measured at room temperature after 20, 40, 60, and 90 min incubation at 37 °C. The results in Figure 3 show that DBNBS spin adduct EPR signal intensity increased as the incubation time increased from 20 to 90 min. Furthermore, the results also showed that the DBNBS spin adduct EPR signal intensity increased from day one through day four postradiation. This suggests that free radical pathways are actively involved in the deterioration of the gut following exposure to γ-radiation.

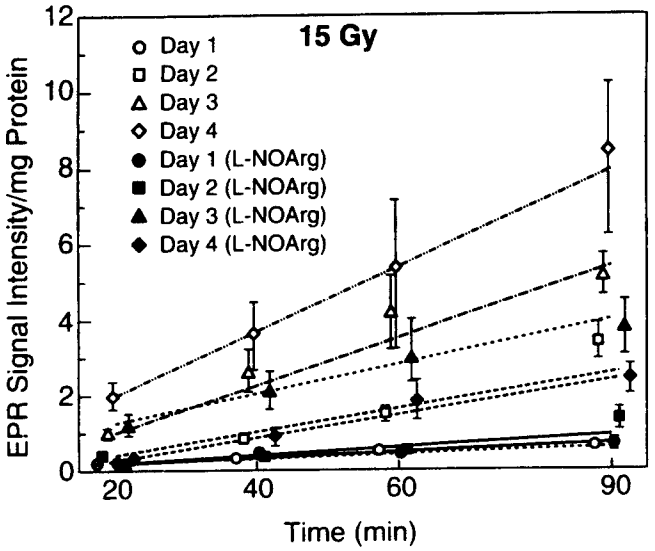

Figure 3. Postirrradiation spin adduct EPR signal intensity as a funtion of incubation time. EPR spectra were obtained 1-4 days postradiation from bathing solutions in the presence and absence of L-NOARG after incubating (37° C) jejunum sections (~ 1 cm) from mice exposed to γ-radiation (15 Gy).

The intestine contains two layers of smooth muscle which are in constant motion (contracting and relaxing) which enable it to propel food through the digestive tract in a process referred to as peristalsis. Increased gut motility, i.e. contractions and relaxations, is known to occur following exposure to ionizing radiation.[23,24] NO· is known to cause smooth muscle relaxation.[25] It has also been implicated in the relaxation phase of intestinal smooth muscle during incubation of jejunum sections with Hex.[6] Since the EPR spectrum

in Figure 2 has a component similar to the spin adduct obtained in the reaction of DBNBS with dissolved NO· gas[22], it is possible that this free radical is also involved in the relaxation phase of intestinal smooth muscle after radiation exposure. In order to determine the involvement of NO· in the radiation effects in the intestine, the effect of L-NOARG (10 mM) on the DBNBS spin adduct EPR signal intensity was measured. L-NOARG is a potent specific inhibitor of the constitutive and inducible forms of NOS.[7,18,19] The results of these experiments are also plotted in Figure 3. At day one postirradiation there is no difference in the DBNBS spin adduct EPR signal intensity in the presence and absence of L-NOARG. At day two postirradiation the DBNBS spin adduct EPR signal intensity is significantly decreased in the presence of L-NOARG. The EPR signal intensity is decreased to approximately the same level as the EPR signal intensity observed at day one postradiation. This suggests that NO· is directly involved in the radiation effects in the intestine at day two postradiation. At day three postirradiation the presence of L-NOARG does not show much of an effect and slightly decreases the DBNBS spin adduct EPR signal intensity. This suggests that although NO· is present other free radical mechanisms are prevalent due to the radiation injury at day three postirradiation. The largest effect exerted by L-NOARG on the DBNBS spin adduct EPR signal intensity is observed at day four postirradiation. In this case and due to the presence of L-NOARG, the DBNBS spin adduct EPR signal intensity has decreased to a similar EPR signal intensity observed for day two postirradiation in the absence of the NOS inhibitor. This result also confirms that a large fraction of the DBNBS spin adduct EPR signal intensity originates from NO·-related pathways at day four postirradiation. However, the results at day four postirradiation in the presence of L-NOARG do not determine the origin of the NO·/NO·-related pathways. It is possible that, due to the severe intestinal injury and hyperemia at day four postirradiation, the NO·/NO·-related pathways do not originate from the intestinal system, but from elevated levels of macrophages and neutrophils. These cells are known to generate NO·.[4] Futhermore, macrophages contain the inducible form of NOS and generate NO· as a major component of their cytotoxic/cytostatic mechanisms.[4]

Pathology observations confirm some of the suggestions derived from the EPR/spin trapping results in Figure 3. Figure 4 shows the photographs obtained at day one through day four postirradiation of jejunum slices (4 μm) using an Olympus Research Photomicroscope (Model: AHBS). At day one postirradiation (panel A) the intestine appears normal and the crypts and villi are intact. At day two postirradiation (panel B) minor changes in the crypts and villi indicate that radiation injury is becoming evident. However, the intestine appears to be sufficiently intact and, therefore, functional. At this stage, it is possible that many of the normal biochemical pathways in the intestine, such as NOS generation of NO·, may be heightened which would lead to the L-NOARG effect observed at day two postirradiation in Figure 3.

At day three postirradiation (panel C) radiation injury is prevalent as seen by loss in crypt cells and blunting of the villi. At this stage, normal functioning of the intestine has ceased (e.g. malabsorption of required nutrients) and it is possible that the biochemical pathways, such as NOS production of $NO^{\cdot}$, are virtually shut down or non-existent. Therefore, it is possible that the slight decrease in the DBNBS spin adduct EPR signal intensity in the presence of L-NOARG at day three postirradiation (Figure 3) does not originate from the intestinal system, but from other sources of $NO^{\cdot}$ such as the the initiation of macrophage activation. At day four postirradiation (panel D) severe radiation injury is evident. Crypt cells and villi are virtually non-existent and the intestine is completely dysfunctional at this stage. This latter observation supports the previous suggestion that, at day four postradiation, the $NO^{\cdot}$/$NO^{\cdot}$-related pathways inhibited by L-NOARG originate from sources such as macrophages and neutrophils and not from the intestinal system.

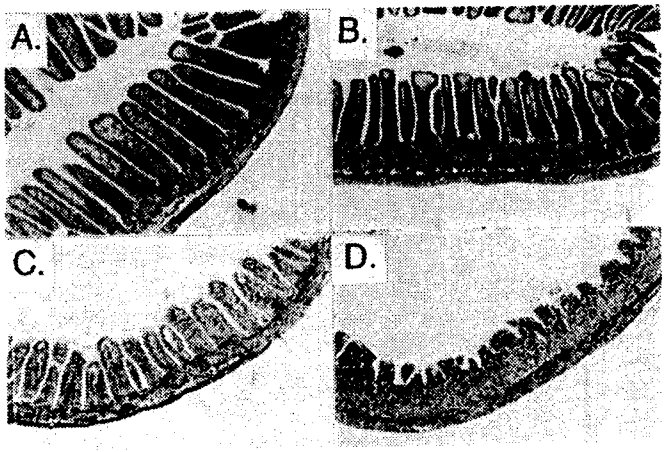

Figure 4. Histopathology of jejunum from mice 1-4 days postradiation (15 Gy). (A) Day 1 ; (B) day 2; (C) day 3; and (D) day 4.

Similar to Hex, radiation affects the motility of the intestine inducing rapid contractions and relaxations.[1,23,24] Whereas the Hex effect on in intestinal motility is immediate, the radiation effects on gut motility are initiated at approximately 48 hrs postirradiation. In a previous report it was shown that the rapid contractions and relaxations, induced by Hex, are abolished when L-NOARG (1-2 mM) is added to the Krebs' bathing solution surrounding a section of jejunum suspended in an organ bath.[6] The effect of L-NOARG on the postirradiation intestinal motility is shown in Figure 5. In these experiments sections of jejunum (~ 1 cm) were suspended (0.5 g passive tension) in an organ bath containing Krebs' buffer.

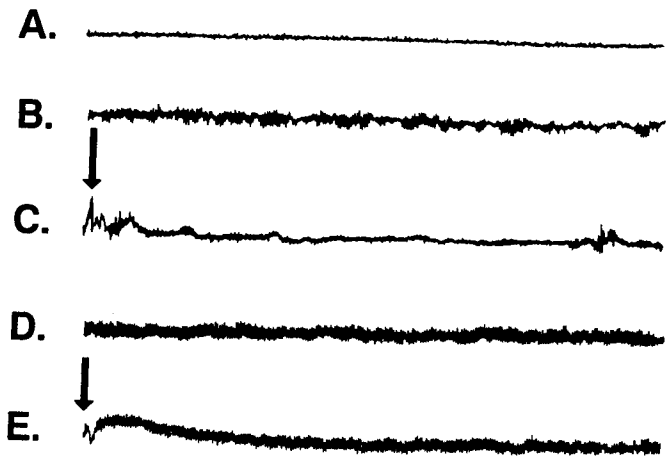

Figure 5. Postirradiation motion in the presence and absence of L-NOARG of jejunum sections (~ 1 cm) from mice exposed to γ-radiation (15 Gy). (A) Control, nonirradiated; (B) day 2 postirradiation, no L-NOARG; (C) day 2 postradiation in the presence of L-NOARG; (D) day 3 postirradiation, no L-NOARG; (E) day 3 postirradiation in the presence of L-NOARG. Jejunum sections were suspended at 0.5 g tension and traces were recorded at the same gain and at a chart speed of 50 mm/s. Each panel represents 400 seconds of the recording.

The contractions and relaxations of the longitudinal smooth muscle were monitored. Figure 5A corresponds to a control nonirradiated jejunum section and shows the normal spontaneous contractions and relaxations expected for a healthy intestine. Figure 5B shows the effects of γ-radiation on longitudinal smooth muscle motility at day two postradiation. In this case the jejunum section is more active showing a substantial increase in contractions and relaxations compared to the control nonirradiated jejunum section (Figure 5A). The increased contractions and relaxations appear to have a degree of spontaneity displaying small areas of lower activity. When L-NOARG (1-2 mM) is added (arrow) to the Krebs' bathing media surrounding the jejunum section described in Figure 5B, an immediate significant decrease in the contractions and relaxations is observed (Figure 5C). Although the contractions and relaxatons are substantially decreased in the presence of L-NOARG, the jejunum section still remains more active when compared to the control jejunum (Figure 5A). The difference between Figure 5B and Figure

5C strongly suggests that NO· is involved in the relaxation phase of the jejunum section at day two postirradiation described in Figure 5B. The EPR/spin trapping results (Figure 3) showed that L-NOARG did not completely reduce the DBNBS spin adduct EPR signal intensity at day 2 postirradiation. These EPR results are consistent with the observation in Figure 5C of a residual increased activity (compared to control jejunum) after L-NOARG addition. This residual increased activity is possibly due to the initiation of intestinal injury caused by the γ-radiation. It is consistent with the pathology observations (Figure 4, panel B) which show the beginning of villi and crypt cell deterioration. Therefore, the residual activity observed in Figure 5C which is independent of NO·/NO·-related pathways is possibly caused by the initiation of radiation induced cellular dysfunction in the crypts and villi and mediated by active oxygen species known to be generated by radiation in cell membranes. At day three postirradiation (Figure 5D) jejunum sections show a significant increase in activity when compared to day two postirradiation (Figure 5B) and control nonirradiated jejunum (Figure 5A). In this case the rapid contractions and relaxations show no degree of spontaneity and are, instead, rythmical. Furthermore, Figure 5E shows that the addition (arrow) of L-NOARG to the jejunum section described in Figure 5D has no effect on the rythmical contractions and relaxations occuring in the jejunum at day three postradiation. The EPR/spin trapping results (Figure 3) suggested the production of some NO· by the small but observable L-NOARG induced decrease in the DBNBS spin adduct EPR signal intensity. However, the result in Figure 5E suggests that the NO· is not generated in the intestinal system and that the increased jejunum activity is independent of intestinal NO·/NO·-related pathways in jejunum at day three postirradiation. These assumptions are consistent with the suggestions derived from the results in Figures 3 and 4 for day three and day four postirradiation, namely, that at day 3 and day 4 postirradiation, respectively, the radiation has sufficiently and totally injured the jejunum (Figure 4, panels C and D) rendering it dysfunctional. Therefore, the observed NO·/NO·-related contribution to the DBNBS spin adduct EPR signal intensity which is inhibited by L-NOARG at days three and four postirradiation (Figure 3) must originate from other sources such as activated macrophages and neutrophils and not from the intestinal system. Due to the deteriorated condition of the jejunum at day four postradiation, it was not possible to suspend these jejunum sections in the organ baths in order to monitor their motility.

The experiments were done using complete jejunum sections containing all components. Therefore, the origin of the mechanism stimulating the increased motility of the jejunum sections at day three postirradiation (not affected by L-NOARG) cannot be predicted. However, previous studies have suggested that radiation induced hypersensitivity of the cholinergic system is directly involved in radiation stimulated intestinal motion.[26,27]

V. CONCLUSIONS

The results show that the production of NO· is detectable by EPR/spin trapping in jejunum incubations exposed to Hex and in incubations of jejunum sections at days two, three and four postradiation. L-NOARG abolishes the Hex effects in the jejunum and the NOS activity is inhibited at a L-NOARG concentration of 10 μM. This suggests that the production of NO· originates from the constitutive form of NOS in the intestinal nervous system. The NO· produced in the presence of Hex is involved in the relaxation phase of the Hex-induced rapid contractions and relaxations. The results also show that radiation injury causes the production of NO· in jejunum incubations at day two, three and four postradiation. However, it appears that NO· production in the intestinal system only occurs at day two postradiation. The NO· produced at this time is involved in the relaxation phase of the postirradiation induced contractions and relaxations. The NO· produced at days three and four postirradiation does not originate from the intestinal system but from other sources possibly activated macrophages and neutrophils. These cells would be present in large quantities in the areas of inflammation and intestinal deterioration caused by radiation injury.

REFERENCES

1. Kagnoff MF, Kivy-Rosenberg E. In vitro contractions of rat jejunum following whole body X-irradiation or drugs. Am J Phys 1969; 216:1057-1063.
2. Gilman AG, Nies AS, and Taylor P. In: *Goodman and Gilman's The Pharmacological Basis of Therapeutics.* New York: Pergamon Press, 1990.
3. Udeinya IJ, Wyche Jr MQ, West WL. Effect of nicotine on the release of endothelium-derived relaxing factor. In: Moncada S, Marletta MA, Hibbs Jr JB, Higgs EA, eds. Biology of Nitric Oxide Vol. 1: Physiology and Clinical aspects. London: Portland Press, 1992: 68-70.
4. Moncada S, Marletta MA, Hibbs Jr JB, Higgs EA. Nitric oxide: physiology, pathophysiology, and pharmacology. Pharmacol Rev 1992; 43:109-142.
5. Steel-Goodwin L, Gray B, Arroyo CM, Carmichael AJ. Nitric oxide in intestinal peristalsis, abstract and poster presented at Nitric Oxide, Implications for Drug Research, Philadelphia, PA, June 1, 1992.
6. Steel-Goodwin L, Gray BH, Arroyo CM, Carmichael AJ. Nitric oxide produced by the intestine relaxes smooth muscle. Submitted for publication.
7. Ishi K, Chang B, Kerwin Jr JF, Huang Z, Murad F. N$^{\omega}$-nitro-L-arginine: a potent inhibitor of endothelium-derived relaxing factor formation. Eur J Pharmacol 1990; 176:219-223.
8. Kerwin Jr JF. EDRF, an emerging target for drug design, Ann Rep Med Chem 1992; 27:69-78.
9. Archer S. Measurement of nitric oxide in biological models. FASEB Journal 1993; 7:349-360.
10. Perkins MJ. In: Gold V, Bethall D, eds. Advances in Physical Organic Chemistry, Vol 17. New York: Academic Press, 1980: 1.
11. Janzen EG. In: Pryor WA, ed. Free Radicals in Biology IV. New York: Academic Press, 1980.
12. Carter RE, Verrelli DM. AFRRI cobalt whole-body irradiator, AFRRI Technical Note, March 1973: 73-3.

13. American Association of Physicists in Medicine, AAPM Task Group 21. A protocol for the determination of absorbed dose from high-energy photon and electron beams. Med Phys 1983: 741-771.
14. Kaur H, Leung RHW, Perkins M. A water-soluble, nitroso-aromatic spin-trap. J. Chem Soc Commun 1981: 142-143.
15. Steel-Goodwin L, Arroyo CM, Gray B, Carmichael AJ. EPR detection of nitric oxide-dependent spin adducts in mouse jejunum. In: Moncada S, Marletta MA, Hibbs Jr JB, Higgs EA, eds. The Biology of Nitric Oxide Vol. 2: Enzymology, Biochemistry and Immunology. London: Portland Press. 1992: 80-84.
16. Smith PK, Krohn RI, Hermanson GT, Mallia AK, Gartner FH, Provenzano MD, Fujimoto EK, Goete NM, Olson BJ, Klerk DC. Measurement of protein using bicinchoninic acid. Anal Biochem 1985; 150:76-85.
17. Freas W, Hart JL, Golightly D, McClure H, Rodgers DR, Muldoon SM. Vascular interaction of calcium and reactive oxygen intermediates produced following photoradiation. J Card Pharmacol 1991; 17:27-34.
18. Gross SS, Steuhr DJ, Aisaka K, Jaffe EA, Levi R, Griffith OW. Macrophage and endothelial cell nitric oxide synthesis: cell-type selective inhibition by N^G-aminoarginine, N^G-nitroarginine, and N^G-methylarginine. Biochem Biophys Res Commun 1990; 170:96-103.
19. Lambert LE, Whitten JP, Baron BM, Cheng HC, Doherty NS. McDonald IA. Nitric oxide synthesis in the CNS, endothelium and macrophages differs in its sensitivity to inhibition by arginine analogues. Life Sci 1991; 48:69-75.
20. Bredt DS, Hwang PM, Snyder SH. Localization of nitric oxide synthase indicating a neural role for nitric oxide. Nature 1990; 347:768-770.
21. Nazaht NB, Yang G, Allen RE, Blake DR, Jones P. Does 3,5-dibromo-4-nitrosobenzenesulphonate spin trap superoxide radicals. Biochem Biophys Res Commun 1990; 166:807-812.
22. Arroyo CM, Kohno M. Difficulties encountered in the detection of nitric oxide ($NO^{\cdot}$) by spin trapping techniques. A cautionary note. Free Rad Res Commun 1991; 14:145-155.
23. Otterson MF, Sarna SK, Moulder JE. Effects of fractional doses of ionizing radiation on small intestinal motor activity. Gastroenterol 1988; 95:1249-1257.
24. Otterson MF, Sarna SK, Lee MB. Fractional doses of ionizing radiation alter postprandial small intestinal motor activity. Dig Dis Sciences 1992; 37:709-715.
25. Murad F, Mittal CK, Arnold WP, Katsuki S, Kimura H. Guanylate cyclase activation by azide, nitro compounds, nitric oxide, and hydroxyl radical and inhibition by hemoglobin and myoglobin. Ad Cyc Nucleot Res 1978; 9:145-158.
26. Rana KZ, Harding RK, Krantis A. Accute effects of ionizing irradiation on intestinal motor activity. The Physiol 1988; 31:A140.
27. Otterson MF, Koch TR, Zhang Z, Leming SC, Sarna SK. Enteric cholinergic enzyme activity is altered by irradiation. J Gastroint Mot 1992; 4:234.

DISTRIBUTION LIST

DEPARTMENT OF DEFENSE

ARMED FORCES RADIOBIOLOGY RESEARCH INSTITUTE
ATTN: PUBLICATIONS DIVISION
ATTN: LIBRARY

ARMY/AIR FORCE JOINT MEDICAL LIBRARY
ATTN: DASG-AAFJML

ASSISTANT TO THE SECRETARY OF DEFENSE
ATTN: AE
ATTN: HA(IA)

DEFENSE NUCLEAR AGENCY
ATTN: TITL
ATTN: DDIR
ATTN: RAEM
ATTN: MID

DEFENSE TECHNICAL INFORMATION CENTER
ATTN: ACQUISITION
ATTN: ADMINISTRATOR

FIELD COMMAND DEFENSE NUCLEAR AGENCY
ATTN: FCIEO

INTERSERVICE NUCLEAR WEAPONS SCHOOL
ATTN: DIRECTOR

LAWRENCE LIVERMORE NATIONAL LABORATORY
ATTN: LIBRARY

UNDER SECRETARY OF DEFENSE (ACQUISITION)
ATTN: OUSD(A)/R&E

UNIFORMED SERVICES UNIVERSITY OF THE HEALTH SCIENCES
ATTN: LIBRARY

DEPARTMENT OF THE ARMY

HARRY DIAMOND LABORATORIES
ATTN: SLCSM-SE

OFFICE OF THE SURGEON GENERAL
ATTN: MEDDH-N

U.S. ARMY AEROMEDICAL RESEARCH LABORATORY
ATTN: SCIENCE SUPPORT CENTER

U.S. ARMY CHEMICAL RESEARCH, DEVELOPMENT, & ENGINEERING CENTER
ATTN: SMCCR-RST

U.S. ARMY INSTITUTE OF SURGICAL RESEARCH
ATTN: COMMANDER

U.S. ARMY MEDICAL DEPARTMENT CENTER AND SCHOOL
ATTN: MCCS-FCM

U.S. ARMY MEDICAL RESEARCH AND MATERIEL COMMAND
ATTN: COMMANDER

U.S. ARMY MEDICAL RESEARCH INSTITUTE OF CHEMICAL DEFENSE
ATTN: MCMR-UV-R

U.S. ARMY NUCLEAR AND CHEMICAL AGENCY
ATTN: MONA-NU

U.S. ARMY RESEARCH INSTITUTE OF ENVIRONMENTAL MEDICINE
ATTN: DIRECTOR OF RESEARCH

U.S. ARMY RESEARCH LABORATORY
ATTN: DIRECTOR

WALTER REED ARMY INSTITUTE OF RESEARCH
ATTN: DIVISION OF EXPERIMENTAL THERAPEUTICS

DEPARTMENT OF THE NAVY

BUREAU OF MEDICINE & SURGERY
ATTN: CHIEF

NAVAL AEROSPACE MEDICAL RESEARCH LABORATORY
ATTN: COMMANDING OFFICER

NAVAL MEDICAL RESEARCH AND DEVELOPMENT COMMAND
ATTN: CODE 42

NAVAL MEDICAL RESEARCH INSTITUTE
ATTN: LIBRARY

NAVAL RESEARCH LABORATORY
ATTN: LIBRARY

OFFICE OF NAVAL RESEARCH
ATTN: BIOLOGICAL & BIOMEDICAL S&T

DEPARTMENT OF THE AIR FORCE

BROOKS AIR FORCE BASE
ATTN: AL/OEBZ
ATTN: OEHL/RZ
ATTN: USAFSAM/RZB

OFFICE OF AEROSPACE STUDIES
ATTN: OAS/XRS

OFFICE OF THE SURGEON GENERAL
ATTN: HQ AFMOA/SGPT
ATTN: HQ USAF/SGES

U.S. AIR FORCE ACADEMY
ATTN: HQ USAFA/DFBL

U.S. AIR FORCE OFFICE OF SCIENTIFIC RESEARCH
ATTN: DIRECTOR OF CHEMISTRY & LIFE SCIENCES

OTHER FEDERAL GOVERNMENT

ARGONNE NATIONAL LABORATORY
ATTN: ACQUISITIONS

BROOKHAVEN NATIONAL LABORATORY
ATTN: RESEARCH LIBRARY, REPORTS SECTION

CENTER FOR DEVICES AND RADIOLOGICAL HEALTH
ATTN: DIRECTOR

GOVERNMENT PRINTING OFFICE
ATTN: DEPOSITORY ADMINISTRATION BRANCH
ATTN: CONSIGNED BRANCH

LIBRARY OF CONGRESS
ATTN: UNIT X

LOS ALAMOS NATIONAL LABORATORY
ATTN: REPORT LIBRARY

NATIONAL AERONAUTICS AND SPACE ADMINISTRATION
ATTN: RADLAB

NATIONAL AERONAUTICS AND SPACE ADMINISTRATION
GODDARD SPACE FLIGHT CENTER
ATTN: LIBRARY

NATIONAL CANCER INSTITUTE
ATTN: RADIATION RESEARCH PROGRAM

NATIONAL DEFENSE UNIVERSITY
ATTN: LIBRARY

U.S. DEPARTMENT OF ENERGY
ATTN: LIBRARY

U.S. FOOD AND DRUG ADMINISTRATION
ATTN: WINCHESTER ENGINEERING AND ANALYTICAL CENTER

U.S. NUCLEAR REGULATORY COMMISSION
ATTN: LIBRARY

RESEARCH AND OTHER ORGANIZATIONS

AUSTRALIAN DEFENCE FORCE
ATTN: SURGEON GENERAL

AUTRE, INC.
ATTN: PRESIDENT

BRITISH LIBRARY
ATTN: ACQUISITIONS UNIT

CENTRE DE RECHERCHES DU SERVICE DE SANTE DES ARMEES
ATTN: DIRECTOR

FEDERAL ARMED FORCES DEFENSE SCIENCE AGENCY FOR NBC PROTECTION
ATTN: LIBRARY

INHALATION TOXICOLOGY RESEARCH INSTITUTE
ATTN: LIBRARY

INSTITUTE OF RADIOBIOLOGY, ARMED FORCES MEDICAL ACADEMY
ATTN: DIRECTOR

KAMAN SCIENCES CORPORATION
ATTN: DASIAC

OAK RIDGE ASSOCIATED UNIVERSITIES
ATTN: MEDICAL LIBRARY

RESEARCH CENTER FOR SPACECRAFT RADIATION SAFETY
ATTN: DIRECTOR

RUTGERS UNIVERSITY
ATTN: LIBRARY OF SCIENCE AND MEDICINE

UNIVERSITY OF CALIFORNIA
ATTN: DIRECTOR, INSTITUTE OF TOXICOLOGY & ENVIRONMENTAL HEALTH
ATTN: LIBRARY, LAWRENCE BERKELEY LABORATORY

UNIVERSITY OF CINCINNATI
ATTN: UNIVERSITY HOSPITAL, RADIOISOTOPE LABORATORY

XAVIER UNIVERSITY OF LOUISIANA
ATTN: COLLEGE OF PHARMACY